Perovskite Light-Emitting Diodes

Antti Nurmesjärvi
Master's thesis
Master's Programme of Chemistry
University of Oulu
2020

Preface

This work is part of my studies in the Master's Programme of Chemistry at University of Oulu, and was carried out at VTT Technical Research Center of Finland during 2020. The work is part of PeroCUBE project funded by European Union.

I would like to thank my supervisors Dr. Riikka Suhonen and PhD, Adjunct Professor Tao Hu for their guidance and advice. Dr. Suhonen provided me with a great opportunity to write a thesis and work in a brilliant research group and an interesting project. Adjunct Professor Hu provided me important guidance and feedback.

I would also like to thank Adjunct Professor Juha Heiskanen for his support during my studies. Your expertise guided me in my development as a scientist, and the work I did during the research project in your lab further convinced me that I should pursue a career as a research chemist. The topic you gave me for my bachelor's thesis led me to the world of perovskites.

Many thanks to my collagues at VTT. The warm and welcoming environment helped me stay motivated, and days of hard work were balanced with laughter. I would like to thank Lic. Phil. Mari Ylikunnari for guidance and Ville Holappa for feedback and comments.

Last, I want to thank my family and friends for support. Annina, I am grateful for your support and the joy you bring to my life. And also, thank you for reviewing the language of this thesis.

Antti Nurmesjärvi

Oulu, December 9, 2020

Abstract

The usage of artificial lighting and displays is increasing all the time. Energy efficient and affordable light-emitting materials are being developed widely. Light-emitting diodes (LEDs) are energy efficient, and LED technology and displays based on LEDs have developed greatly in the recent years. In the year 2014, the first research article related to a perovskite LED (PeLED) that is functional in room temperature was released.

The light-emitting material in PeLED has ABX_3 stoichiometry and perovskite structure. The most common A-cations used in perovskites in PeLEDs are methylammonium, formamidinium and cesium (Cs^+). The most common B-cation is lead (Pb^{2+}) and X-anion is a halide or a mixture of halides. Lead halide perovskites are interesting light-emitting materials, since they can be readily solution processed with inexpensive methods. The emission of lead halide perovskites can be tuned across the whole visible spectrum by changing the composition, and the emission colors are bright due to narrow emission.

There are multiple challenges in PeLED development. Especially the efficiency of blue PeLEDs needs to be improved. Furthermore, there are challenges related to health and stability. The perovskite used in PeLEDs contains lead, which is poisonous, and perovskites are often solution processed from toxic solvents such as dimethylformamide. The biggest challenges in perovskite stability are sensitivity to moisture, oxygen, illumination and heat. Moreover, the stability is affected by mechanical stress, reactions caused by electric bias and reactions between materials used in PeLEDs.

In this thesis, the most common perovskite materials, PeLED architectures, and their characterizations are introduced. Challenges in PeLED development are discussed, especially stability. Perovskite stability can be increased by e.g. perovskite substitution, additives, morphology control and optimization of PeLED structure.

Tiivistelmä

Keinovalaistuksen ja näyttöjen määrä kasvaa maailmassa jatkuvasti. Energiatehokkaita ja edullisia valoa emittoivia materiaaleja kehitetään paljon. Valoa emittoivat diodit (light-emitting diode, LED) ovat energiatehokkaita, ja erilaiset LED teknologiat ja niihin perustuvat näytöt ovatkin kehittyneet lähivuosina nopeasti. Vuonna 2014 julkaistiin ensimmäinen tutkimus huoneenlämmössä toimivasta perovskiitti LED:sta (PeLED).

PeLED:n valoa emittoivalla materiaalilla on ABX_3 koostumus ja perovskiitin kiderakenne. PeLED:ssa käytettävissä perovskiiteissa yleisimmät A-kationit ovat metyyliammonium, formamidinium ja cesium (Cs^+). Yleisin B-kationi on lyijy (Pb^{2+}) ja X-anionina käytetään halidia tai niiden seosta (Cl^-, Br^-, tai I^-). Lyijyhalidi-perovskiitit ovat erityisen kiinnostavia materiaaleja, sillä niitä voidaan valmistaa liuoksista edullisesti ja helposti. Lyijyhalidi-perovskiittien emissiota voidaan säätää koko näkyvän valon aallonpituusalueella muuttamalla niiden koostumusta, ja niiden kapea emissiospektri mahdollistaa kirkkaat värit.

PeLED:en kehityksessä on vielä lukuisia haasteita. Erityisesti sinisten PeLED:en hyötysuhde vaatii vielä kehittämistä. Lisäksi haasteina on mm. terveysriskit ja stabiilisuus. PeLED:t sisältävät myrkyllistä lyijyä ja niiden valmistuksessa käytetään myrkyllisiä liuottimia, kuten dimetyyliformamidia. Suurimmat haasteet stabiilisuudessa ovat herkkyys kosteudelle, hapelle, valolle ja lämmölle. Lisäksi stabiilisuuteen vaikuttaa mekaaninen rasitus, sähkövirran aiheuttamat reaktiot ja PeLED:ssa käytettyjen materiaalien keskinäiset reaktiot.

Tässä tutkielmassa esitellään yleisesti PeLED:ssa käytettäviä perovskiittimateriaaleja, yleisiä PeLED:en rakenteita ja niiden karakterisointia. Lisäksi tutkielmassa perehdytään PeLED:en kehityksen haasteisiin, erityisesti stabiilisuuteen. Perovskiittien stabiilisuutta voidaan parantaa esimerkiksi vaihtamalla perovskiitin koostumusta, käyttämällä lisäaineita, muokkaamalla perovskiittikerroksen morfologiaa ja optimoimalla PeLED:n rakenne.

Contents

The research leading to these results has received funding from the European Union's Horizon 2020 research and innovation programme under grant agreement No. 861985 of the PeroCUBE project.

Abbreviations and symbols

Abbreviations

2D	two-dimensional
3D	three-dimensional
4F-PEA	4-fluoro-phenethylammonium
Ac	acetate
AcN	acetonitrile
AFM	atomic force microscopy
AM	air mass
BA	butylammonium
BCP	bathocuproine
CB	conductive band
CIE	International Commission on Illumination (Commission Internationale de l'Eclairage)
CNT	carbon nanotube
DDDA	4,9-dioxa-1,12-dodecanediamine
DMF	*N,N'*-dimethylformamide
DMSO	dimethyl sulfoxide
EBL	electron blocking layer
EDEA	2,2'-(ethylenedioxy)diethylamine
EDX	electron dispersive x-ray spectroscopy
EL	electroluminescence
EML	emitting layer
EQE	external quantum efficiency
ETL	electron transport layer
EU	European Union
F8	poly(9,9-di-n-octylfluorenyl-2,7-diyl)
FA	formamidinium
FTO	fluorine tin oxide
FWHM	full width at half maximum
GBL	γ-butyrolactone
HBL	hole blocking layer
HI	hydriodic acid
HMDA	hexamethylenediamine
HOMO	highest occupied molecular orbital

HTL	hole transport layer
IR	infrared
ITO	indium tin oxide
LCD	liquid-crystal display
LED	light-emitting diode
Li-Fi	light fidelity
LUMO	lowest occupied molecular orbital
MA	methylammonium
NMA	1-naphthylmethylammonium
NMR	nuclear magnetic resonance
NW	nanowire
OA	oleylamine
ODEA	2,2'-[oxybis(ethyleneoxy)]diethylamine
OLED	organic light-emitting diode
PAA	polyacrylic acid
PBA	4-phenylbutylammonium
PCBM	[6,6]-phenyl-C61-burytic acid methyl ester
PEA	2-phenylethylammonium
PEDOT:PSS	poly(3,4-ethylenedioxythiophene polystyrene sulfonate
PeLED	perovskite light-emitting diode
PEO	poly (ethylene oxide)
PEOXA	poly(2-ethyl-2-oxazoline)
PET	polyethylene terephthalate
PL	photoluminescence
PLED	polymer light-emitting diode
PLQY	photoluminescence quantum efficiency
poly-HEMA	poly(2-hydroxyethyl methacrylate)
poly-TPD	poly(4-butyltriphenylamine
PSC	perovskite solar cell
PTAA	poly[bis(4-phenyl)(2,4,6-trimethylphenyl)amine]
PVK	poly(9-vinylcarbazole)
PVP	polyvinyl pyrrolidone
QD	quantum dot
QLED	quantum dot light-emitting diode
RGB	red, green, and blue
RH	relative humidity
RT	room temperature

SEM	scanning electron microscope
SIMS	secondary-ion mass spectrometry
Spiro-OMeTAD	2,2',7,7'-tetrakis[N,N-di(4-methoxyphenyl)amino]-9,9'-spirobifluorene
TCE	transparent conductive electrode
TEM	transmission electron microscope
TF	tolerance factor
TFB	poly[9,9-dioctylfluorenyl-2,7-diyl)-*co*-(4,4'-(*N*-(4-sec-butylphenyl)diphenylamine)]
TPBi	2,2',2''-(1,3,5-Benzinetriyl)-tris(1-phenyl-1-H-benzimidazole)
TRL	technology readiness level
TTDDA	4,7,10-trioxa-1,13-tridecanediamine
U.S.	United States
UV	ultraviolet
UV-VIS	ultraviolet-visible
VB	valence band
WHO	World Health Organization
XPS	X-ray photoelectron spectroscopy
XRD	X-ray diffraction

Symbols

c	speed of light
e	elementary charge
eV	electron volt
Eg	Bandgap energy
h	Planck's constant
n_i	oxidation state
r_i	radius
T	Goldschmidt tolerance factor
V	voltage
λ	wavelength
μ	octahedral factor
ν	photon's frequency
τ	tolerance factor τ

1 INTRODUCTION

1.1 Background

The first organic-inorganic hybrid perovskite light-emitting diode (PeLED) was constructed by Era et al. in 1994, but it was functional only in liquid nitrogen temperature.[1] They predicted that a hybrid material could combine desirable attributes from both, organic and inorganic, materials. PeLEDs gained attention again in 2014, when the first research article concerning room temperature functional PeLED was released.[2]

Organic-inorganic hybrid perovskites have been intensely studied since 2009 when methylammonium lead iodide perovskite was used as an absorbing material in a solar cell for the first time. The PeLED research has taken a lot of influence from perovskite solar cell (PSC) research, because same materials are used in both technologies and the device architecture is similar. Other technologies related to PeLEDs are organic light-emitting diodes (OLEDs), polymer light-emitting diodes (PLEDs), and quantum dot light-emitting diodes (QLEDs).

The progress of OLEDs, QLEDs and PeLEDs is shown in Figure 1. External quantum efficiency (EQE), current efficiency and luminance are important metrics of LED technologies. PeLEDs are a new technology, which has developed remarkably fast, and the development has not yet shown signs of slowing down.

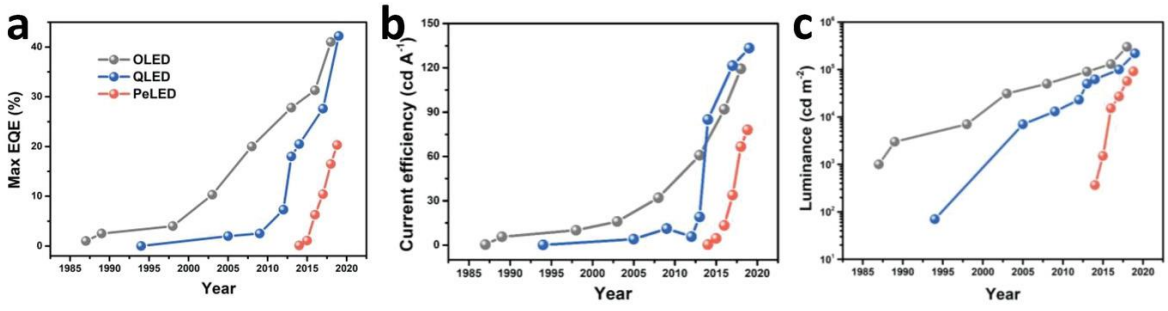

Figure 1. Timelines of OLED, QLED and PeLED development. a) maximum EQE, b) current efficiency, and c) luminance. Reprinted with permission.[3] © 2019 WILEY-VCH Verlag GmbH & Co. KGaA, Weinheim.

1.2 Motivation

The usage of artificial lighting increases all the time. United States of America (USA) Department of Energy estimates that the electricity consumption of lighting in USA was 641 TWh in 2015, which accounts for 17% of total electricity consumed in USA. The amount of newly installed lamps and other luminaires increased from around 7 billion in 2001 to 8.7 billion in 2015.[4]

Environmentally friendly lighting technologies are needed. LEDs are a good option since they have high luminous efficacy. Inorganic LEDs are already widely used, and according to USA Department of Energy, more than 2353 million LED units were installed in year 2018. The annual energy cost savings from these LEDs were around $14.7 billion, and they estimate that savings would approach $56 billion if all lighting sources were switched to the best available LEDs.[5]

Traditional inorganic LEDs need high material purity and expensive processing techniques, which increases prices and thus slows the shift from e.g., incandescent lamps to LEDs. OLEDs are another interesting option, but emitting materials used in OLEDs generally need complex synthesis, which increases costs.[6] OLEDs are currently not widely used in lighting, but they are widely used in displays.

PeLEDs have a long list of desirable properties for lighting sources and displays, such as solution processability, high luminous efficacy, transparency, high color purity and color tunability. In addition, PeLEDs are thin and can be fabricated on flexible substrates to make flexible LEDs. Essentially, PeLEDs have a potential to be a cheap and efficient option for lighting and displays that is easy to manufacture. Nevertheless, there are many challenges, such as material and device stability and environmental issues.

1.3 Structure of the thesis

Background and motivation of this thesis have been presented in this chapter. Chapter 2 defines the theoretical principles of LEDs and introduces some relevant LED applications. In chapter 3, the perovskite materials for perovskite light-emitting diodes, with theories to predict perovskite stability, are discussed. The most common perovskite light-emitting diode

architectures are introduced, along with non-perovskite materials used in other layers of PeLEDs. In chapter 4 the most important characterization methods for PeLED research are introduced. The most important challenges in PeLED development are discussed in chapter 5. Finally, chapter 6 summarizes this thesis and gives conclusions of this work with discussion about the future of perovskite light-emitting diodes.

2 LIGHT-EMITTING DIODES

2.1 Working principle of a light-emitting diode

A traditional light-emitting diode (LED) is a P–N junction diode that is fabricated from semiconducting materials. Electrons are injected from the n-side and holes are injected from the p-side. Electrons and holes recombine in the semiconducting material and emit light. A graphical presentation of a P–N junction LED is shown in Figure 2.[7]

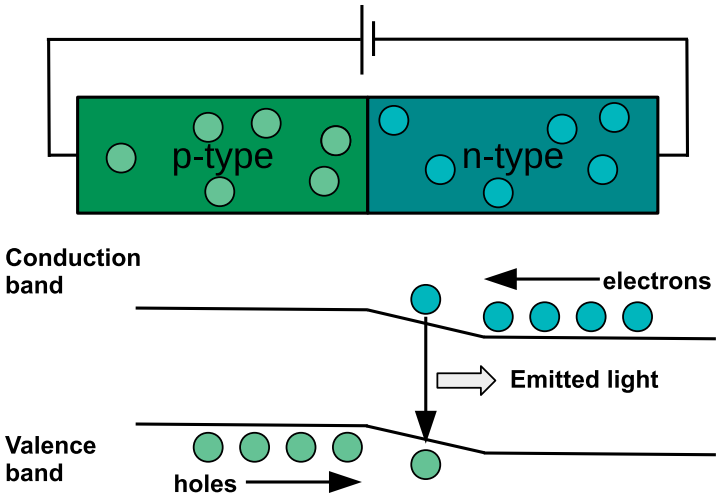

Figure 2. Graphical presentation of a P-N junction LED.

The recombination of electrons and holes can be radiative or non-radiative. In radiative recombination, an electron moves from the conduction band to the valence band to recombine with a hole, and a photon is emitted. The non-radiative recombination can never be completely eliminated, but it can be minimized in order to increase the efficiency of the LED.

Bandgap energy E_g is the energy difference between the valence band and conductive band. Different LED materials have different bandgap energies. The energy of a photon emitted from the LED is related to the bandgap (equation 1).

$$h\,\nu \approx E_g \tag{1}$$

where h is Planck's constant, ν is the photon's frequency and E_g is bandgap energy.

The voltage applied to the LED (V) multiplied by the elementary charge (e) is equal to the photon energy hν (equation 2). This only applies to an ideal LED, and there are various effects that can lead to small changes in the diode voltage.

$$e\,V = h\,\nu \tag{2}$$

where e is the elemental charge, V is diode voltage, h is the Planck constant and ν is photon's frequency.

From equations (1) and (2) it can be derived that the energy of the emitted photon is related to the energy of the electron injected to the LED. The radiative electron–hole recombination requires that the drive voltage is larger than or equal to the bandgap energy. The diode voltage is given by equation (3):

$$V = \frac{h\,\nu}{e} \approx \frac{E_g}{e}. \tag{3}$$

where V is voltage, h is Planck's constant, ν is photon's frequency, e is elementary charge and E_g is bandgap energy.

Stranks et al. list four requirements for an efficient electroluminescence (EL) emission for a LED: 1) The ratio of electrons and holes that are injected to emitting material should be close to one. 2) Current leakage should be minimized: no carriers should leave the diode without recombining. 3) Non-radiative recombination should be minimized. All electron-hole recombinations should be radiative. 4) The photons generated in the emitting layer should be efficiently extracted.[8] EL is discussed in more detail in section 4.1.1.

2.2 Wavelengths and colors

The wavelength of the emission is directly related to the photon energy. Photon energy hν is Planck constant times the frequency of the photon. The wavelength can be calculated with equation (4):

$$\lambda = \frac{h\,c}{E_g} \approx \frac{1240}{E_g} nm \tag{4}$$

where λ is the wavelength and c is the speed of light.

For a common perovskite used in green PeLEDs, $CsPbBr_3$, bandgap energy E_g is around 2.36 electron volts (eV) in room temperature. This corresponds to a wavelength of roughly 525 nm.

Most LED applications are in visible light range, and the recipient of the emission is human eye. The human eye is able to detect emission with wavelength range 390–720 nm. The human eye can also detect light with wavelengths below or above the range, but the sensitivity is low. The human eye is the most sensitive with green light with 555 nm wavelength (Figure 3). The photon energies, wavelengths and corresponding colors are summarized in Table 1. It should be noted that color is subjective and there is no clear boundary between colors, the transition between colors is fluid.

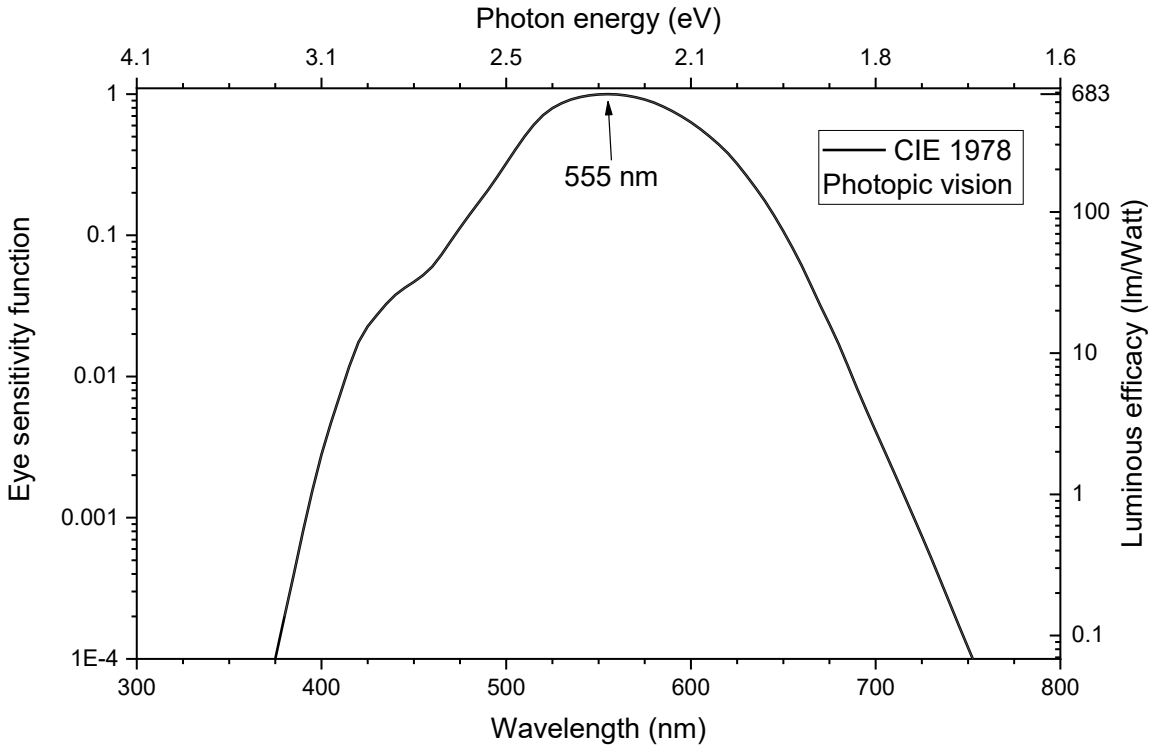

Figure 3. CIE 1978 Eye sensitivity function.

Table 1. Photon energies, wavelengths and corresponding colors.[9]

Photon energy (eV)	Wavelength	Color
< 1.72	> 720	Infrared
1.72–1.98	625–720	Red
1.98–2.07	600–625	Orange
2.07–2.18	570–600	Yellow
2.18–2.41	515–570	Green
2.41–2.53	490–515	Cyan
2.53–2.73	455–490	Blue
2.73–3.18	390–455	Violet
> 3.18	< 390	Ultraviolet

The human eye has three cone cells that are sensitive in the red, green and blue color range. The chromaticity space by International Commission on Illumination (Commission Internationale de l'Eclairage, CIE) (Figure 4) is based on the spectral sensitivity of the cone cells to perceive human color vision. With coordinates x and y, one is able to specify how the human eye detects the emission.

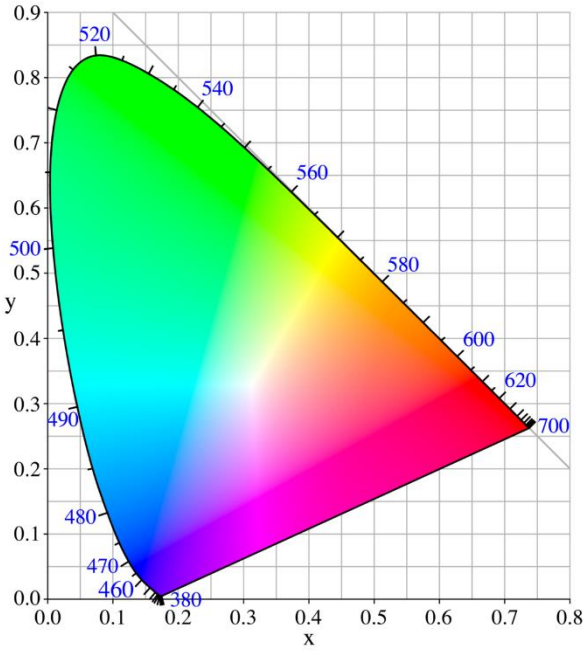

Figure 4. CIE chromaticity space.[10]

White LEDs can be made with multiple structures (Figure 5). The white LED with single emitting layer can have a single emitting layer (EML) with broad emission, so that it seems white, or the layer can be a mixture of red, green and blue (RGB) emitting materials (Figure 5a). It is possible to get white emission with separate RGB layers that are stacked in a single LED (Figure 5b), stacked RGB LEDs (Figure 5c), or parallel RGB pixels (Figure 5d). If the pixels are small and the gap between then is narrow, human eye observes it as white light. This (Figure 5d) is a general structure used in OLED displays. The advantage in structures c and d is that the different light pixels can be adjusted separately, and the system can produce different colors. Fifth possibility is to use only an ultraviolet (UV) or a blue led and down-converting materials on top of it (Figure 5e).

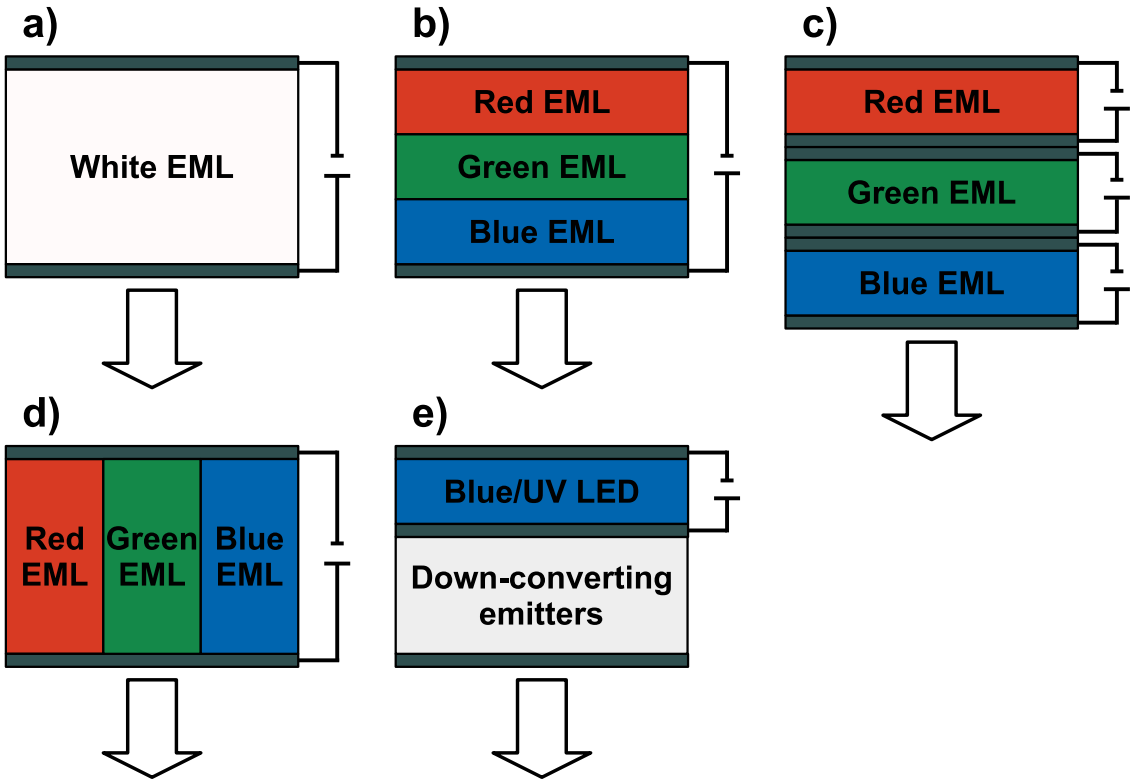

Figure 5. General structures of white LEDs. a) Structure with a single white-emitting-layer. b) Structure with multiple emitting layers. c) Stacked RGB structure. d) Pixelated structure. e) Down-converting structure. Arrows show the direction of emission.

The down-converting materials need to have strong photoluminescence (PL). As an example, Dai et al. made perovskite nanoparticles with near 100 % photoluminescence quantum efficiency (PLQY) and used a thin perovskite film on an inorganic blue LED,

resulting in efficient down-converting green LED.[11] It is important that the stacked layers are in the right order: the emitting materials used in LEDs generally absorb emission with wavelength shorter than its emission wavelength, which means that the red EML can absorb the emission of green and blue EMLs, and green EML can absorb the emission of blue EML. The absorbance is avoided in structures b and c, and it is utilized in structure e.

2.3 Applications of light-emitting diodes

Two largest areas of application for LEDs are lighting and displays. USA department of energy estimated that out of 8.7 billion new stationary luminaires installed in the USA in 2015, about 700 million (8 %) were LEDs.[4] The amount of displays is hard to cover, but to include a few examples: Over 1.5 billion smartphones were sold in 2019[12] and many OLED screens are commonly used in smartphones. Other popular screen technology is liquid-crystal display (LCD), in which LEDs are commonly used as the backlight. OLEDs and LED backlit LCD displays are also widely used in computer monitors and televisions. The market for smartwatches is constantly increasing, and e.g., every Apple Watch series released so far has had an OLED display. In addition, Apple Watch Series 6 contains a blood oxygen sensor, which consists of four LEDs and four photodiodes.

Obviously, lighting and displays are potential applications also for PeLEDs. In both cases, PeLEDs can enable things that cannot be achieved with present technology. Since PeLED emission wavelength is easily tunable, it is possible to make LEDs with specific wavelengths. This can be beneficial in e.g., high color purity displays, human circadian lighting and lighting for agriculture. In addition, it is possible to make transparent PeLEDs, which leads to applications like transparent displays and lighting inside windows.

In addition, PeLEDs can be turned on and off relatively quickly, which enables the usage in light fidelity (Li-Fi) applications. For example $CsPbBr_3$ nanocrystals have a PL lifetime of approximately 7 nanoseconds.[13] Li-Fi is a wireless communication technology where data is transmitted with light. Generally, a light source is flashed and the emitted light is detected by a photodiode. Li-Fi enables data transfer speeds up to several gigabits per second. Perovskites can be used as an emitting material in LEDs and as an absorbing material in photodiodes, and it is even possible that the same perovskite diode acts as a LED and a photodiode.[14]

In order for display to have a wide color gamut, it needs to have suitable green, red and blue primary colors. Rec. 2020 is a recommendation for display technology that defines the primary color wavelengths and coordinates in CIE 1931 chromaticity diagram. The coordinates are listed in Table 2 and shown in Figure 6. The white coordinate D65 in the Figure 6 corresponds to a 6500 K white light, which is a normal daylight. All colors inside the triangle can be reached with only the three primary colors in the corners of the triangle. Since the emission of PeLEDs is easily tunable and narrow, it is possible that these coordinates can be reached more accurately compared to other LED technologies. To the best of my knowledge, fully PeLED based displays have not been demonstrated yet, but Yin et al. demonstrated a backlighted LED where $CsPbBr_3$ perovskite was used as a down-converting material to achieve green color. They reached a high color gamut and were able to proof that a perovskite material can be used as a down-converting material in a display.[15]

Table 2. Rec. 2020 primary color coordinates and wavelengths[16]

Color	Red	Green	Blue	White
Coordinates (x, y)	(0.708, 0.292)	(0.170, 0.797)	(0.131, 0.046)	(0.3127, 0.3290)

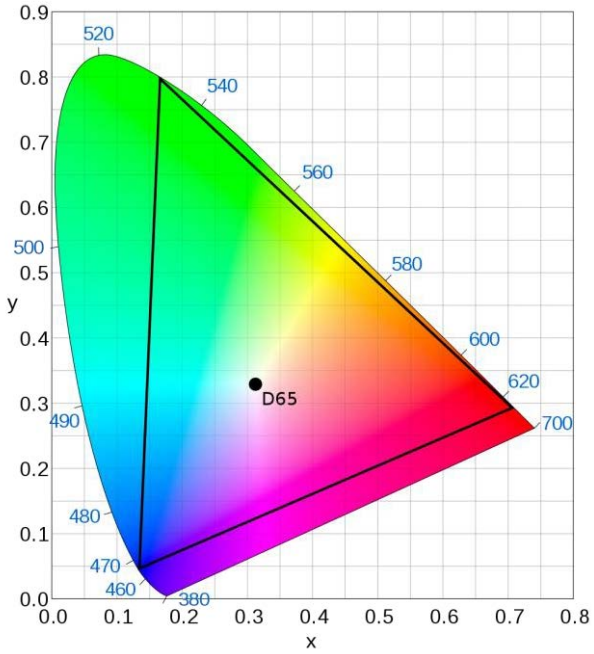

Figure 6. CIE 1931 chromaticity diagram. The black triangle shows Rec. 2020 color gamut.[17]

The lighting affects human body in many ways. For example, the production of melatonin, which is the hormone that controls sleep-wake cycle, is decreased after a long-term exposure to certain wavelengths of blue light. LED emission wavelength is narrow and tunable, and PeLED emission is especially narrow and the tuning is relatively easy. With PeLEDs as lighting source it is possible to avoid specific undesirable wavelengths.[18]

3 PEROVSKITE LIGHT-EMITTING DIODES

Although first perovskite-based LED devices were made in 1994, the technology gained more attention in 2014 when the first room-temperature functional PeLED was made. In only 6 years, highest EQE of PeLED has increased from 0.76% to over 24% and is expected to increase even higher.

PeLEDs have many attracting properties. PeLED color can be tuned over the whole visible light wavelength region (about 400 to 785 nm), as will be later discussed in section 3.1.4. In addition, the emission full width at half maximum (FWHM) is very narrow compared to other LEDs, which enables very pure color LEDs[19]

Other advantages of PeLEDs are related to the fabrication: the elements in perovskites are very earth-abundant, so there is no shortage of materials and the material costs are moderate. Perovskites can be solution processed, and the defect density of solution processed perovskites is quite low. Moreover, perovskites have a comparably high tolerance for defects. Solution processing is faster and cheaper compared to e.g., thermal evaporation in high vacuum that is needed for some emitters used in OLEDs. The processing temperatures are also lower than those used to fabricate traditional inorganic LEDs, which saves energy and enables e.g., usage of flexible substrates such as polyethylene terephthalate (PET), which has a melting point around 250 °C.

Perovskite structure and most common perovskite compositions used in PeLEDs are introduced in section 3.1. In section 3.2, the architecture of PeLEDs is discussed, and in section 3.3, the most common materials used in PeLEDs are discussed.

3.1 Perovskite structure

3.1.1 *Perovskite crystal structure*

Originally perovskite was the name of a mineral composed of calcium titanate ($CaTiO_3$) which was found in 1839 and named after a Russian mineralogist L. A. Perovski. The term is later used to describe compounds with similar crystal structure as $CaTiO_3$. Perovskites have ABX_3 stoichiometry, where A and B are cations and X is an anion, most commonly

oxide (O^{2-}) or a halide. Perovskite crystal lattice contains a network of BX_6 octahedra with A-site cations in the cavities. A perfect cubic perovskite structure is rare. Most perovskites have orthorhombic or tetragonal distortion, due to the size difference between the A-site cations, B-site cations, and X-site anions (Figure 7).

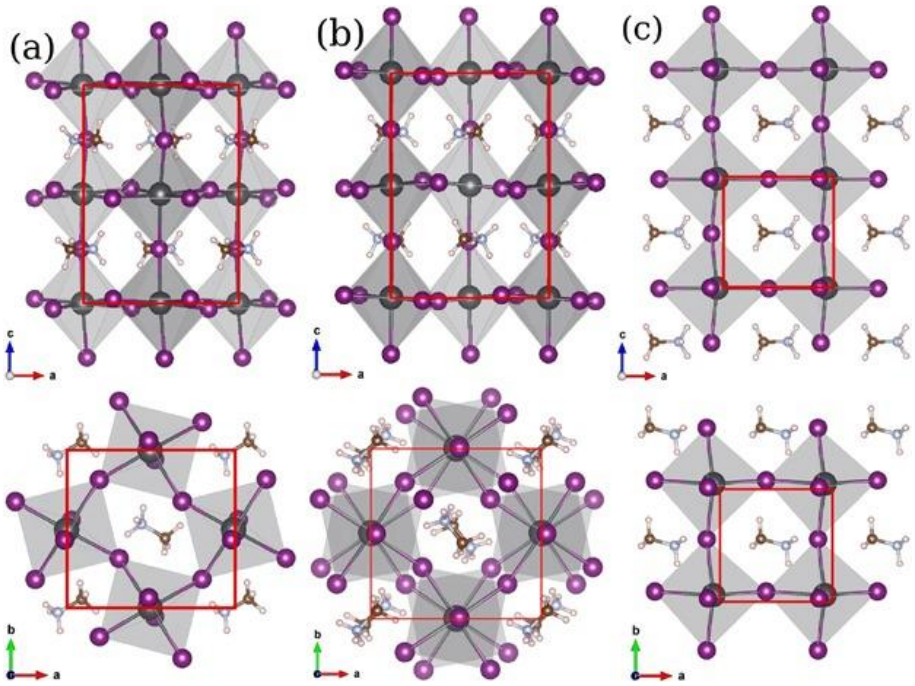

Figure 7. (a) orthorhombic, (b) tetragonal and (c) cubic phases of $MAPbI_3$ perovskite. Top row is in a-c plane, bottom row is in a-b plane. Reprinted with permission.[20] © 2016 WILEY-VCH Verlag GmbH & Co. KGaA, Weinheim.

There are vast amounts of compounds with perovskite structure. A few materials are widely used in PeLED research, and they are similar to the materials used in PSCs. Since PeLEDs are a relatively new technology, it is possible that the perovskites which are now widely used will be replaced by some other perovskites with superior properties. In this section, the most common perovskite compositions for PeLED applications are introduced.

Organic-inorganic hybrid perovskites have an organic cation in the A-site. Most common organic A-site cations are methylammonium (MA) (**2**) and formamidinium (FA) (**5**). In some structures, a mixture of cations is used. Other organic A-site cations include e.g. ammonium (**1**)[21], hydrazinium (**3**)[22], azetidinium (**4**)[23], ethylammonium (**6**)[24], acetamidinium (**7**)[25] and guanidinium (**8**)[26]. Some organic cations form non-perovskite phases when used as the only A-site cation, but a small portion of them can be added to substitute FA or MA, to improve perovskite layer quality, device performance or stability.

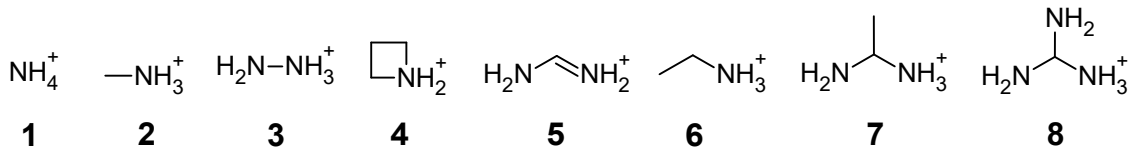

Figure 8. Selected organic A-site cations. Ammonium (1), Methylammonium (2), hydrazinium (3), azetidinium (4), formamidinium (5), ethylammonium (6), acetamidinium (7) and guanidinium (8).

In all-inorganic perovskites, inorganic A-site cation is used. Most common inorganic A-site cation is Cesium (Cs^+), and it can form perovskite structure alone. Other inorganic A-site cations such as rubidium (Rb^+), potassium (K^+) and sodium (Na^+) are used in some studies as additives, but they are too small to form stable perovskite structure alone.[27–31] Some perovskite materials used in state-of-the-art PSCs and PeLEDs contain a mixture of organic and inorganic A-site cations. Perovskite compositions such as $FA_xCs_{1-x}PbX_3$ are common, and even structures with four A-site cations are used.[29] Formulas of organic A-site cations are presented in Figure 8, and ionic radii of organic and inorganic A-type cations are presented in Figure 9

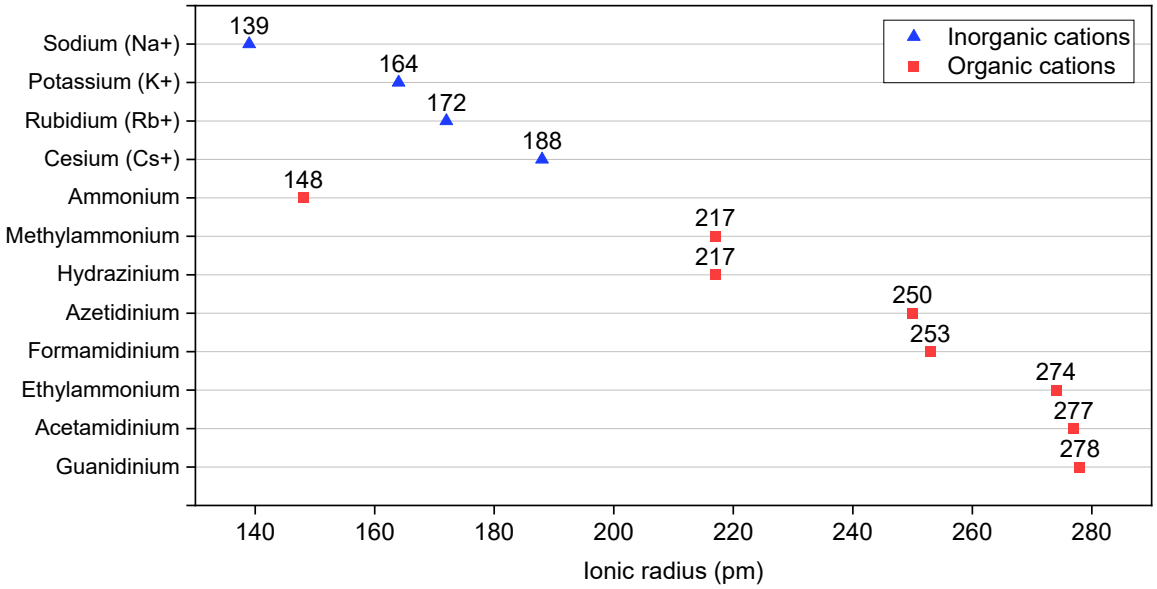

Figure 9. Calculated ionic radii of organic A-site cations and ionic radii of inorganic A-site cations.[32,33]

Most common B metal is lead (Pb^{2+}), but since lead is toxic, other metals are also considered. Tin (Sn^{2+}) is the most common substitute for lead, but it oxidizes easily to Sn^{4+} under ambient conditions, leading to degradation of perovskite. Other B metals include germanium (Ge^{2+}), silver (Ag^+), bismuth (Bi^{3+}), antimony (Sb^{3+}), indium (In^{3+}) and copper (Cu^{2+}). In so-called

double perovskite, a mixture of +1 and +3 charged cations is used, resulting in A_2BCX_6 structure, where B has +1 charge and C has +3 charge.[34] $Cs_2AgInCl_6$ is an example of such material, and it has been successfully used in a white LED.[35]

In most reported PeLEDs, X is a halide-anion. In some cases, a mixture of iodide and bromide or bromide and chloride is used, but iodine and chlorine are rarely mixed because of the size difference. Chlorine doping in iodine-based perovskite is possible only at small percentages (3–4%)[36] Even though halides are the most common X-site materials, it is possible to substitute them with other anions. Jiang et al. replaced two iodides with thiocyanate ions (SCN^-) and used the resulting $MAPb(SCN)_2I$ as an active light-absorbing perovskite material in a solar cell.[37]

3.1.2 *Theories to predict properties and stability of perovskites*

There is a vast amount of possible perovskite compositions, and many compositions remain unexplored. Tolerance factors (TFs) can be used to predict if a chemical composition will form a stable perovskite structure. Goldschmidt tolerance factor (equation 5) is generally used as a guideline to estimate the stability of a perovskite:

$$t = \frac{r_A + r_B}{\sqrt{2}(r_A + r_X)} \tag{5}$$

where r_i is the radius of ion i.

When t is between 0.8 and 1, a solid-state perovskite is expected. If $t > 1$, cation in A-site is too large, and it can prevent the formation of perovskite structure. If $t < 0.8$, the A-site cation is too small, and it can lead to non-perovskite structure. As can be seen from the equation (5), increase in r_A or r_X makes the t-value smaller, and increase in r_B raises the t-value. As an example, t-values of $MAPbI_3$, $MAPbBr_3$, and $MAPbCl_3$ are 0.912, 0.927, and 0.938, respectively.

In 2015, Kieslich et al. calculated t values for over 2300 perovskite compositions using the Goldschmidt TF. They found that there were at that time over 600 potential unexplored perovskites with t values between 0.8 and 1. In their study, they included only amines in the A site, excluding other options like inorganic cations cesium Cs^+ and rubidium Rb^+.[38]

While t is widely used, it has limitations. It was first used in 1926 to describe perovskites with ABO_3 structure, and it works well with oxide- and fluoride-based perovskites ($X = O^{2-}$, F^-). The most common X-site anions in PeLEDs are heavier halides, ($X= Cl^-$, Br^-, I^-), and Goldschmidt TF identifies such perovskites with much lower percentage.[39] More precise methods to predict perovskite stability for heavier halides have been developed. The application of t can be expanded with octahedral factor μ, introduced by Travis W et al. in 2016 (equation 6):[39]

$$\mu = \frac{r_B}{r_X} \tag{6}$$

where r_i is ionic radius of ion i. When μ is larger than 0.41, the B-site anion can coordinate octahedrally with the X-site anion. With μ smaller than 0.41, the ions would overlap, and such combinations are not able to form a continuous perovskite structure. Goldschmidt TF together with octahedral factor can predict the perovskite stability more precisely than Goldschmidt TF alone.

Since t and μ are based on geometry, they can predict if the perovskite structure is geometrically possible, but they do not predict if perovskite structure actually forms. In 2019, a new data-based TF τ was presented by Bartel et al. (equation 7).[33]

$$\tau = \frac{r_X}{r_B} - n_A\left(n_A - \frac{r_A/r_B}{\ln(r_A/r_B)}\right) \tag{7}$$

where n_A is the oxidation state of ion A, r_i is the ionic radius of species i, and $r_A > r_B$. τ-value less than 4.18 indicates that a perovskite structure forms. The new TF τ includes the octahedral factor μ in its first term ($r_X/r_B = \mu^{-1}$). τ was tested on a set of 576 compounds, and it correctly identified 92 % of compounds as perovskites and non-perovskites. τ is adaptable also to double perovskites with formula A_2BCX_6.[33]

When TFs are used, the radii of organic cations is a challenge. Molecular ion radii depend on the ionic counterparts. Kieslich et al. suggested that the ionic radii for a set of nitrogen-based A-site cations can be calculated with equation 8:

$$r_{Aeff} = r_{mass} + r_{ion} \tag{8}$$

where r_{mass} is the distance between the center of mass of the molecule and the furthest non-hydrogen atom in the molecule, and r_{ion} is the ionic radius of the furthest non-hydrogen atom.[32] These calculations are dependent on the B-site cation and X-site anion.

The properties of mixed perovskites, such as $Cs_xFA_{1-x}PbBr_3$, follow Vegard's Law (equation 9).[40–43] The law is seldom obeyed perfectly, but it can be a useful tool to predict e.g. the stability of mixed perovskites. Vegard's law is an empirical rule discovered by Vegard in 1921, and it states that when two similar compounds A and A' are mixed, the lattice parameter of the resulting mixture is a weighted mean of the lattice parameters of A and A'. The components A and A' need to have the same crystal structure.[44]

$$a_{A_{(1-x)}A_x} = (1-x)a_A + xa_{A'} \tag{9}$$

where a_i is the lattice parameter a of species i.

TFs can be calculated for mixed perovskites using Vegard's law. It should be noted that TFs are even more inaccurate for mixed perovskites, and they can be used only as a tool to predict the stability. It is possible that a mixed perovskite does not form a single mixed phase but separate phases, and TFs are not able to predict if phase segregation happens.[45]

3.1.3 *Two-dimensional perovskite-like structures*

Perovskites discussed in sections 3.1.1 and 3.1.2 are called three-dimensional (3D) perovskites, because the network of BX_6 octahedra is continuous in three dimensions. Perovskite quantum dots (QDs) are called zero-dimensional perovskites and perovskite nanowires (NW) are called one-dimensional perovskites, based on the shape of the nanoparticle. Two-dimensional (2D) perovskites can be divided to two groups. The first type of 2D perovskite can be described as a 2D ABX_3 perovskite, an ABX_3 perovskite grown in the nanoplatelet structure. A 2D perovskite can also be made by using a large organic cation in the A position, resulting in a stacked structure where single layers of BX_6 octahedra are separated with a layer of organic cations as can be seen in Figure 10. Sometimes only a part of the A-site cations is substituted with long cations, and the structure can be generalized with a formula $L_2A_{n-1}B_nX_{3n+1}$, where L is a long cation and n defines the number of PbX_4 layers between the long cations. When n=1, the formula is L_2BX_4, and such materials are called 2D perovskites, Ruddlesden-Popper phases or Dion-Jacobson phases. When $n\rightarrow\infty$,

structure resembles ABX_3 structure. Materials between n=1 and n=∞ are called quasi-2D perovskites, 2D/3D perovskites, or layered perovskites.

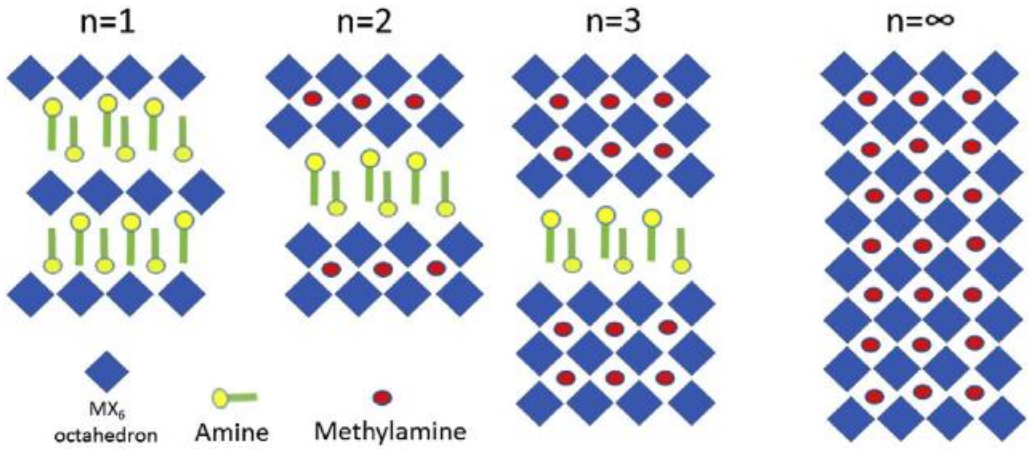

Figure 10. Schematic of layered perovskite-like structures with long amines. When n=∞, the structure is ABX_3, with n=1, structure is L_2BX_4. Reprinted with permission.[46] © 2017 Elsevier Inc.

Most common large cation used in 2D perovskites is 2-phenylethylammonium (PEA) (**9**)[1,47–53]. Other large cations include e.g. 4-fluoro-phenethylammonium (4F-PEA) (**10**)[54,55], 4-phenylbutylammonium (PBA) (**11**)[56,57], 1-naphthylmethylammonium (NMA) (**12**)[58,59], butylammonium (BA) (**13**)[60–65], and oleylamine (OA) (**14**)[66,67]. The chemical structures of large cations (**9–14**) are presented in Figure 11. 2D perovskites are generally more resistant for humidity, heat and stress than commonly used 3D perovskites[49,50,68], and 2D perovskites have good film formation properties[58]. 2D/3D perovskite structures can combine some properties of 2D and 3D perovskites. However, the fabrication conditions and perovskite composition must be carefully designed, since bulky large cations can prevent charge transport, leading to a drop in the efficiency of radiative recombination.[47] The structure can be hard to optimize so that <n> is constant throughout the structure.[47,58,60]

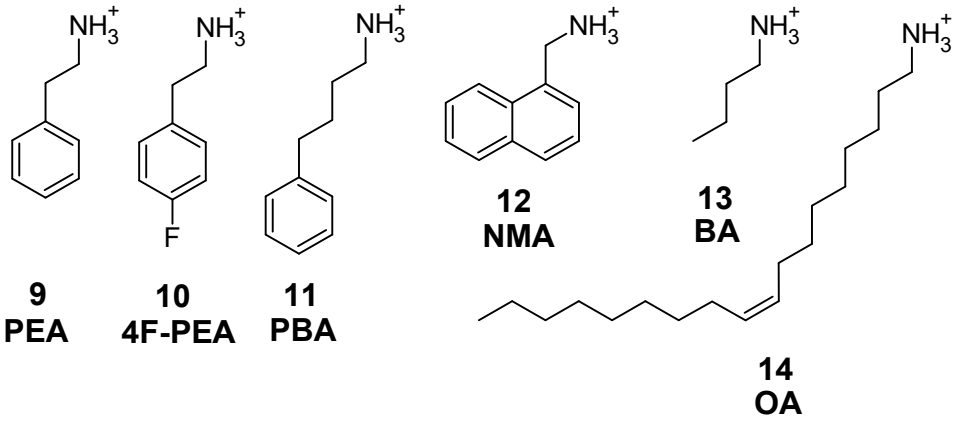

Figure 11. Large organic cations used in layered organic-inorganic hybrid metal halides. PEA (9), 4F-PEA (10), PBA (11), NMA (12), BA (13) and OA (14).

There is debate if 2D and quasi-2D structures should be called perovskites, since they do not have an ABX_3 stoichiometry, the BX_6-octahedra is not continuous and the properties of the materials differ from properties of perovskites[69,70]. Akkerman and Manna recommend that materials that do not meet the criteria of perovskite should be called something else that describes the material, not perovskites. Terms such as hybrid organic–inorganic metal halide and organic-inorganic layered metal halide could be used. In this thesis, they are called 2D/3D perovskite structures.

3.1.4 *Bandgap tuning in perovskite light-emitting diodes*

The bandgap of the light emitting material in LED is directly related to the wavelength of the emission. The bandgap can be tuned by changing any of the three components, A, B or X.[42,43,71–73] Vegard's law, which was introduced in section 3.1.2, can also be applied to perovskite band gap tuning. The bandgap of a semiconductor is more or less linearly dependent to lattice parameters. When the lattice parameter gets smaller, the interatomic distance decreases, which leads to a higher binding energy for valence electrons and a higher bandgap. Zhang et al. have studied $FA_{(1-x)}Cs_xPbBr_3$ with x=0–0.6, and when FA is replaced by smaller Cs, the lattice parameter decreases and bandgap increases, leading to a blue-shift in the emission. The PL peak shifts from 531 to 519 nm.[43] Zhang et al. have also studied $CsPb_{(1-x)}Sn_xBr_3$ with x =0–0.7, and by replacing lead with smaller tin, the lattice parameter decreases, bandgap increases, and a blue shift is observed. The PL peak wavelength shifts from 520 to 496 nm.[41] In perovskite materials, a common way to tune the bandgap is changing the halide composition. Noh et al. demonstrated in 2013 that the bandgap and wavelength of $MAPbI_{3-x}Br_x$ can be tuned between 1.58 eV (786 nm) and 2.28 eV (544 nm)

respectively. Smaller bromide leads to a decreased lattice parameter and thus a higher band gap energy.[42] Protesescu et al. demonstrated in 2015 that $CsPbX_3$ ($X=Cl^-$, Br^-, I^- or a mixture of halides) nanocrystals have emission spectra tunable over the visible spectral region. Pure $CsPbCl_3$ has the highest bandgap and the shortest wavelength (~410 nm), Pure $CsPbI_3$ has the lowest bandgap and the longest wavelength (~700 nm). The bandgap tuning of $CsPbX_3$ is shown in Figure 12.[71]

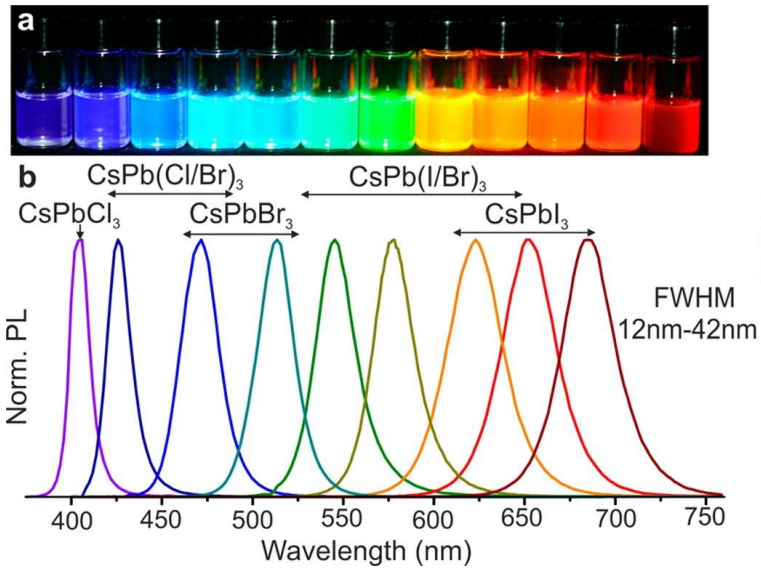

Figure 12. Bandgap tuning of $CsPbX_3$ nanoparticles. a) $CsPbX_3$ nanocrystal colloidal dispersions under UV illumination, b) Photoluminescence spectra of $CsPbX_3$ samples. Reprinted with permission.[71] © 2015, American Chemical Society.

2D/3D perovskite structures are another option to tune bandgap. The bandgap depends on n in $L_2A_{n-1}BX_{3n+1}$. As n increases, bandgap decreases and emission wavelength gets longer.[47] This applies also to 2D ABX_3 perovskites, where n is the number of PbX_6 layers in a platelet. In 2017, Kumar et al. studied 2D $FAPbBr_3$ perovskites with the platelet thickness of 7 to 10 layers, and they achieved a ultrapure green LED with a wavelength of 529 nm and a color close to the Rec. 2020 standard.[74]

A third way to tune bandgap is to control the crystal size and morphology of the crystals. In 2015, Song et al. demonstrated that in addition to bandgap tuning with halides, PL wavelength of $CsPbBr_3$ QDs increases when the QD size is increased.[73] Huang and Lu et al. have demonstrated that the wavelength of $MAPbBr_3$ can be tuned from 450 to 530 nm by changing the morphology.[75,76]

3.2 Common architectures of perovskite light-emitting diodes

The simple LED architecture is a layer of light-emitting material between two electrodes. One of the electrodes needs to be transparent so that the emission can escape the device. Typically, there are other layers between electrodes and the light-emitting layer to enhance the properties of the LED. Hole transport layer (HTL) is used to transfer holes from anode to valence band of perovskite, and electron transport layer (ETL) is used to transfer electrons from cathode to conduction band of perovskite. The holes and electrons recombine in the perovskite layer, emitting light. Sometimes an electron blocking layer (EBL), or a hole blocking layer (HBL) is used to prevent the leakage of holes and electrons to the opposite direction. In addition to the functional layers, there is a substrate material, on which the LED is built.

The devices can be constructed in two ways: the electrons can be injected from the substrate side and holes from the other side, or the other way. The structures are called n-i-p and p-i-n, where p means positive, n means negative and i means intrinsic. General PeLED structures are shown in Figure 13.

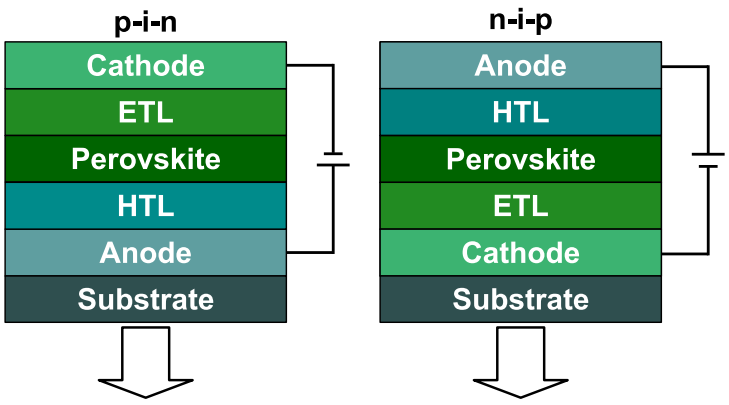

Figure 13. p-i-n and n-i-p architectures used in PeLEDs.

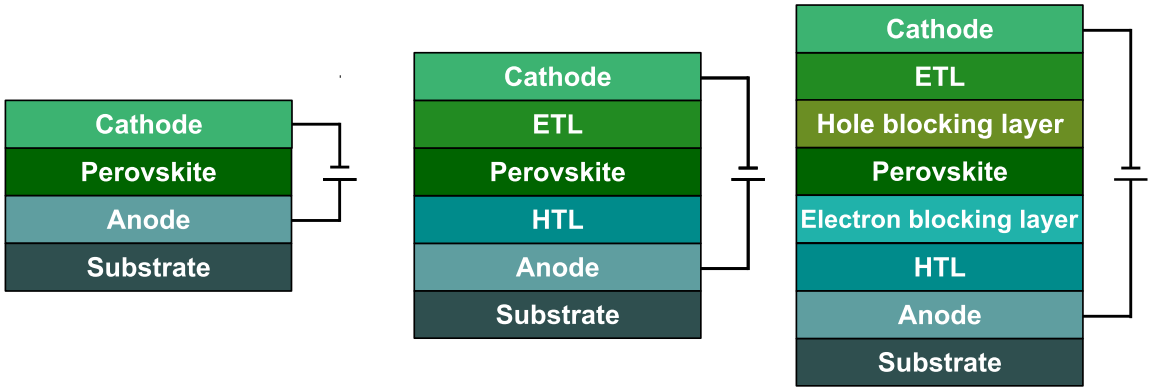

Figure 14. Device architectures with different amounts of layers.

Three p-i-n PeLED architectures with different amounts of layers are shown in Figure 14. Not all LED applications need the state-of-the-art effective LEDs, sometimes a less effective LED is enough, and it can save money. Some perovskite LEDs are functional even without HTL or ETL, and a simpler architecture is much cheaper, faster, and more environmentally friendly to manufacture since there are fewer processing steps and less materials used. There are multiple reports on single-layer perovskite LEDs, where a perovskite or a perovskite-related material is sandwiched between electrodes.[46,55,66,77,78] It is possible to increase PeLED stability and performance with additional layers, but some common ETL and HTL materials are expensive, need vacuum deposition techniques and highly controlled environment. This increases the manufacturing costs and complicates the upscaling. Furthermore, some ETL and HTL materials are moisture sensitive, and while they can increase the efficiency, it is possible that they reduce the stability of the LED.

All the layers have varying thicknesses, but generally all layers except the substrate are thinner than 200 nm. To reduce material usage and costs, it is reasonable to use as thin layers as possible, as long as is does not have any negative effects on device efficiency or stability. In PeLEDs, the optimal thickness of the perovskite layer is 35–40 nm, according to Zhao et al.[79] They tested different thicknesses using $MAPbI_3$, $Cs_{0.2}FA_{0.8}PbI_{2.8}Br_{0.2}$, $FAPbI_3$ and $FAPbBr_3$ based LEDs, and with all perovskite materials the layer thickness of 35–40 nm led to higher EQE and better stability when compared to thicker layers (80–160 nm). Zhao et al. used a structure where indium tin oxide (ITO) anode thickness is 150 nm, HTL thickness is 25 nm, ETL thickness is 40 nm and cathode thickness is 100 nm. The device was built on a 0.7 mm thick glass substrate, and the perovskite thickness was varied.[79] In addition to the experimental results by Zhao et al, Jung et al. have made optical simulations on layer

thicknesses. They varied the thickness of ITO and perovskite layers in a device with Glass/ITO (anode)/HTL/Perovskite/ETL/cathode structure and found that optimal thickness of ITO anode is 200 nm and optimal thickness of perovskite is 30 nm. They state that the refractive indices of ITO and perovskite are higher than the other layers, and the optimal layer thicknesses lead to more efficient light outcoupling and higher efficiency. They have also made simulations with varying ETL and HTL layer thicknesses, and the results indicate that the ETL and HTL thicknesses have less impact on the efficiency of the PeLED.[80]

The common architecture of PeLED is greatly influenced by PSCs and OLEDs. Shi et al. predict that an optimal structure for a PeLED would be much different, and they propose a new "insulator-perovskite-insulator" architecture, where the perovskite layer is sandwiched between two ultrathin insulating layers made of lithium fluoride LiF. LiF blocks current leakage and prevents exciton quenching that happens at HTL/perovskite and ETL/perovskite interfaces, but the thin layer of only a few nanometers allows electrons to tunnel through it. They achieve a 30-fold increase in current efficiency, and an increased device stability. Their strategy is very different from other PeLEDs, and they show that it is possible that the device architecture and materials might change.[81]

3.3 Materials in perovskite light-emitting diodes

Most common substrate material is glass. The LED is built on a substrate material, and in most devices, the emitted light escapes the device through the substrate. In such devices, substrate needs to be transparent at least on the wavelength of emitted light. PET is a common flexible substrate.[82]

The bottom electrode must be transparent because the light emitted from the LED passes through it. The most common transparent conducting electrodes (TCE) are indium doped tin oxide (ITO) and fluorine doped tin oxide (FTO). Indium is a rare metal, and new materials have been researched to replace ITO. Some promising materials are graphene[83], carbon nanotubes (CNTs), and metal NWs. A good TCE is conductive, transparent, light, flexible, cheap, and scalable for mass production.[84]

The main requirements for top electrodes are conductivity and a suitable work function. If the top electrode is reflective, it can reflect the emission and increase the illuminance of the

LED. On the other hand, transparent top electrode enables transparent LEDs. Top electrode is deposited last, so all other materials of the device need to withstand the deposition conditions, e.g., high temperature or vacuum. Common top electrode materials are gold, silver, and aluminum. Top electrodes for transparent PeLEDs include CNTs, graphene and metal NWs, or some more complex multilayer systems, such as Al/ITO/Ag/ITO used by Xie et al.[85]

HTL and ETL materials are used to match the energy levels and charge carrier injection between the electrodes and the emitting layer. Both materials need to be conductive, and it would be optimal that the HTL and ETL used would have similar charge transporting characteristics, so that equal amounts of holes and electrons are injected to the emitting layer.

ETLs include ZnO, TiO_2, SnO_2, bathocuproine (BCP) (**15**) and 2,2',2"-(1,3,5-benzinetriyl)-tris(1-phenyl-1-H-benzimidazole) (TPBi) (**16**). The chemical structure of organic ETLs is presented in Figure 15.

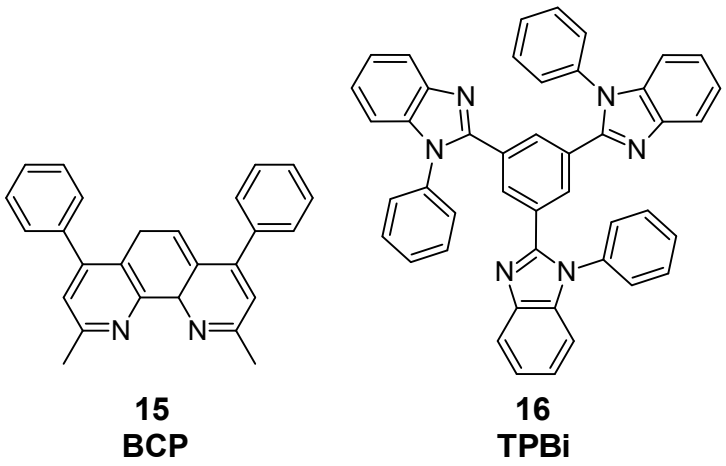

Figure 15. Chemical structure of organic ETL materials used in PeLEDs.

HTL materials used in PeLEDs include NiO_x, poly(9,9-di-n-octylfluorenyl-2,7-diyl) (F8) (**17**), poly(3,4-ethylenedioxythiophene) polystyrene sulfonate (PEDOT:PSS) (**18**), poly(4-butyltriphenylamine) (poly-TPD) (**19**), poly[bis(4-phenyl)(2,4,6-trimethylphenyl)amine] (PTAA) (**20**), Poly(9-vinylcarbazole) (PVK) (**21**), N2,N2,N2′,N2′,N7,N7,N7′,N7′-octakis(4-methoxyphenyl)-9,9′-spirobi[9H-fluorene]-2,2′,7,7′-tetramine (spiro-OMeTAD) (**22**) and poly[(9,9-dioctylfluorenyl-2,7-diyl)-co-(4,4′-(N-(4-sec-butylphenyl)diphenyl-amine)] (TFB) (**23**). The chemical structure of organic HTLs is presented in Figure 16.

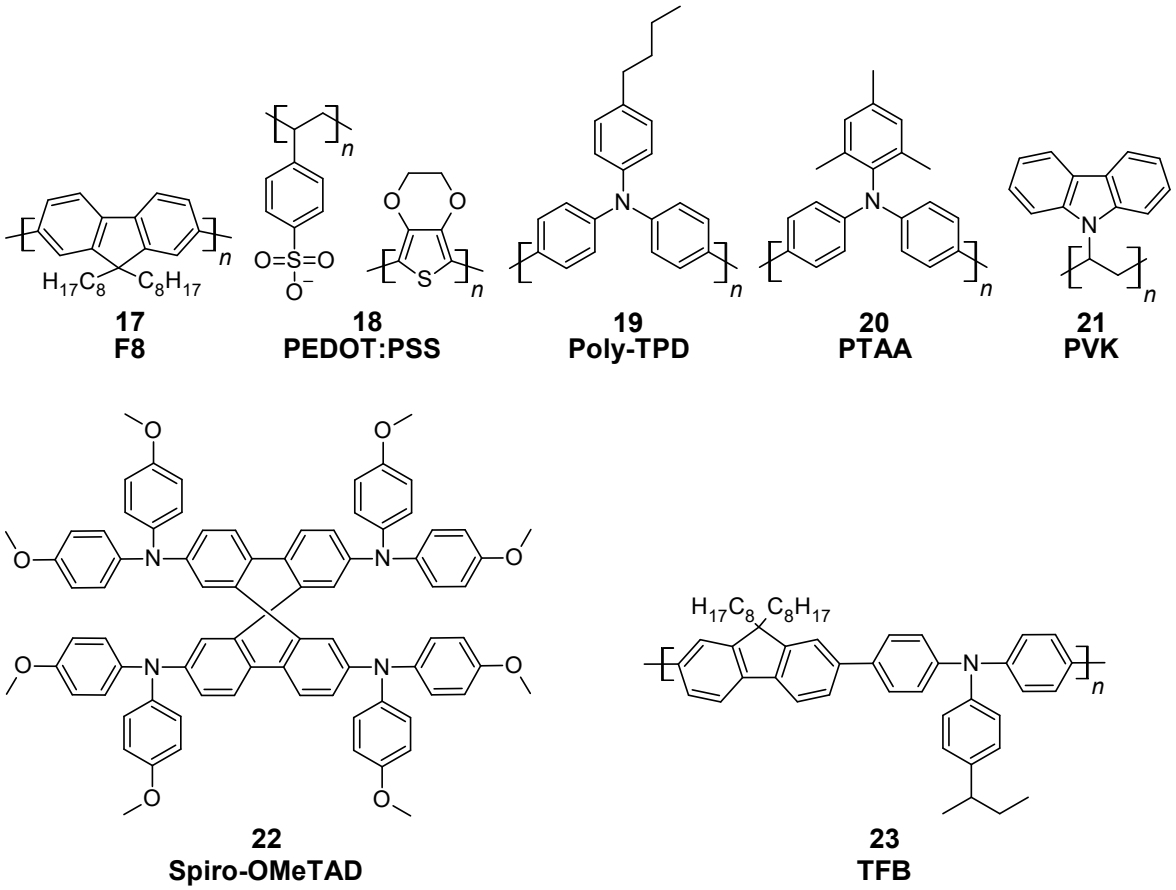

Figure 16. Chemical structure of organic HTL materials used in PeLEDs.

The best ETL and HTL materials depend on the color of the led, since the energy levels of adjacent layers need to match. As an example, Xiao et al. used poly-TPD as a HTL with $MAPbI_3$ and PVK with $MAPbBr_3$. HOMO energy levels for poly-TPD and PVK are 5.6 eV and 5.8 eV respectively, and conduction band energy levels are 5.4 and 5.9 eV for $MAPbI_3$ and $MAPbBr_3$ respectively.[62] Energy levels of $CsPbX_3$ perovskites and selected other materials are presented in Figure 17.

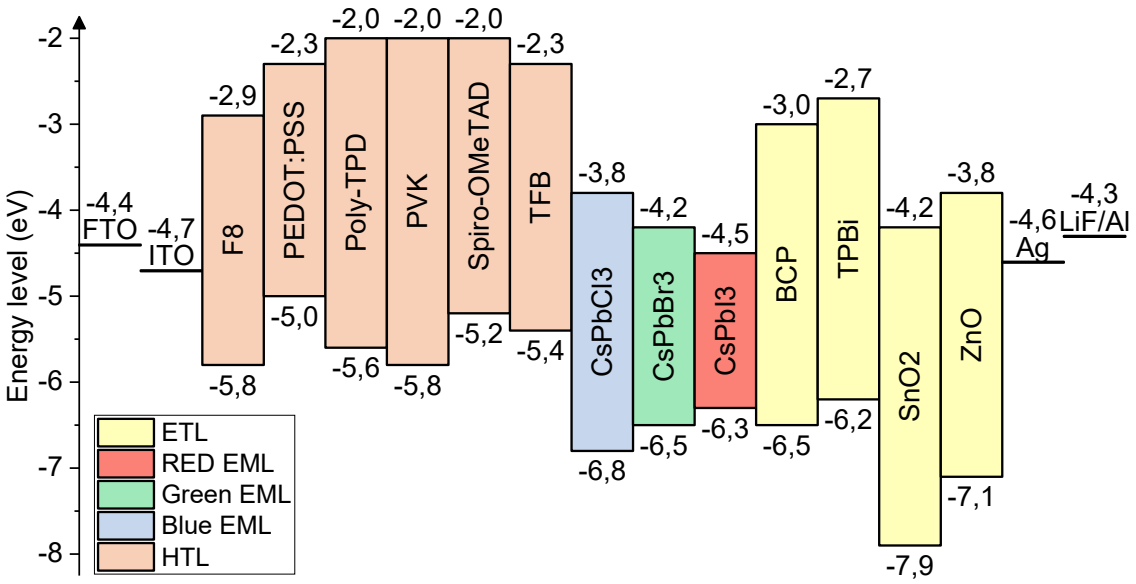

Figure 17. Energy levels of selected materials used in PeLEDs. Electrodes are marked only with work functions. Energy levels are taken from multiple sources.[2,62,86–90]

The energy levels need to match in two ways: the HTL must have matching HOMO (highest occupied molecular orbital)/valence band (VB) energy levels with electrode and perovskite layer to allow hole transportation from electrode to perovskite. At the same time, the LUMO (lowest unoccupied molecular orbital)/conductive band (CB) energy level must be high enough to block electron transportation from perovskite to HTL. In proportion, the ETL must have matching LUMO/CB energy levels with electrode and perovskite layer to allow electron transportation from electrode to perovskite, and at the same time the HOMO/VB energy level must be low enough to block hole transportation from perovskite to ETL. The energy level matching is demonstrated in Figure 18. In Figure 18a, the HOMO/VB energy level has a good match for hole transportation to perovskite, but the LUMO/CB energy level is too low, and it allows the leakage of electrons. In a similar manner, the LUMO/CB energy level of ETL has a good match for electron transportation from cathode to perovskite, but a high HOMO/VB energy level allows the leakage of holes. In Figure 18b, HTL and ETL have large bandgaps, which helps to prevent leakage. In some cases, additional layers are used to enhance electron and hole blocking or to balance electron and hole injection.

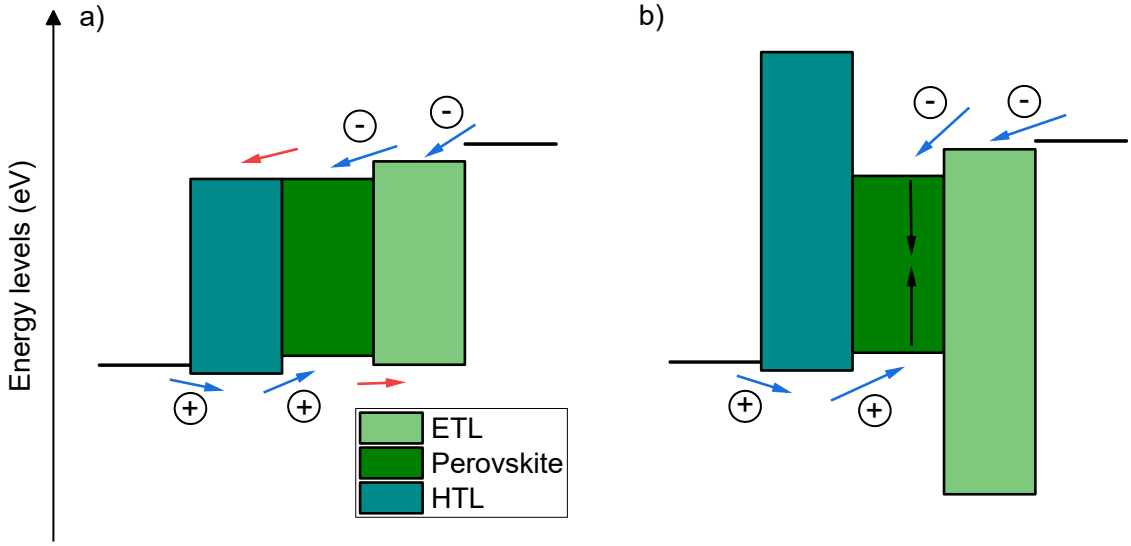

Figure 18. A graphical presentation of a) electron leakage with small bandgap charge transport layers and b) electron and hole blocking of large bandgap charge transport layers. Blue arrows show desirable transportation of electrons and holes, red arrows show undesirable leakage.

PSC development has been most beneficial for red and infrared (IR) PeLEDs, since perovskites used in PSCs have a bandgap at IR area. ETL and HTL materials developed for PSCs have matching energy levels with red and IR PeLEDs. Since the green and blue emitting perovskites have wider bandgaps, the energy levels are different, and the energy levels of HTL and ETL materials used in PSCs do not match as well as with red and IR emitting perovskites.

In some cases, the perovskite is built into a host matrix. Various polymers have been used, e.g. a commercially available polyimide precursor PI2525 (**24**)[91], poly(ethylene oxide) (PEO) (**25**)[77], poly(2-hydroxyethyl methacrylate) (Poly-HEMA) (**26**)[92] and poly(2-ethyl-2-oxazoline) (PEOXA) (**27**)[93] (Figure 19). PEO is a conductive polymer, so it enables the transportation of electrons. PI2525 is an insulator, and it blocks electron transportation directly between HTL and ETL. PEOXA was used with $CsPbBr_{0.6}I_{2.4}$ perovskite, and it interacts with the metal cations of the perovskite, improving the phase stability of the perovskite and preventing formation of non-perovskite phase. In addition, PEOXA increases the number of nucleation sites of perovskite during fabrication, which leads to a smaller particle size. There are multiple justifications for usage of host matrix, including protecting the perovskite and passivating the surfaces, which both can improve stability. In some cases,

polymer can improve the morphology of the perovskite layer, e.g., decrease surface roughness and crystal size.

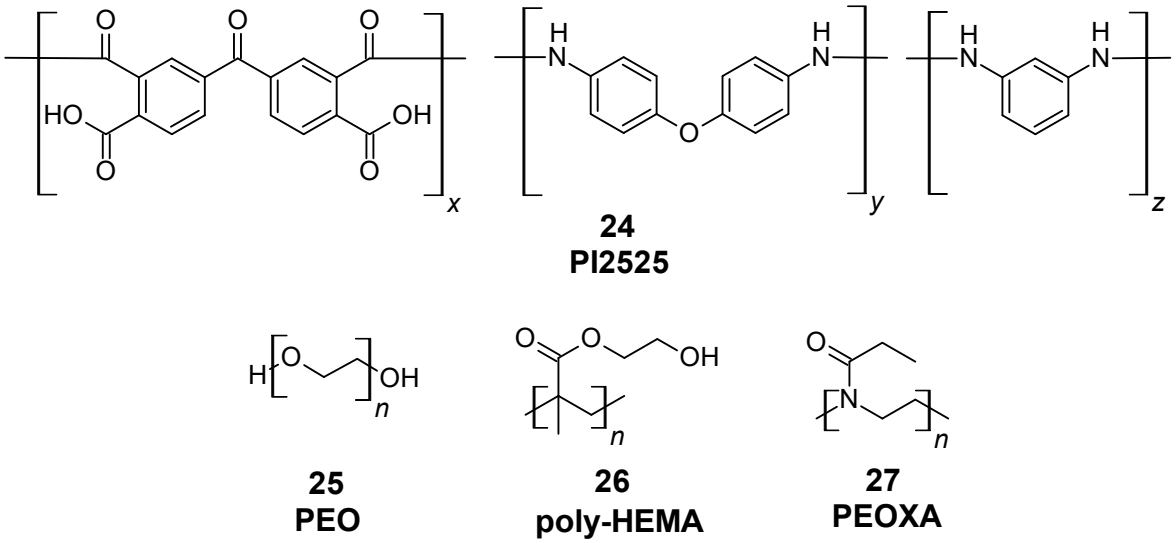

Figure 19. Chemical structure of polymer materials used in composites with perovskites. PI2525 (24), PEO (25), poly-HEMA (26) and PEOXA (27).

4 CHARACTERIZATION METHODS FOR PEROVSKITE LIGHT-EMITTING DIODES

4.1 Characterization of device performance

The research article *High-Efficiency Polycrystalline Perovskite Light-Emitting Diodes Based on Mixed Cations* by Cho et al. will be used as an example on the PeLED performance characterization. They studied PeLEDs based on $FA_{1-x}Cs_xPbBr_3$ perovskites with x between 0 and 1.[94]

4.1.1 *Photoluminescence and electroluminescence*

Photoluminescence (PL) is a phenomenon where a sample emits light after it absorbs light. The sample is illuminated, and the energy of the absorbed photons excites electrons in the sample. When the excited electrons return

to the ground state, they recombine with holes and the sample emits photons with the energy of the band gap. The photons that are used for sample illumination must have higher energy than the bandgap of the LED. The peak of PL emission is at the bandgap of the emitting material.

PL can be used to determine or confirm the bandgap energy, to gain information about uniformity of the sample and in some cases to detect sample impurities. In PeLED research, PL emission quality (wavelength) and emission intensity are both important parameters. Figure 20 shows PL characterizations made by Cho et al. The most important thing is emission wavelength: it blue shifts as the amount of FA gets higher (Figure 20a). Figure 20b shows the PLQY dependency on the composition: highest PLQY is achieved with composition $FA_{0.9}Cs_{0.1}PbBr_3$. Figure 20c shows PL lifetime with different cation compositions. Figure 20d shows PL as a function of temperature. PL is dependent on temperature, and as temperature gets higher, non-radiative recombination increases, which decreases the PL intensity. Figure 20e shows PL lifetime under continuous illumination, and Figure 20f shows the recovery of PL after continuous illumination. Continuous illumination clearly decreases PL, and PL of mixed cation perovskites decreases slower. In addition, PL of mixed cation perovskites recovers faster and the recovery is more complete.[94]

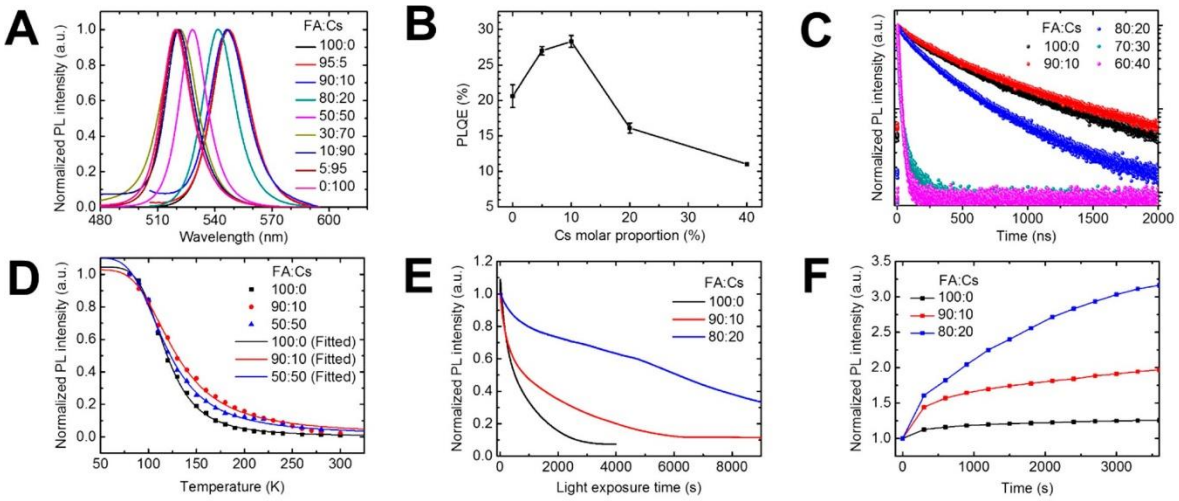

Figure 20. Photoluminescence in PeLED characterization. (A) Normalized PL spectra. (B) PLQY as a function of Cs proportion. (C) PL lifetime, (D) Normalized PL as a function of temperature, (E) PL under continuous illumination, (F) Recovery of PL after the measurement of PL under continuous illumination. Reprinted with permission.[94] © 2018, American Chemical Society.

Electroluminescence (EL) is a phenomenon where a sample emits light when an electric current pass through it. It is the main function of LED, so it is important that it is accurately measured and precisely reported. The EL emission peak is at the bandgap energy just like the PL emission peak. The color of the emission (peak wavelength), its FWHM, and the chromaticity coordinates (x,y) are obtained from EL spectrum. Normalized EL spectra and chromaticity coordinates of $FA_{1-x}Cs_xPbBr_3$ PeLEDs by Cho et al. are presented in Figure 21. In the same way as the emission peak of PL, EL emission peak shifts to blue when the amount of Cs increases.[94]

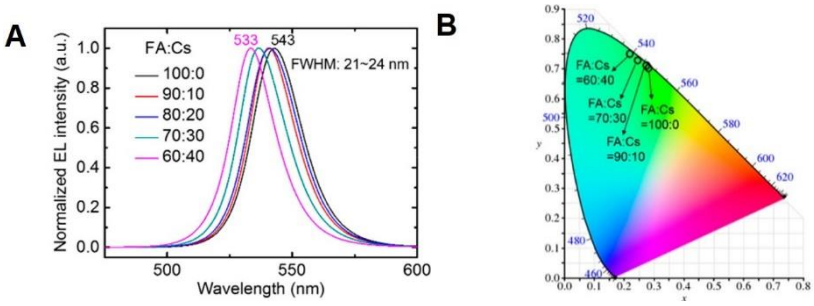

Figure 21. a) Normalized EL spectra of $FA_{1-x}Cs_xPbBr_3$ PeLEDs and b) CIE 1931 chromaticity diagram with the coordinates of the $FA_{1-x}Cs_xPbBr_3$ PeLEDs fabricated by Cho et al. Reprinted with permission.[94] © 2018, American Chemical Society.

There are many factors that affect PL and EL intensity. Excitation power is the most obvious factor, but temperature, atmosphere, and sample storage prior to measurements can also affect the PL and EL intensity and efficiency.[95] In many devices, PL and EL are not equal, and generally PL intensity is higher than EL intensity. One reason for this is a difference in hole and electron injection to the emitting material. In PL, the holes and electrons are created simultaneously when the photon is absorbed, which leads to an equal number of electrons and holes. In EL, depending on the device, there can be a difference in electron and hole injection from the electrodes.[8]

In LED characterization, external quantum efficiency (EQE) is the ratio of photons emitted from the LED to the electron–hole pairs injected into the LED (equation 10).

$$\mathrm{EQE} = \frac{\text{Photons emitted from the LED}}{\text{Electron}-\text{hole pairs injected into the LED}} \tag{10}$$

Photoluminescence quantum efficiency (PLQY) is defined as the ratio of photons emitted to the photons absorbed (equation 11).

$$\mathrm{PLQY} = \frac{\text{Photons emitted}}{\text{Photons absorbed}} \tag{11}$$

Quantum efficiencies are given in percentages.

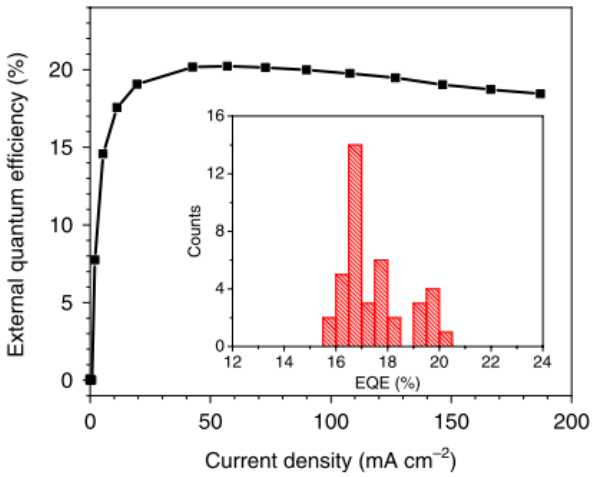

Figure 22. External quantum efficiency as a function of current density for a $FAPbI_3$ baser IR PeLED. Inset: distribution of EQE values of 40 devices. Reprinted with permission.[96] © Springer Nature.

Quantum efficiencies are always dependent on the carrier density, and especially EQE is often reported in a graph as a function of current density, luminance or voltage.[97] An example of a good, steady EQE is shown in Figure 22. EQE reaches its peak 20.2% with a current density of 57 mA cm^{-2} and EQE stays quite steady with higher current densities.[96]

4.1.2 *Radiance and luminance*

The radiant flux means the energy emitted by the LED in watts per meter ($W \cdot m^{-1}$), and it is often used per wavelength. Radiance means the radiant flux by a LED surface per angle and the unit is watts per steradian per square meter ($W \cdot sr^{-1} \cdot m^{-2}$), and it is often used per wavelength. Because the human eye is not evenly sensitive to different colors, luminance is used. Human eye is the most sensitive for light with 555 nm wavelength, and the human eye sensitivity follows the curve in CIE photopic luminosity function (Figure 23) in well-lit conditions. At 555 nm, one watt can generate a maximum of 683 lumen light. The luminosity function is used to calculate luminous efficacy, luminous flux and luminance of a LED.[98]

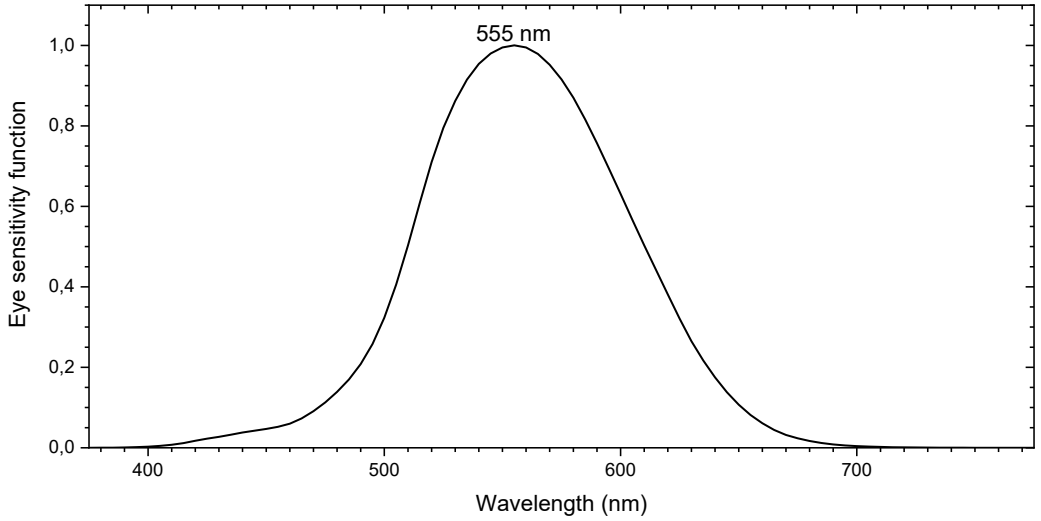

Figure 23. 1978 CIE photopic luminosity function.

Luminous flux is the amount of light that takes into consideration the sensitivity of the human eye. The photopic luminosity function is used to weigh the radiant flux. The ratio of luminous flux to radiant flux is called luminous efficacy, which describes the proportion of visible light from the total emission.[98]

Similar to radiance, luminance is the luminous flux by a LED per angle. The unit of luminance is candela per square meter (cd m^{-2}). Luminous power efficiency ($lm \cdot W^{-1}$) is an

important parameter to compare LEDs and other lighting devices. It gives the amount of luminous flux per input electrical unit power. Increasing luminous efficiency can save energy, since a light with same luminous flux uses less energy.[98] As an example of the magnitude, Finnish lighting company Airam produces a consumer LED that produces 806 lumens with 8 watts, which means a luminous power efficiency of around 100 $lm \cdot W^{-1}$.[99]

In addition, current efficiency (cd A^{-1}) is a widely used parameter. The units based on the luminance are often used with the development of visible-light LEDs, but when the emission is non-visible, e.g., IR light, radiance-based units are used.

Operating luminance of displays is at least 100 cd m^{-2}, and in some applications, a luminance of over 1000 cd m^{-2} is required. LED light bulbs have varying luminance values for different purposes, but a common luminance for interior lighting is around 800 lumens.

A graphical report of the variation of luminance is often used, since it gives a lot of information about the device performance. Cho et al. presented the luminance of their $FA_{1-x}Cs_xPbBr_3$ based PeLEDs as a function of current density (Figure 24a) and the current density as a function of voltage (Figure 24b). When voltage is increased, the current density and the luminance increase.[94]

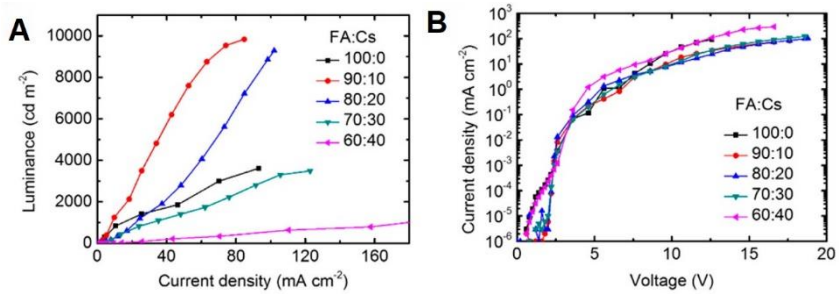

Figure 24. Characterization of $FA_{1-x}Cs_xPbBr_3$ PeLEDs. a) Luminance as a function of current density and b) Current density as a function of voltage. Reprinted with permission[94] © 2020, American Chemical Society.

4.1.3 *Device lifetime and stability*

Device lifetime can be characterized in many different ways, and there is much variety in the characterization. For example, EQE or luminance can be measured over a period of time and plotted as a function of time. The common values for lifetime are T_{50} and T_{95} values,

which is the time it takes that the measured value drops to 50% or 95% of the initial value, respectively. The measurement conditions should be constant and reported. If one study reports a lifetime T_{85} measured under constant current density of 100 mA cm^{-2} and other study reports a lifetime T_{50} measured under constant current density of 10 mA cm^{-2}, it is hard to compare the results.

Some PeLEDs have reportedly had issues with color instability. Color instability can be detected with a continuous EL measurement. Color stability is often related to ion migration and phase separation in mixed halide systems, as is the case in study by Li et al. (Figure 25). $CsPbBr_{1.5}Cl_{1.5}$ perovskite separates to Br- and Cl-rich areas and since $CsPbBr_3$ has lower bandgap energy than $CsPbCl_3$, the bromide-rich areas need less energy to emit light than the chloride-rich areas. Only bromide rich areas emit light, and the emission shifts to longer wavelength.[100] The color stability should also be measured with varying voltage to make sure that the emission wavelength is constant under a wide voltage range.[97]

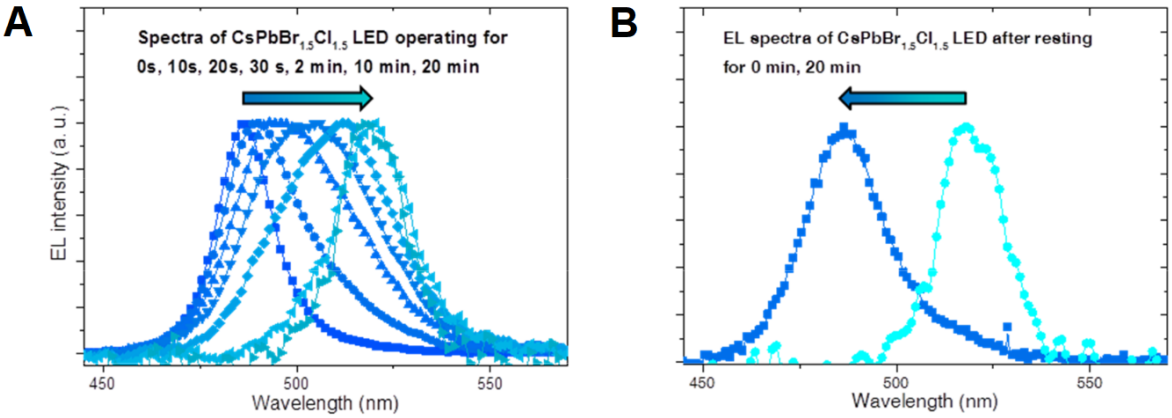

Figure 25. Evolution of EL spectra of $CsPbBr_{1.5}Cl_{1.5}$ based LED (A) operated at 5.5 V and (B) after resting. Reprinted with permission.[100] © 2016, WILEY-VCH Verlag GmbH & Co. KGaA, Weinheim.

51 institutions released a consensus for the stability assessment of PSCs in January 2020.[101] It is based on the International Summit on Organic Photovoltaic Stability protocols, with additional processes that take into account perovskite properties, such as ion migration. They state that it is hard to compare the results from different publications if the test conditions are different and the reported parameters are inconsistent, and they think that unified stability testing protocol would be important for the research community. The stability protocols include dark storage testing, outdoor testing, light soaking testing, thermal cycling testing

and light-humidity-thermal cycling testing. No such recommendation is yet available for PeLEDs.

In addition to operational stability, shelf stability is also important: the PeLED device should not degrade upon storage. BAI:$MAPbI_3$ based PeLEDs by Xiao et al. did not degrade for 8 months in N_2 atmosphere.[62] It is a good start, but obviously PeLEDs need to be stable in air for even longer times in order to enable large scale production and usage.

To the best of my knowledge, the most stable PeLEDs were made by Wang et al. in 2020. The IR-LEDs had $FAPbI_3$ nanocrystals embedded in molecule 4,4'-diaminodiphenyl sulfone (DDS) and had a lifetime T_{50} of 100 hours. The T_{50} was defined as the time when the EQE drops to 50% of the initial value and it was measured at a constant current density of 20 mA cm^{-2}. Furthermore, the LED also had a moderately high efficiency, with 17.3% EQE.[102]

PeLED stability is discussed in more detail in section 5.1.

4.1.4 *Hysteresis*

Hysteresis is a characteristic of a system where the system does not fully return to its initial state after it has been under stress. It can be said that the system is dependent on its history. In LEDs, hysteresis can mean that depending on scan rate and scan direction, some values, e.g., EQE, luminance, and radiance measurements can have different values. Tan et al. reported hysteretic behavior in the first room-temperature PeLED. A forward–reverse bias scan gives higher EQE and radiance than reverse–forward bias scan.[2]

Hysteresis is a common problem in perovskite devices. PeLEDs suffer from hysteresis, and it can lead to incorrect results in device characterization. The PeLED hysteresis has not been thoroughly studied, but it is thought to be related to ion migration and vacancies in the perovskite.[62]

Xiao et al. studied BAX:$MAPbX_3$ devices with X = I^-, Br^- and various BAX:$MAPbX_3$ ratios. They used various scanning rates and directions to study hysteresis in their devices. Their most efficient devices with both halides had the BAX:$MAPbX_3$ molar ratio of 20:100, showing also reduced hysteresis compared to the devices without BAX, and being less dependent on the scanning rate. Based on their characterizations they think that $MAPbX_3$

forms small grains, BAX forms a thin layer on top of $MAPbX_3$ grains and fills grain boundaries, which leads to a better performance. Since the PeLED hysteresis is associated with ion migration that happens at grain boundaries, they conclude that the passivation of grain boundaries with BAX leads to suppressed hysteresis.[62]

Cho et al. studied the effect of temperature on the hysteresis of $CsPbBr_3$ based PeLEDs. The hysteresis area, which is the area between the forward and reverse scan curves, increases exponentially as temperature increases. This is explained by temperature-dependence of ion migration. Their IV-measurements are shown in Figure 26.[103]

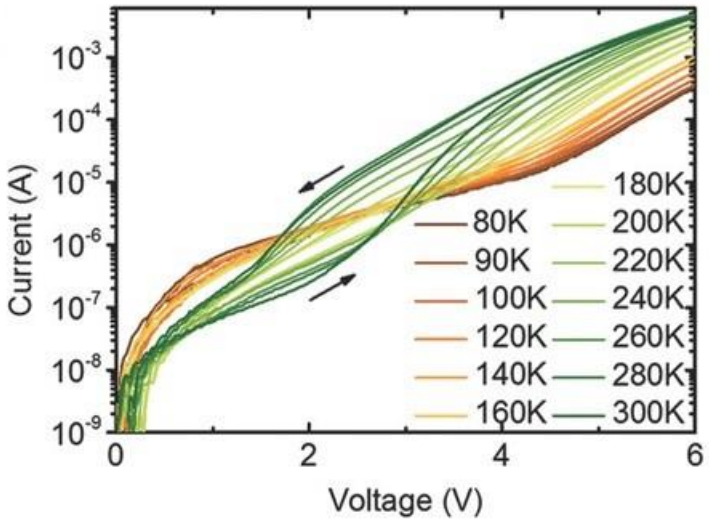

Figure 26. Current-voltage hysteresis of CsPbBr3 based LED with varying temperature. Reprinted with permission.[103] © 2017 WILEY-VCH Verlag GmbH & Co. KGaA, Weinheim

4.2 Characterization of perovskite layer

Most perovskite layers are solution processed. As a study by Fassi et al. highlights, tiny changes in perovskite precursor solution stoichiometry can lead to big changes in film morphology, and film morphology affects device performance.[104] It is important to characterize the perovskite layer and its interfaces with adjacent layers thoroughly. The most common methods used are shortly introduced here as background information for chapter 5. The methods introduced here are electron microscopy, x-ray diffraction (XRD), x-ray photoelectron spectroscopy (XPS) and Optical absorption spectroscopy, also known as ultraviolet-visible (UV-vis) absorption spectroscopy. Other methods are also used, e.g.

nuclear magnetic resonance spectroscopy (NMR)[105], solid-state NMR[48], atomic force microscopy (AFM)[60,61,106,107], IR spectroscopy[105,108,109], and secondary-ion mass spectrometry (SIMS)[107]. With every method, it is possible to get different kind of information from the sample, and it is important to confirm the interpretations and results with multiple methods.

4.2.1 *Electron microscopy*

The wavelength of visible light restricts the resolution of optical microscopes to roughly 200 nm. Instead of optical light source, electron microscopes use an electron beam. When the electron beam hits the sample, electrons can interact with the sample in multiple ways. If the sample is thin enough (<100 nm), electrons can transmit through it, and transmitted electrons can be used in transmission electron microscopy (TEM). Electrons can also scatter from the sample, generate secondary electrons, and generate Auger electrons. Backscattered and secondary electrons are used in scanning electron microscopes (SEM), Auger electrons are used in a different instrument called Auger electron spectroscope. In addition to electrons, an electron beam can generate x-ray from the sample, and many SEM and TEM instruments are equipped with electron dispersive x-ray (EDX) detector. A portion of electrons also get absorbed in the sample. A graphical illustration of electron beam interaction with a sample is shown in Figure 27.

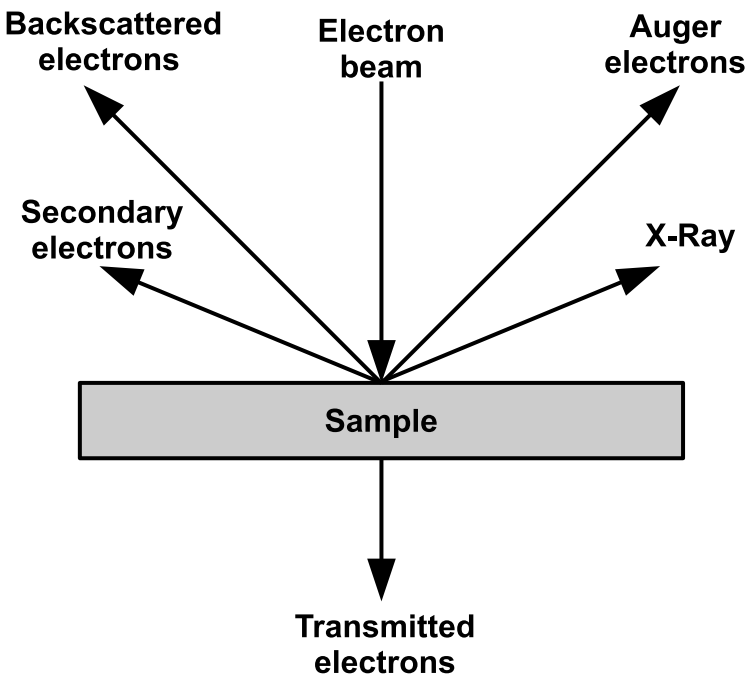

Figure 27. Interactions of electron beam in the sample. Secondary electrons, backscattered electrons and x-ray are used in SEM, Transmitted electrons and x-rays are used in TEM. Redrawn from reference.[110]

SEM is a widely used tool for characterization. It is possible to get nanoscale imaging of the sample surface. In perovskite research, it is often used to study the morphology and particle size of the sample. A cross-sectional image can be used to measure layer thicknesses and to study the interfaces between layers. SEM takes a 2D image of the sample, and it cannot be used to quantitatively determine the surface roughness. Since SEM is widely available, fast, and nondestructive, it is used in majority of perovskite research.

Transmission electron microscopy (TEM) can get to the scale of 0.1 nm, which is small enough to see the lattice planes in a crystal structure, as can be seen in Figure 28. Figure 28a shows multiple nanocrystals of a $CsPbBr_3$ sample. Figure 28b shows a more magnified image of one nanocrystal, where the lattice constant is detected from the lattice fringe. TEM is not as widely used as SEM, since the instruments are much more expensive, and the measurements are more time consuming.

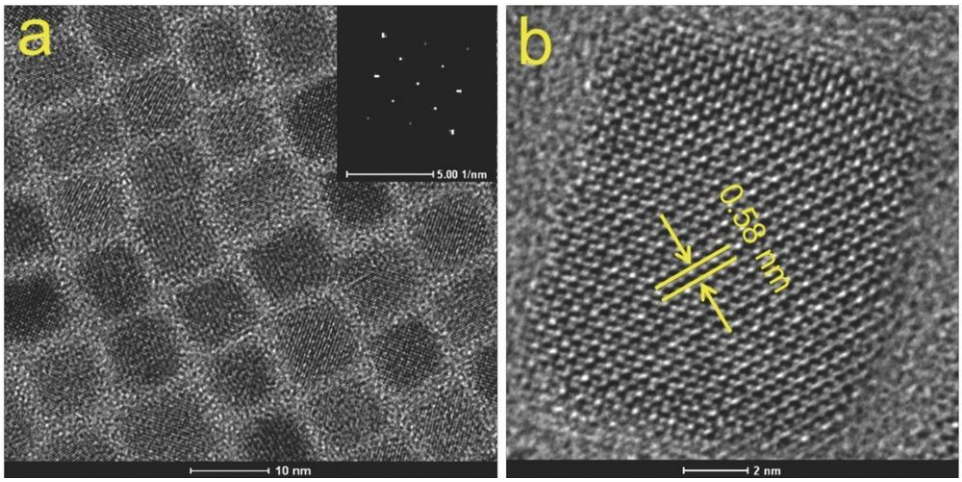

Figure 28. TEM images of $CsPbBr_3$ nanoparticles. (a) scale bar is 10 nm and inset shows selected area electron diffraction. (b) Scale bar is 2 nm. Reprinted with permission.[73] © 2015 WILEY-VCH Verlag GmbH & Co. KGaA, Weinheim

SEM and TEM can be used for elemental mapping based on EDX.[107] Elemental mapping can be used to evaluate how different elements are distributed in the perovskite layer, and to gain information about the ratio of different elements. It can be used to study ion migration in perovskite layer and the whole device. Elemental mapping of EDX is shown in Figure 29[111] and the usage of EDX to determine the elemental ratio is introduced in chapter 4.2.5.

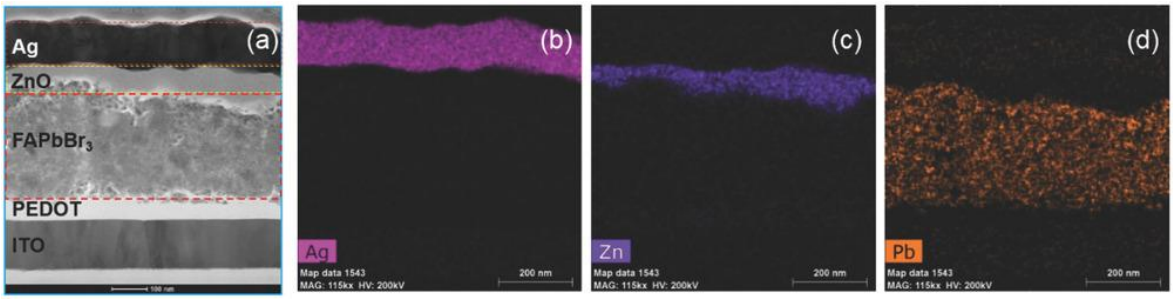

Figure 29. a) Cross sectional TEM image of a PeLED. EDX elemental mapping of b) Ag, c) Zn, and d) Pb. Reprinted with permission.[111] © 2018 WILEY-VCH Verlag GmbH & Co. KGaA, Weinheim

4.2.2 *Optical absorption spectroscopy*

Absorption of UV and visible light can be used to get qualitative information about the materials. The absorbance correlates with the PL and EL peaks, as can be seen in Figure 30. The absorbance spectra have a sharp edge near the PL peak, and absorb emission with shorter wavelengths than the PL peak.

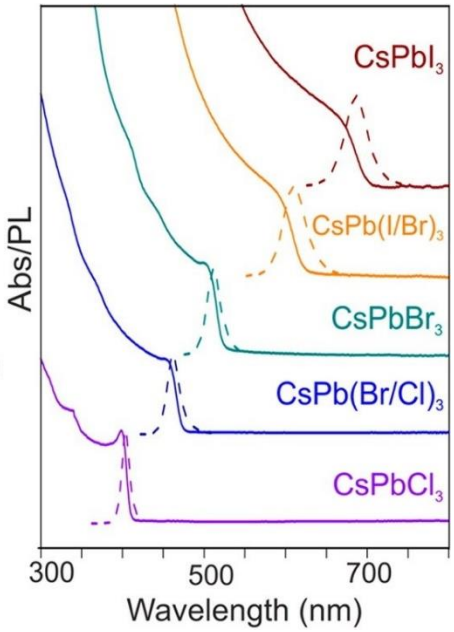

Figure 30. Absorbance (solid line) and photoluminescence (dashed line) of $CsPbX_3$ perovskites. Reprinted with permission.[71] © 2015, American Chemical Society.

Absorption spectroscopy is also a good tool to get information of quasi-2D structures, as seen in Figure 31. The sample prepared with only MABr and $PbBr_2$ as precursors (<n>=∞) has only one peak around 530, and the sample prepared with only PEABr and $PbBr_2$ (<n>=1) has only one peak around 400 nm. The other samples were prepared with a mixture of MABr, PEABr and $PbBr_2$ (<n> between 2 and 5), and there are multiple peaks in their absorbance spectra, since the samples contain multiple phases with different values of x ($PEA_2MA_{x-1}Pb_xBr_{3x+1}$.

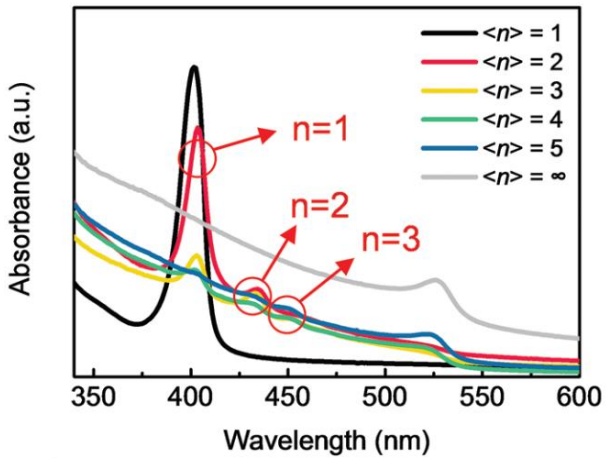

Figure 31. Absorption spectra of $PEA_2MA_{x-1}Pb_xBr_{3x+1}$ perovskite films with x=1–5 and ∞. Reprinted with permission.[47] © 2019, WILEY-VCH Verlag GmbH & Co. KGaA, Weinheim

4.2.3 *X-ray diffraction*

X-ray diffraction (XRD) can be used to study perovskites. XRD can be measured from a powder, a thin-film, or a single-crystal. It is a nondestructive method, and it is a very commonly used to characterize perovskites. XRD can give a lot of information of the sample, and a few useful cases are introduced in this section.

In XRD, the diffraction of an x-ray radiation from the sample is used to characterize the material. XRD is based on Bragg's law (equation 12)

$$n\lambda = 2d\sin(\theta) \tag{12}$$

where n is an integer, λ is the wavelength of the x-ray radiation, d is the lattice spacing. A common x-ray in XRD is Cu Kα with wavelength $\lambda = 1.5418$ Å.

XRD is used to identify the composition and structure of the materials by comparing with standard diffraction files from databases, such as International Centre for Diffraction Data. It can be used to estimate the purity of the perovskite. If no peaks of impurities are detected, it can be concluded that the impurity is less than 0.5 wt% or smaller than the detection limit of the diffractometer. It can also be used to detect the different phases of the same material. As an example, the perovskite and non-perovskite phases of $FAPbI_3$ diffract the x-rays differently, resulting in a distinct XRD patterns.[112]

An example of XRD pattern is shown in Figure 32. The peaks of $FAPbBr_3$ are at 14.84°, 21.04°, 29.88° and 33.54°, and they correspond with (100), (110), (200), and (210) Miller indices. As the amount of Cs increases, the peaks shift slightly towards higher 2θ values, since Cs is smaller than FA, and when the amount of Cs increases, the lattice constant decreases. The lattice constant of $FA_{1-x}Cs_x$ roughly follows Vegard's law. With Cs content higher than 20%, an additional peak at 12.5° appears, and it is assigned to $PbBr_2$ impurity.[94]

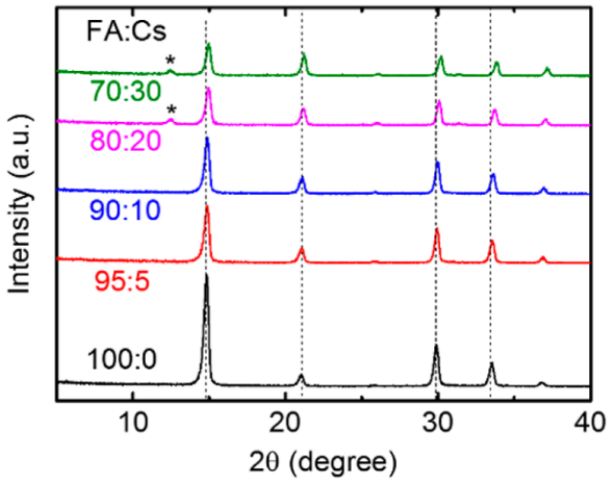

Figure 32. XRD pattern of $FA_{1-x}Cs_xPbBr_3$ thin film samples with various FA:Cs ratios. Reprinted with permission.[94] © 2018, American Chemical Society.

The measurement depth of XRD depends on the sample, but it can be up to tens of micrometers. This means that XRD gives information about the bulk of the material, and together with a surface analytical method such as XPS, it can be used to find out if the bulk and surface have different properties.

4.2.4 *X-ray photoelectron spectroscopy*

X-ray photoelectron spectroscopy (XPS) also uses x-ray as the source, but the detector detects photoelectrons instead of x-ray radiation. The surface of the sample is irradiated with x-rays, and the energy of the x-ray radiation can release an electron from the sample. The electron energy is measured, and it is possible to detect the element, but also its chemical state. The data is reported with a spectrum that has photoelectron energy (eV) on x-axis, and the count of electrons (a.u.) on y-axis. A typical XPS spectra of a $MAPbI_3$ is presented in Figure 33.[113]

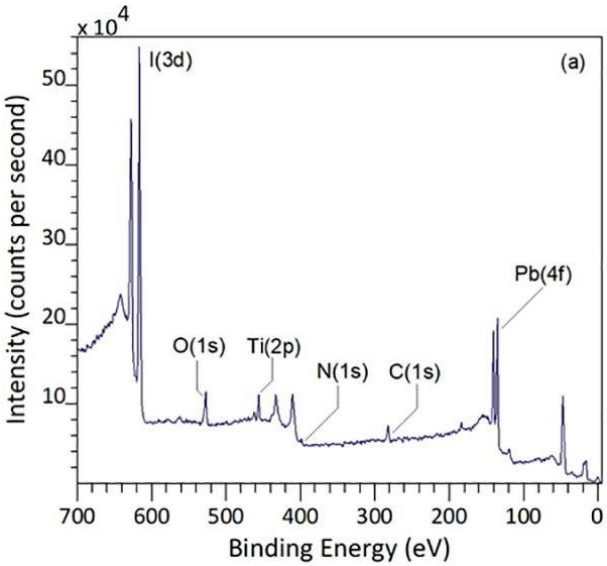

Figure 33. XPS spectrum of a $MAPbI_3$ film on TiO_2. Titanium and oxide are detected since the surface coverage of the perovskite is not complete. Reprinted with permission.[113] © 2019, Elsevier B.V.

Figure 34 shows XPS spectra from a study by Akbulatov et al. The spectra were measured from a sample of $FAPbBr_3$ before and after aging, and from a $PbBr_2$ sample. The decomposition of $FAPbBr_3$ sample cannot easily be detected from the Br $3d_{5/2}$ peaks since the binding energy of the bromine in $FAPbBr_3$ and $PbBr_2$ overlap, but decomposition can be clearly seen from the Pb $4f_{7/2}$ peak.[114]

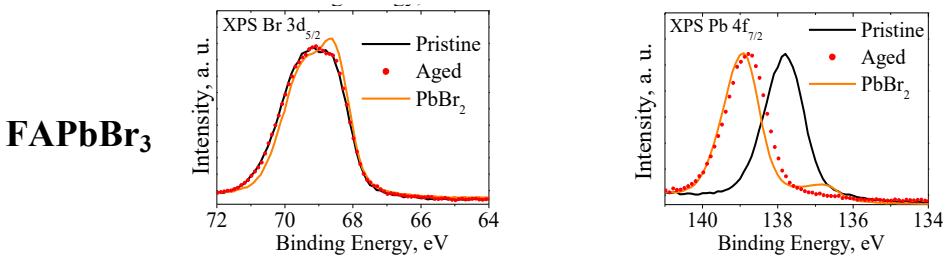

Figure 34. XPS spectra of $FAPbBr_3$ and $PbBr_2$ at 64–72 eV and 134–142 eV. Reprinted with permission.[114] © 2020, Elsevier B.V.

XPS is a surface analytical method, and the photoelectrons escape only from a thin, around 10 nanometers thick layer of the surface of the sample. XPS can be used to determine the composition of a thin layer in the top of the sample, and together with a bulk method, such as XRD, it is possible to compare bulk and surface decomposition of the sample.

4.2.5 *Research example: Thermal decomposition of perovskites*

Akbulatov et al. characterized the thermal decomposition of various perovskites in 2020.[114] Their main tools for characterization were SEM, UV-vis absorbance, XRD, XPS, AFM and mass spectrometry. AFM was used to characterize the morphology of perovskite surfaces and mass spectrometry was used to characterize the volatile degradation compounds. SEM, XRD, XPS and UV-vis absorbance are used to characterize the changes in the film. They use a large variety of methods to confirm their results, and e.g., the usage of XRD together with XPS can reveal whether the decomposition happens on the surface, in the bulk or both.

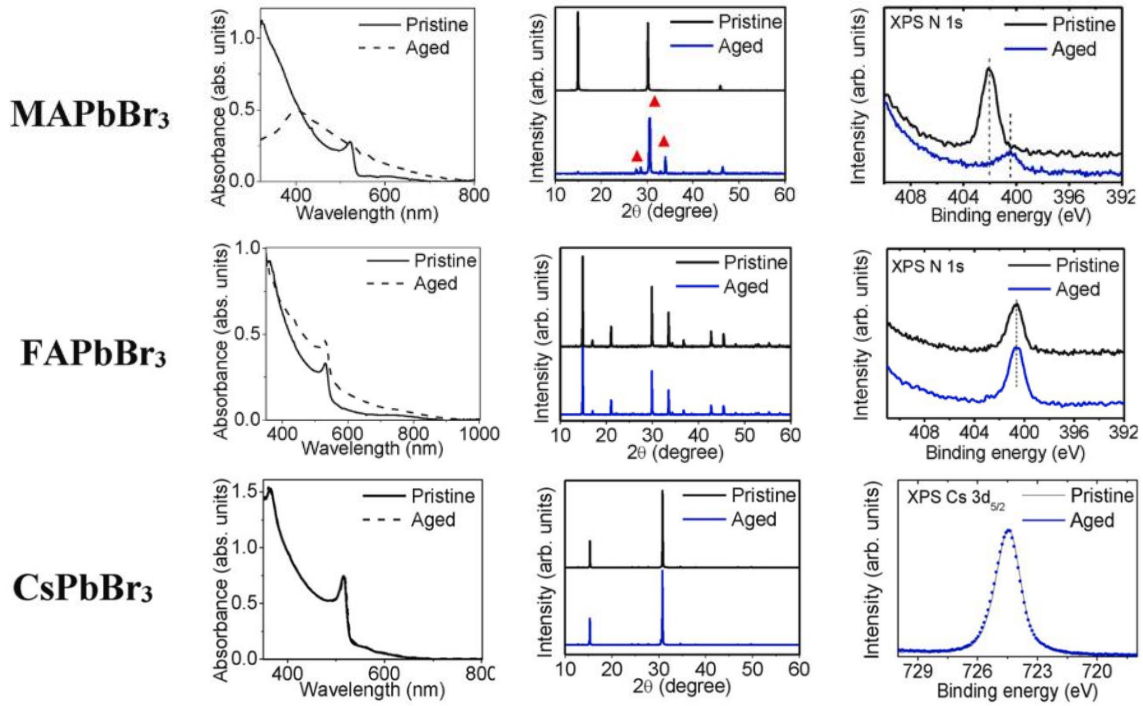

Figure 35. UV-vis absorbance (left), XRD-patterns (middle) and XPS-spectra (right) for $MAPbBr_3$, $FAPbBr_3$ and $CsPbBr_3$ before and after annealing. Reprinted with permission.[114] © 2020, Elsevier B.V.

UV-vis absorption spectra, XRD-pattern and XPS spectra of $MAPbBr_3$, $FAPbBr_3$ and $CsPbBr_3$ before and after aging are shown in Figure 35. It can be clearly seen that the absorbance peak of $MAPbBr_3$ disappears, the absorbance of $FAPbBr_3$ gets stronger, and that the absorbance of $CsPbBr_3$ does not change. The absorbance of $FAPbBr_3$ probably increases because of light scattering in the aged sample. In the XRD-patterns of $MAPbBr_3$, aged sample has new peaks, and the peaks of pristine sample disappear. The peaks marked with red triangle are assigned to $PbBr_2$, which is a decomposition product of $MAPbBr_3$. In the XRD-patterns of $FAPbBr_3$ and $CsPbBr_3$ no peaks appear nor disappear. In the XPS spectrum

of $MAPbBr_3$, the high peak at around 402 eV corresponds to the 1s electron of the nitrogen atom in MA, and it disappears during the aging. In the XPS spectrum of $FAPbBr_3$, the peak at around 401 eV corresponds to the 1s electron of nitrogen in FA, and the peak show no change after aging. $CsPbBr_3$ does not contain nitrogen, so the peak of Cs $3d_{5/2}$ is used instead. There is also no change in the XPS spectrum of $CsPbBr_3$.

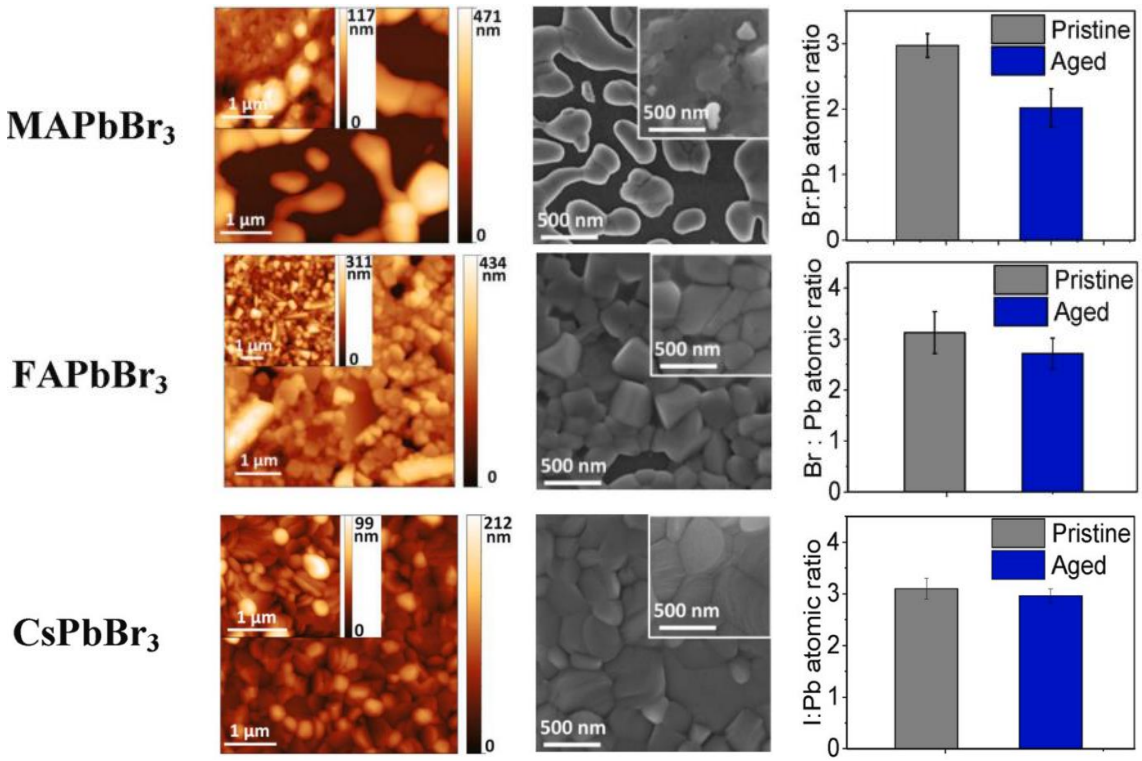

Figure 36. AFM images (left), SEM images (middle) and SEM-EDX data (right) from $MAPbBr_3$, $FAPbBr_3$ and $CsPbBr_3$ samples before and after annealing. Insets in AFM and SEM images are before annealing. Reprinted with permission.[114] © 2020, Elsevier B.V.

In addition, the samples were characterized with SEM, AFM and SEM-EDX (Figure 36). AFM and SEM images show clear changes in $MAPbBr_3$ layer morphology, small changes in $FAPbBr_3$, and no changes in $CsPbBr_3$. The Br:Pb ratios from SEM-EDX analysis support the findings from absorbance, XRD and XPS studies: the ratio of Br and Pb atoms in pristine $MAPbBr_3$ is 3, and the ratio drops to 2 after aging, which is the Br:Pb ratio in the decomposition product, $PbBr_2$. The other decomposition products are volatile, and are not present in the perovskite anymore. The Br:Pb ratio of $FAPbBr_3$ drops slightly, which indicates that only a part of $FAPbBr_3$ decomposed. The Br:Pb ratio of $CsPbBr_3$ seems to drops slightly, but the drop is so small that the change is inside the tolerance limit. Other methods confirm, that $CsPbBr_3$ did not degrade under these conditions.

5 CHALLENGES

PeLED technology has been intensely studied only for a short period of time, and most of the research has been done in laboratory scale. In technology readiness level (TRL), PeLED fabrication is currently between levels 3 and 4 out of 9. The concept of PeLED fabrication is proven, and the technology is validated in laboratory scale, but not yet in relevant environment.[115] The long-term goal is mass production of PeLEDs for various applications, but there is still a lot of work to be done. In this thesis, stability, efficiency, and challenges related to environment and health are discussed.

5.1 Stability challenges and perovskite degradation

Since PeLEDs are a relatively new field of research, there is not yet much research on the stability of PeLED devices. Similar perovskite materials are used in PSCs, and the PSCs are facing similar stability issues. Some of the research referenced in this chapter studied the properties of perovskites in PSCs, but the results apply, at least partly, to PeLEDs. In some cases, the cause of degradation is known, but the mechanisms remain undiscovered. Some degradation mechanisms only apply to specific perovskites.

To some extent, the stability can be enhanced with encapsulation, but encapsulation is not discussed in this thesis. Even if the LED is properly encapsulated, the perovskite material needs to be intrinsically stable, and PeLEDs should be functional over varying circumstances, e.g., a large temperature range.

There are also challenges with stability of other layers, e.g., charge transport layer [6,6]-phenyl-C61-burytic acid methyl ester (PCBM) is sensitive to oxygen and water. Stability of other layers is discussed here only if it is related to perovskite stability, i.e., usage of some other layer affects stability of perovskite.

In all applications, the degradation of the perovskite is a sum of many variables, but it is important to study how different things affect the perovskite. In this thesis, most common degradation methods and their prevention is discussed in section 5.1.1. Other general strategies to increase stability are discussed in section 5.1.2. Strategies to improve stability are summarized in section 5.1.3.

5.1.1 *Causes of degradation*

MA was the most common A-site cation for a long time and iodine is the most common halide in PSCs. The stability of MA-based perovskites, especially $MAPbI_3$, have been most widely studied. There are some studies about perovskites with FA and Cs cations, but degradation of other perovskite compositions, such as mixed-cation structures or 2D/3D perovskites, has not been studied as thoroughly.

Different perovskite compositions face different kinds of stability challenges. For example, some degradation compounds of perovskites with organic A-site cations are volatile, whereas the analogous degradation compounds of Cs-based perovskites are non-volatile. As another example, some perovskite compositions can also form non-perovskite phases in operation temperature, which can cause problems.

It seems that when the most severe degradation methods are eliminated, some other degradation methods become dominant. For example, early $MAPbI_3$-based PSCs had a device lifetime of a few hours, and as Senocrate et al. stated, from a thermodynamics point of view, the most severe causes for degradation of $MAPbX_3$ perovskites are moisture and oxygen.[116] With encapsulation, moisture and oxygen induced degradation can be greatly reduced, and the device lifetime can be increased. When the moisture and oxygen induced degradation is prevented, it is easier to study other degradation mechanisms. Some degradation methods are harder to eliminate: the intrinsic instability of the perovskite material can be hard to eliminate without substitution or doping, and since a LED needs to be able to emit light, exposure to light cannot be prevented, and photostability can be an issue. There is no section for light-induced degradation, but the effect of illumination is discussed in sections 5.1.1.3 and 5.1.1.5.

The degradation of a bare perovskite layer and a perovskite layer in a device can be different. If the degradation releases gaseous compounds, the gases get trapped inside the device and can hasten or alter the degradation.[117] On the other hand, if the gaseous compounds can escape the device, the perovskite layer would slowly wear out and only the non-volatile species such as PbI_2 would remain.

5.1.1.1 Thermal stability of perovskites

There are dissenting opinions about thermal stability of $MAPbX_3$. Calorimetric measurements indicate that stability increases in the order of Cl>Br>I, and that both $MAPbI_3$ and $MAPbBr_3$ would be unstable in room temperature even without being exposed to light, water, or oxygen.[118] On the other hand, Senocrate et al. think that there are solvent–precursor and precursor–precursor interactions that need to be taken into account, and thus the calorimetric measurements cannot be directly applied.[116] Either way, even if $MAPbX_3$ perovskites are thermally stable in room temperature, PeLEDs need to be stable also in elevated and lowered temperatures.

Akbulatov et al. studied the thermal stability of a series of lead perovskites with three A-site cations (MA^+, FA^+, and Cs^+) and two halides (Br^- and I^-). The perovskites were stored in nitrogen atmosphere at 90 °C for 20 hours. The chamber was dark and O_2 and H_2O levels were less than 0.1 ppm, to eliminate effects caused by light, moisture, and oxygen. Thermal stability increases in the order $MAPbX_3$<<$FAPbX_3$<$CsPbX_3$, which also correlates with the volatility of MAX>>FAX>CsX. SEM-EDX data shows that the halogen to lead ratio decreases from 3 to around 2 for $MAPbI_3$ and $MAPbBr_3$, but it drops only a little for $FAPbI_3$ and $FAPbBr_3$. This indicates that $MAPbX_3$ perovskites degraded almost completely to PbX_2 and volatile compounds, and $FAPbX_3$ perovskites degraded only partly. $CsPbX_3$ perovskites do not form volatile compounds, and no change in the Br:Pb ratio was observed. To confirm the decomposition compounds, they heated the perovskites to 200–300 °C and examined the volatile compounds with mass spectrometry. They propose equation (13) as a general reaction for $APbX_3$ perovskites, equation (14) as the thermal degradation of MAI and reactions presented in Figure 37 as the degradation of FAI.[114]

$$\begin{aligned} APbX_3 &\rightleftharpoons PbX_2 + AX \\ AX &\rightarrow \text{Volatiles} \end{aligned} \tag{13}$$

$$\begin{aligned} CH_3NH_3I &\rightleftharpoons CH_3I + NH_3 \\ CH_3I &\rightleftharpoons :CH_2 + HI \\ :CH_2 &\rightarrow CH_2 = CH_2 \\ CH_3I + HI &\rightleftharpoons CH_4 + I_2 \end{aligned} \tag{14}$$

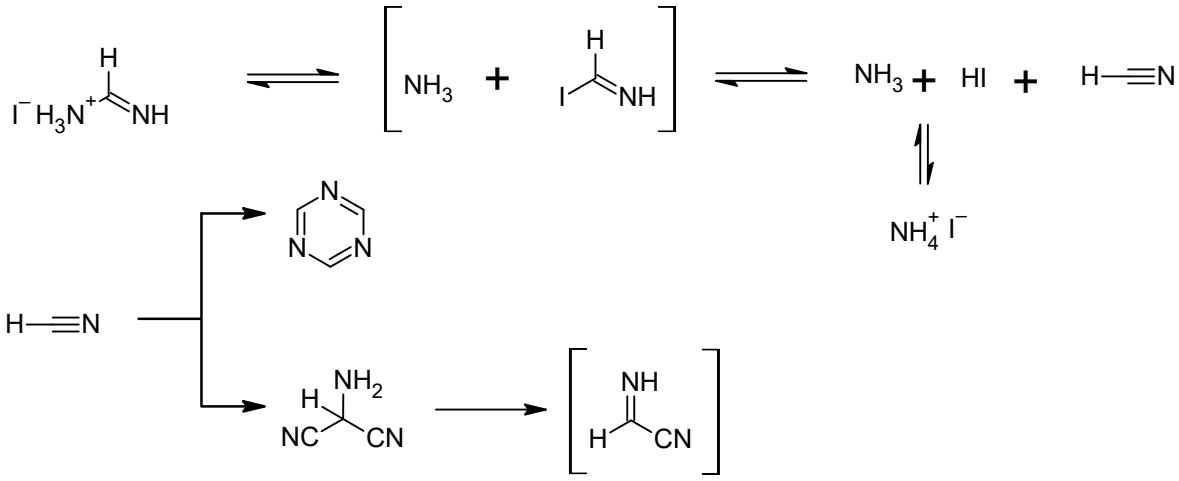

Figure 37. The proposed reactions of thermal degradation of FAI.[114]

Akbulatov et al. also found that the mass spectrum of ABX_3 decomposition has the same peaks as the decomposition of corresponding AX ($MAPbI_3$ and MAI, $FAPbI_3$ and FAI). This further proves that ABX_3 with organic A-site cation first degrades to PbX_2 and AX, and AX further decomposes. It should be noted that these compounds formed when perovskites were heated to 200–300 °C, and it is likely that the degradation compounds and/or their ratio are different when the degradation happens in room temperature. Juarez-Perez et al. reported that the volatile compounds detected are different in room temperature and 300 °C. In room temperature $MAPbI_3$ degradation resembles the equation (15) instead of equation (14). For $MAPbBr_3$, degradation in room temperature follows equation (16), whereas in 300 °C the degradation follows equation (17).[119]

$$MAPbI_3 \rightarrow PbI_2 + Pb^0 + I_2 + CH_3NH_2 + CH_3I + HI + NH_3 \quad (15)$$

$$MAPbBr_3 \rightarrow CH_3NH_2 + HBr \quad (16)$$

$$MAPbBr_3 \rightarrow NH_3 + CH_3Br \quad (17)$$

Akbulatov et al. studied bare perovskites, and it is possible that a perovskite in a device, sandwiched between other layers and encapsulated, would degrade in a different way. Their XPS and XRD studies are mostly consistent, so it is not possible to make conclusions if the degradation starts from the surface, bulk, or both. The only inconsistency is with $FAPbBr_3$: Pb 4f XPS spectra shows signs of degradation, but the XRD pattern does not. This indicates that decomposition happens on a thin layer on the sample's surface, but not in the bulk.[114] Fan et al. studied thermal decomposition of $MAPbI_3$ in situ with TEM, and found that the

degradation of $MAPbI_3$ starts from the surface of $MAPbI_3$ and the perovskite degrades layer-by-layer, meaning that it is possible to slow down or eliminate the degradation by protecting the perovskite surface.[120]

Lin et al. studied the thermal stability of $MAPbI_3$ and corresponding 2D/3D perovskite structures. They tested spin coating a solution of BA in chlorobenzene and BAI in isopropanol on a $MAPbI_3$ layer, and found that the methods resulted in different reactions (equations 18 and 19).[68]

$$2BA + MAI + MAPbI_3 \rightarrow BA_2PbI_4 + 2MA \uparrow \quad (18)$$

$$2BAI + nMAPbI_3 \rightarrow BA_2MA_{n-1}Pb_nI_{3n+1} + MAI \quad (19)$$

After the BA treatment only a BA_2PbI_4 layer (n=1) was discovered in XRD pattern, but after treatment with BAI, layers with n=1, 2, 3 and 4 were discovered. Both treatments increased the solar cell performance and thermal stability. According to their conclusions, the 2D and 2D/3D perovskites fill grain boundaries and cover the surface of $MAPbI_3$ perovskite, which greatly reduces degradation of $MAPbI_3$ that starts from the surfaces.[68] This is also supported by the results of Sutanto et al. They studied the effect of 2D perovskite on thermal stability. They coated a triple A-site cation mixed-halide perovskite $FA_{0.8}MA_{0.12}Cs_{0.08}Pb(I_{0.88}Br_{0.12})_3$ with a thin 2D perovskite layer and annealed the samples in 50 °C. They used two 2D perovskites, PEA and 2-thiophenemethylamine. When heated, only the 2D layer changes its structure, while the 3D perovskite is protected and shows no signs of degradation. The 2D layer transforms into a mixed phase which does not decrease device performance.[51]

Quan et al. found that the stability of $PEA_2MA_{n-1}Pb_nI_{3n+1}$ perovskites compared to $MAPbI_3$ is increased because of the higher van der Waals interactions. They found that the energy needed to remove PEAI from the surface of perovskite is 0.91 eV, which is only 0.55 eV for MAI. In their theoretical calculations, the values were independent of the amount of layers n. In the experimental test of PSC stability, the PSCs with n=10, n=40 and n=60 all had superior stability compared to the 3D perovskite with n=∞.[49]

5.1.1.2 Phase transitions of perovskites

A perovskite LED should be stable within a large temperature range to extend usability in different applications. Common perovskite materials undergo phase transitions, which can restrict their usability. Phase transition temperatures of some common perovskites are listed in Table 3. Generally, perovskites have a cubic phase in high temperature, and when temperature is lowered, they undergo a phase transition from cubic to tetragonal to orthorhombic phases. The common perovskite $MAPbI_3$ is in cubic phase in high temperatures and transits to a tetragonal phase in 327 K and to orthorhombic phase in 162 K. Temperatures higher than 327 K are often used in the preparation of the perovskite layer and other layers of the LED device, which means that the perovskite undergoes phase transitions during the preparation. Even though cubic and tetragonal phases are both photoactive and the difference in the structure is small, continuous phase transitions can affect the structure's stability and leave the device under strain.

Table 3. Phase transition temperatures of selected perovskites

Perovskite	Non-perovskite phase	Low symmetry phase	Mid symmetry phase	High symmetry phase	Ref.
Structure	Orthorhombic or hexagonal	Orthorhombic or tetragonal	Tetragonal	Cubic	
$MAPbI_3$		<162 K	162–327 K	>327 K	[112,121]
$FAPbI_3$	<438 K	<140 K	140–285 K	>285 K	[122,123]
$CsPbI_3$	<588 K			>588 K	[122]
$MAPbBr_3$	<145 K	150–155 K	155–237 K	>237 K	[121]
$FAPbBr_3$		<125 K	150–250 K	>275 K	[124]
$CsPbBr_3$		<361 K	361–403 K	>403 K	[125]
$MAPbCl_3$		<173 K	173–179 K	>179 K	[121]

As can be seen in Table 3, $FAPbI_3$ and $CsPbI_3$ have non-perovskite phases in room temperature. $CsPbI_3$ turns from non-perovskite phase to a cubic perovskite phase at 588 K (315 °C), and slowly converts back to non-perovskite phase when cooled to room temperature. Similarly, the non-perovskite perovskite transition of $FAPbI_3$ happens at 438 K (165 °C).[122] The phase transitions start from the grain boundaries.[126] The structures of $FAPbI_3$ and $CsPbI_3$ phases are shown in Figure 38.

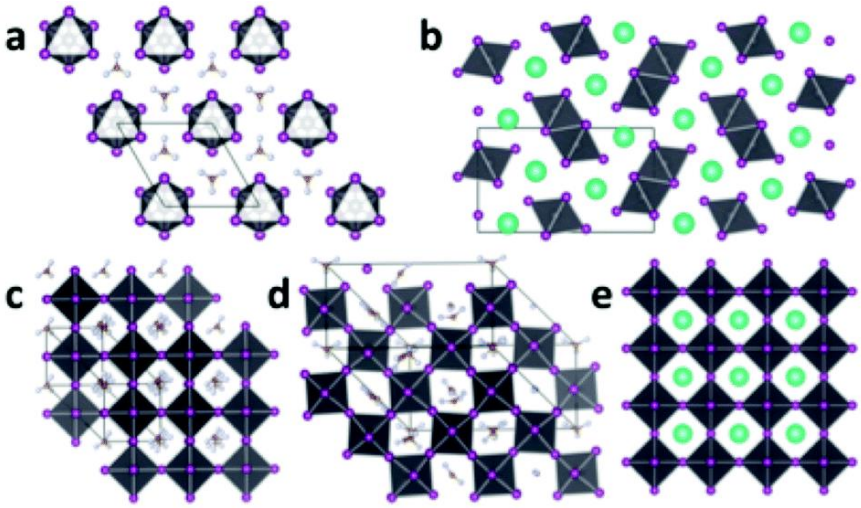

Figure 38. Various phases of $FAPbI_3$ and $CsPbI_3$. a) Hexagonal non-perovskite phase of $FAPbI_3$, b) orthorhombic non-perovskite phase of $CsPbI_3$, c) cubic phase of $FAPbI_3$, d) tetragonal phase of $FAPbI_3$, e) cubic phase of $CsPbI_3$. Reprinted with permission.[127] © 2015, Royal Society of Chemistry

However, when a small part of FA is substituted with Cs or vice versa, the transition temperature can be lowered, and perovskite phase can be stable even in room temperature. The transition temperatures of $FA_{0.85}Cs_{0.15}PbI_3$ and $FA_{0.3}Cs_{0.7}PbI_3$ are dropped to 125 °C (398 K) and 160 °C (433 K) respectively. For $FA_{0.85}Cs_{0.15}PbI_3$ compared to pure $FAPbI_3$, the phase stability was increased and thermal degradation was reduced.[122] In addition, perovskite phases of $FAPbI_3$ and $CsPbI_3$ have similar structure and volume per stoichiometric unit ($FAPbI_3$ 256 Å, $CsPbI_3$ 250 Å), whereas non-perovskite phases have very different structure (Figure 38a–b) and volume ($FAPbI_3$ 256 Å and $CsPbI_3$ 222 Å). A large mismatch in structure can make phase mixing unfavorable.[127] The composition engineering can be taken even further: Saliba et al. made a series of triple A-site cation mixed-halide perovskite $Cs_x(MA_{0.17}FA_{0.83})_{(1-x)}Pb(I_{0.83}Br_{0.17})_3$ and used them in PSCs. MA increases the stability of the photoactive α-phase of FA, and even a small amount of cesium (x=0.05) increased the solar cell performance and the device lifetime. The addition of bromide further increases the stability.[128]

Even though the phase transition is reversible, it may not be possible without material degradation. Yun et al. stored $FAPbI_3$ samples in 150 °C in N_2 atmosphere and in ambient conditions, and in both cases, the sample turned completely to PbI_2 and volatile compounds in 12 hours.[126] The transition temperature of $FAPbI_3$ is 165 °C, so $FAPbI_3$ starts to degrade before it reaches the phase transition temperature. Yun et al. studied only non-encapsulated

perovskite layers, so it is possible that a perovskite layer in encapsulated device could withstand the temperature better.

5.1.1.3 Moisture induced degradation of perovskites

In 2015, Leguy et al. discovered that the hydration of $MAPbI_3$ is reversible. The hydration happens in two steps, first there is a reaction of one water molecule with every $MAPbI_3$ unit, and after that, a second water molecule reacts with the $MAPbI_3$ unit (equation 20). The structures of hydrated phases are presented in Figure 39. Even the dihydrated product can turn back to $MAPbI_3$ in dry conditions. In excess water, the dihydrated product can degrade irreversibly (equation 21).[129]

$$4\,CH_3NH_3PbI_3 + 4H_2O \rightleftarrows 4[CH_3NH_3PbI_3 \cdot H_2O] \rightleftarrows (CH_3NH_3)_4PbI_6 \cdot 2H_2O + 3PbI_2 + 2H_2O \quad (20)$$

$$(CH_3NH_3)_4PbI_6 \cdot 2H_2O(s) \xrightarrow{H_2O(l)} 4CH_3NH_3I(aq) + PbI_2(s) + 2H_2O(l) \quad (21)$$

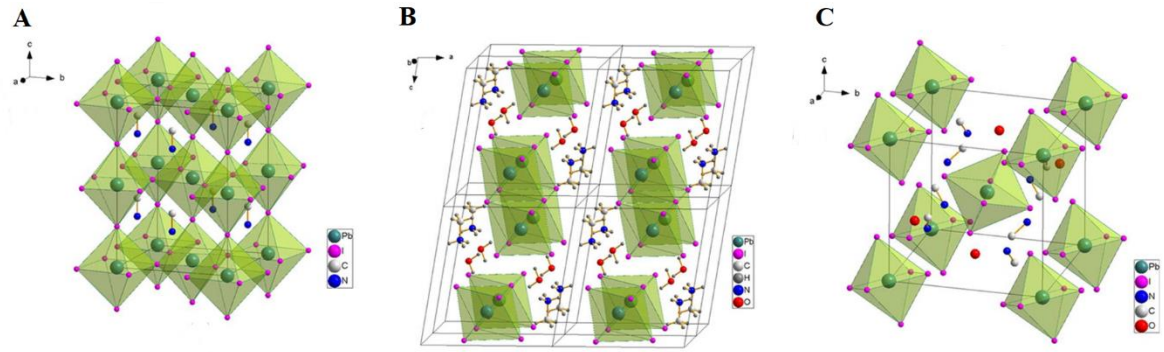

Figure 39. (A) Structure of cubic $MAPbI_3$. (B) Structure of monohydrated phase, $MAPbI_3 \cdot H_2O$. (C) Structure of dihydrated phase, $MA_4PbI_6 \cdot 2H_2O$. Hydrogens are not displayed in (A) and (C). Reprinted with permission.[129] © 2015, American Chemical Society

The second part of reaction (20) produces water. The reaction can be at least partly self-sustaining, since the water that is produced in the second reaction can act as a reagent in the first reaction. Leguy et al. stored $MAPbI_3$ based PSCs in 77% relative humidity (RH). After three hours, solar cell performance dropped significantly, and when the degraded PSC was stored in dry nitrogen for five hours, the device performance recovered almost to the initial state. They suggest that the moisture induced degradation starts from the grain boundaries,

and the hydrated phase in the grain boundaries isolate the $MAPbI_3$ grains from each other, which restricts the transportation of charge carriers and leads to a decrease in performance. In dry conditions, the hydrated phase turns back to perovskite, since the reaction is reversible.[129]

Christians et al. studied degradation of $MAPbI_3$ in dark and illuminated conditions with varying humidity. They found that it is faster under illumination. They also suggest that hydrogen bonding between water molecules and A-site cations weaken the interaction between A cation and BX_6 octahedra. [130] This also means that moisture can boost degradation caused by other degradation methods including oxygen, light or heat. On the other hand, it seems that a stronger interaction between A-site cations and BX_6 octahedra results in improved moisture resistance. The interaction can be strengthened e.g., by A-, B- or X-site substitution. Lee et al. studied $FA_{1-x}Cs_xPbI_3$ systems and found that a 10 % substitution of FA with Cs improved the moisture stability significantly. They suggest that incorporation of Cs, which is smaller than FA, leads to decreased lattice parameters, which leads to stronger interaction between FA-cations and iodide.[131]

Yun et al. studied the effect of humidity on $FAPbI_3$. When $FAPbI_3$ sample was stored in N_2 atmosphere, there were no changes in the XRD pattern or appearance of the sample, and when the sample was stored in 30% humidity for 90 days, there was no change in appearance and only a tiny peak in XRD pattern suggesting formation of non-perovskite phase. However, in 50% humidity, the sample started to turn from black to yellow, and the XRD pattern showed a significant peak of non-perovskite phase and of PbI_2. When the sample was dipped into water, it immediately turned yellow, and according to XRD it completely decomposed to PbI_2.[126]

Marchezi et al. studied the degradation of $Cs_xFA_{1-x}Pb(Br_yI_{1-y})_3$ mixed-cation mixed-halide perovskites in ambient conditions with varying temperature. They used six samples with varying cation and halide composition, with x=0.10, 0.17 or 0.20, and y=0.17 or 0.38. The samples were studied with XRD, SEM, UV-vis absorbance and XPS. According to their findings, different compositions have different degradation paths (Figure 40). 2H intermediate phase is a hexagonal non-perovskite phase similar to the one in Figure 38a, 4H and 6H phases are intermediate phases that still have 3D network of PbX_6 octahedra, even though those are not perovskite phases. There is no degradation observed when the RH is

below 40%, but when RH is increased to 60%, all samples show some signs of degradation. The most stable sample was $Cs_{0.2}FA_{0.8}Pb(Br_{0.17}I_{0.83})_3$, and results of the study indicate that higher cesium content increases stability, and higher bromide content decreases stability.[132] The addition of a right amount of bromide is found to enhance the stability of the perovskite.[128] Based on these results, it is important to carefully determine the optimal ratios in mixed-cation and mixed-halide perovskites.

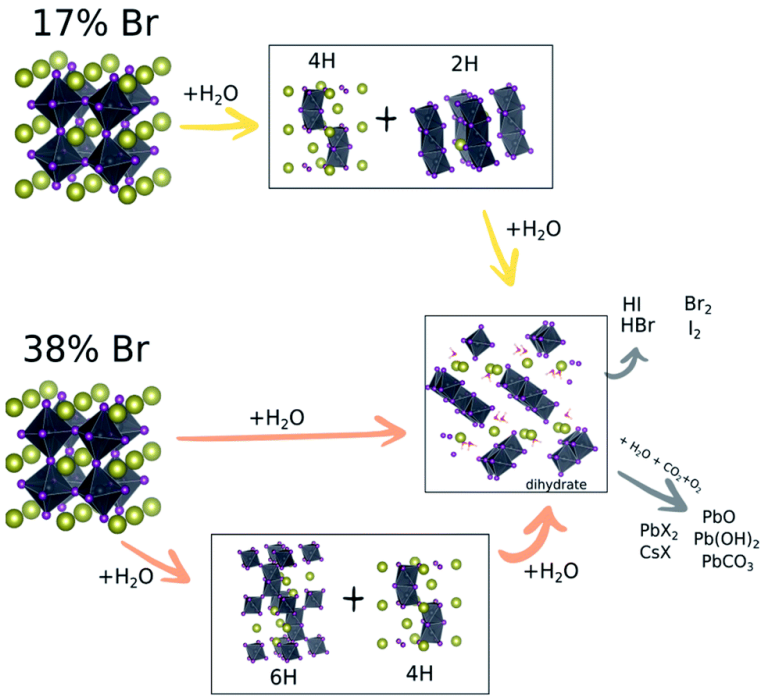

Figure 40. Degradation paths of $Cs_xFA_{1-x}Pb(Br_yI_{1-y})_3$ perovskites. Reprinted with permission.[132] © 2020, Royal Society of Chemistry.

The effect of halide seems to be different in MA-based perovskites. Noh et al. studied $MAPb(I_{1-x}Br_x)_3$ systems and found that with x>0.2, the humidity resistance was much higher. They conclude that the addition of bromide, which is smaller than iodide, results in smaller lattice parameter, which likely leads to stronger interaction between A-site cation and BX_6 octahedra, and thus improves moisture resistance.[42] In a similar manner, Jiang et al. improved moisture resistance by replacing two iodides in $MAPbI_3$ with thiocyanate (SCN^-). Their PSCs with $MAPb(SCN)_2I$ had superior stability compared to PSCs with $MAPbI_3$.[37]

Smith et al. studied $MAPbI_3$ and a layered structure $PEA_2MA_{n-1}Pb_nI_{3n+1}$ and their usage in PSCs. The layered structure with n=3 shows much greater moisture resistance than $MAPbI_3$.[50] 2D and layered perovskite structures have enhanced moisture stability over their

3D equivalents, because of the hydrophobicity of the common long A-site cations. The usage of long A-site cation increases the formation energy of the perovskite layer, leading to improved stability.[49]

Wygant et al. studied the effect of moisture on BA and MA based 2D/3D perovskite structures, and suggest that the perovskite surface undergoes reaction (22):

$$BA_2MA_{n+1}Pb_nI_{3n+1} \xrightarrow{H_2O} BA_2MA_nPb_{n-1}I_{3(n-1)+1} + MAPbI_3 \qquad (22)$$

The 2D/3D perovskite structure reacts to form a single layer of $MAPbI_3$ and a lower-n phase. Equation (23) shows the reaction of n=4 phase.

$$BA_2MA_3Pb_4I_{13}(n=4) \xrightarrow{H_2O} BA_2MA_2Pb_3I_{10}(n=3) + MAPbI_3 \qquad (23)$$

Wygant et al. suggest that only a thin layer of 2D perovskite on top of 3D perovskite will increase the stability because the reaction (22) with water does not degrade the perovskite: it forms lower-n phases that is increasingly more stable. In addition, BA is hydrophobic, which makes it harder for water to interact with the 3D perovskite under the BA-based 2D perovskite layer.[63]

It is possible to enhance the moisture-resistance with additives. Fairfield et al. found that the addition of PEO (**25**), polyacrylic acid (PAA) (**28**) or polyvinyl pyrrolidone (PVP) (**29**) to $MAPbI_3$ prevents the formation of hydrated phase (reaction 20). They suggest that addition of polymers affects the ability of MA-ions to form hydrogen bonds with water molecules.[133]

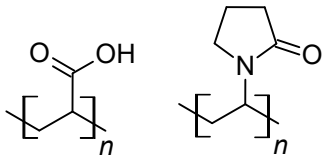

PAA **28** **PVP** **29**

Figure 41. Chemical structure of polymers polyacrylic acid (28) and polyvinyl pyrrolidone (PVP)

Excess moisture is harmful for perovskite, but some amount of air humidity can be necessary in the fabrication of perovskite layer. Eperon et al. studied the perovskite layer fabrication

in different RH, and the exposure to moisture during the film fabrication increases material quality and PL. They suggest that the presence of moisture during film formation reduces trap state density, which leads to better performance.[134]

5.1.1.4 Oxygen induced degradation of perovskites

Oxygen can react with $MAPbI_3$ with reaction (24):

$$4CH_3NH_3PbI_3 + O_2 \rightarrow 4PbI_2 + 2I_2 + 2H_2O + 4CH_3NH_2 \quad (24)$$

Aristidou et al. calculated that enthalpy of reaction (24) is +1.60 eV per O_2 molecule, which indicates that oxygen induced degradation does not happen spontaneously. However, when $MAPbI_3$ is exposed to light and oxygen, the formation of superoxide O_2^- and photoexcited $MAPbI_3^*$ leads to reaction (25):

$$4CH_3NH_3PbI_3^* + O_2^- \rightarrow 4PbI_2 + 2I_2 + 2H_2O + 4CH_3NH_2 \quad (25)$$

Calculated enthalpy of reaction (25) is −1.40 eV per O_2 molecule. The value is negative, which means, that in the presence of oxygen and illumination, $MAPbI_3$ is unstable.[135]

Small perovskite grain size is desirable in PeLEDs for efficiency. However, the smaller crystal size of $MAPbI_3$ leads to higher amount of photo-induced superoxide formation, which degrades the perovskite. Aristidou et al. conclude that there is a direct correlation between the superoxide O_2^- generation, degradation rate and $MAPbI_3$ crystal size. They propose a mechanism where O_2 diffuses in the perovskite through the grain boundaries and the reaction (25) starts from grain surfaces.[135]

Oxygen-induced degradation starts from the surfaces, and it can be reduced by passivating perovskite grain boundaries with additives. Aristidou et al. spin coated solutions iodide and chloride salts of MA, PEA and trimethylsulfonium (MAI, MACl, PEAI, PEACl, Me_3SI) on $MAPbI_3$ to passivate grain boundaries and defects. All iodide salts decreased the formation of superoxide and increased stability, whereas chloride salts did not affect superoxide formation nor stability. They predict that superoxide formation happens in iodide vacancies, and that the addition of iodide salts fills the iodide vacancies in the film, suppressing superoxide formation and leading to increased stability.[135]

The oxygen induced degradation of other perovskites have not been studied as precisely as $MAPbI_3$.

5.1.1.5 Ion migration in perovskites

Ion migration is speculated to contribute to many undesirable phenomena in perovskites, such as hysteresis and phase separation. Ion migration in perovskites is not well understood, and some important questions related to ion migration are: (1) Is ion migration possible in the material? (2) Which ions can migrate? (3) How easily ions migrate and under what conditions? (4) Can ion migration be prevented or decreased? (5) How complete is the migration? and (6) Are the effects permanent or do the migrated ions return when the device is not under stress? There are no answers for all of these questions related to perovskites, and the answers vary within different perovskites.

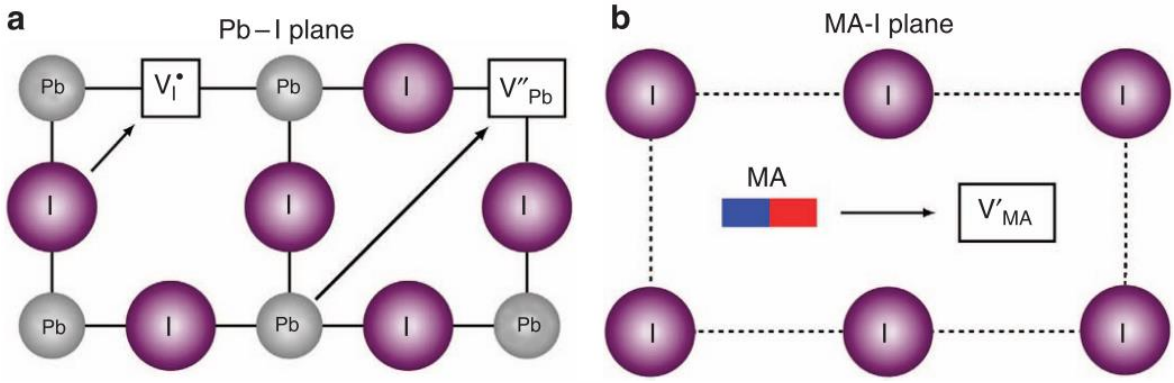

Figure 42. Ion migration in $MAPbI_3$. (a) Iodine and lead migration illustrated in the Pb–I plane, (b) MA migration illustrated in the MA–I plane. Reprinted with permission.[136] © 2015, Springer Nature.

The ion migration in the bulk happens within the ion vacancies. In addition to the vacancies, the ions can migrate within grain boundaries and surfaces. Ion migration is characterized by activation energy (E_A), and it is affected by the characteristics of the material, such as ionic radius, ion charge and crystal structure. Ion migration rate is also affected by temperature.[137] Eames et al. have calculated the activation energies for ionic migration in $MAPbI_3$ to be 0.58 eV, 0.84 eV and 2.31 eV for I^-, MA^+ and Pb^{2+} respectively. The migration routes used in calculations are shown in Figure 42.[136] Iodide migration has the lowest activation energy, suggesting that iodide ions are the most favorable ions to migrate. High activation energy for Pb^{2+} migration suggests that Pb^{2+} ions do not easily migrate.[137] In addition to ions from the perovskite, it is possible that some other ions migrate in the perovskite layer, such as Ag^+

or H^+ ions from other layers used in the PeLED, or some ions from the degradation of the perovskite.

DeQuilettes et al. studied the properties of $MAPbI_3$ under illumination. First, they illuminated the samples with air mass (AM) 1.5 sunlight for 60 minutes, and then stored them in dark for 450 minutes. PL lifetime and PL intensity increase under continuous illumination. After the illumination and storage in dark, the average PL of the sample was approximately the same as before illumination, but it was more uniform: the spots that initially had the brightest emission, were less bright, and the spots that were initially darkest, had brighter emission. When they illuminated only small spots, they found that iodine redistributes away from the area that is illuminated. They conclude that light-soaking is able to redistribute iodide in the sample, and a more uniform distribution of iodide and iodide vacancies lead to a more uniform PL.[138]

Light-induced ion migration has been a problem in mixed-halide and mixed-cation perovskites. In 2015 Hoke et al. studied a set of $MAPb(Br_xI_{1-x})_3$ perovskites. PL emission peak shifted from around 770 nm for x=0 to shorter wavelength when bromide content was increased (around 535 nm for x=1). However, under continuous illumination of samples with $0.2<x<1$, an additional PL peak appears at around 740 nm. In less than a minute of light soaking, the new peak gets more intense than the original peak and after five minutes in the dark, the PL spectra returns to the initial state before illumination. Light soaking makes ions migrate to iodide- and bromide-rich domains, and the iodide-rich domains dominate the PL since their bandgap is smaller. The mechanisms are not clear, but they suggest that the relaxation from segregated-halide phases to the initial mixed-halide phase is driven by the lattice strain and entropy.[139]

Xiao et al. studied ion migration in $MAPbI_3$ and $BA_2MA_2Pb_3I_{10}$. They also studied how 0.25 sun illumination affects ion migration. They found that in $MAPbI_3$, ion migration starts to dominate electric conduction in temperatures higher than 280 K, and that the activation energy for ion migration in $MAPbI_3$ is higher (0.83 eV) in dark conditions than under illumination (0.33 eV), which indicates that illumination increases ion migration. In $BA_2MA_2Pb_3I_{10}$, ion migration was negligible in temperatures under 350 K, both in dark and under illumination. In addition, they have calculated the formation energies of MA and I vacancies in $MAPbI_3$ and $BA_2MA_2Pb_3I_{10}$. Formation energies for MA vacancy are 5.72 eV

and 6.94 eV for $MAPbI_3$ and $BA_2MA_2Pb_3I_{10}$ respectively, and for I vacancy are 3.44 eV and 5.46 eV for $MAPbI_3$ and $BA_2MA_2Pb_3I_{10}$, respectively. The higher formation energies in $BA_2MA_2Pb_3I_{10}$ indicates that it is harder for ion vacancies to form in 2D/3D perovskite structure than in 3D perovskite. The formation energy for iodide vacancy is smaller than formation energy of MA vacancy for both materials, which further proves that the migration of iodide-ions is more favorable than migration of MA ions.[64]

Yun et al. discovered that ion migration happens in the grain boundaries of $FAPbI_3$.[126] It could be possible to reduce ion migration in grain boundaries by grain boundary passivation with passivating agents. Wu et al. have used Lithium halides to passivate the grain boundaries, and among other things, incorporation of LiBr in a $CsPbBr_3$ decreased ion migration. In addition, it increased EQE, brightness, and operational lifetime.[140] Other surface passivating agents include e.g. diamines (Figure 43). Hexamethyldiamine (HMDA) (**30**), 2,2'-[oxybis(ethylenoxy)]diethylamine (ODEA) (**31**), 2,2'-(ethylenedioxy)-diethylamine (EDEA) (**32**), 4,7,10-trioxa-1,13-tridecanediamine (TTDDA) (**33**) 4,9-dioxa-1,12-dodecanediamine (DDDA) (**34**) are all symmetric and contain amino-groups in both ends of the alkyl chain. According to Xu et al. the amino-group can passivate iodide vacancies on the perovskite surface by Pb–N interaction. The two electron pairs of O atoms can also interact with Pb^{2+} to passivate defects. The length of the alkyl chain between N and O and O and O affects the passivation, and in their studies with $FAPbI_3$ based PeLEDs, ODEA works best. ODEA passivated device has highest EQE, and ODEA passivation increased lifetime T_{50} (measured as radiance at constant current density 25 mA cm^{-2}) from 1.5 hours to 20 hours.[141]

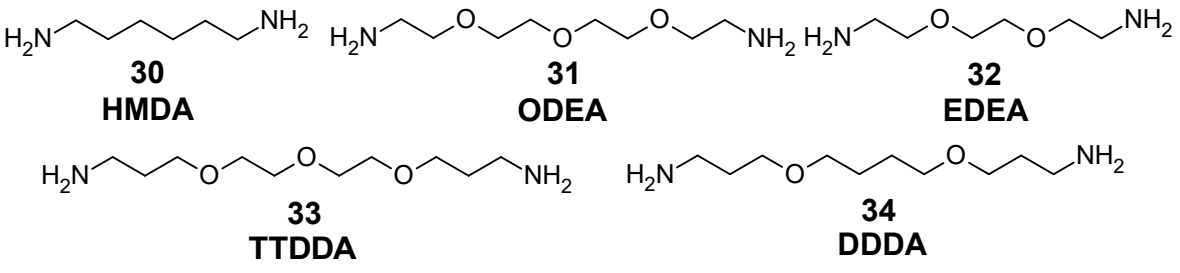

Figure 43. Chemical structures of diamine molecules used as passivating agents.

5.1.1.6 Mechanical stress as a cause of perovskite degradation

Rolston et al. studied the mechanical fragility of PSCs based on $MAPbI_3$. They used double-cantilever beam tests to study the fracture resistance of the PSCs. All PSCs had fracture resistance lower than 1.5 J m^{-2}, which is extremely low and shows that PSCs are extremely fragile. They suggest that a reasonable fracture resistance for PSCs is at least 10 J m^{-2}, and it is a reasonable goal for PeLEDs too. In their tests with devices, the most fragile part of PSC was organic charge transport layers and the interface between organic transport layers and perovskite.[142]

Zhao et al. studied mechanical stress of $MAPbI_3$ films with long cation additives. They tested five different long cations, and each of them increased the fracture energy of the perovskite film. Additionally, the additives decreased particle size and size distribution, increased PLQY, EQE and stability. The fracture energy of $MAPbI_3$ was 0.67 J m^{-2}, and the highest fracture energy 1.6 J m^{-2} was achieved with dodecylammonium (**35**) iodide. They found a correlation between alkyl chain length and fracture energy: the longer the alkyl chain, the higher the fracture energy. In addition, a fluorinated long cation 4-fluorobenzylammonium (**36**) iodide increased the fracture energy more than non-fluorinated equivalent, benzylammonium (**37**) iodide. Chemical structure of compounds **35**-**37** is shown in Figure 44. They suggest that the increased fracture energy is caused by the electron-withdrawing properties of fluoride, which increases the polarity of the amine.[143]

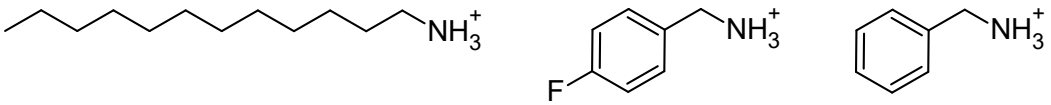

35 **36** **37**

Figure 44. Chemical structures of dodecylammonium (35), benzylammonium (36) and 4-fluorobenzylammonium (37).

The PeLED devices must work and be stable over a broad temperature range. Zhao et al. studied the thermal expansion of $MAPbI_3$ perovskite and found that its linear expansion coefficient is $6.1 \cdot 10^{-5}$ K^{-1}. Typical values for glass and ITO are $0.37 \cdot 10^{-5}$ K^{-1} and $0.85 \cdot 10^{-5}$ K^{-1}, respectively. The linear expansion coefficient for $MAPbI_3$ is over seven times higher than for glass. When the perovskite layer is prepared in an elevated temperature and cooled down to room temperature, the perovskite is left under strain because it is unable to shrink. This can cause stress in a perovskite film built on glass substrate.[144] Other perovskites have

even higher values, $FAPbI_3$ and $FASnI_3$ have linear expansion coefficient values of $6.8 \cdot 10^{-5}$ K^{-1} and $7.3 \cdot 10^{-5}$ K^{-1} respectively.[124] PET has thermal expansion coefficient of around $2–8 \cdot 10^{-5}$ K^{-1}, which is much closer than that of perovskites, and according to the studies by Zhao et al, usage of a substrate with better matching expansion can reduce stress and increase stability.[144]

Wang et al. studied the effect of strain on 2D/3D $BA_2MA_{n-1}Pb_nI_{3n+1}$ perovskite structures. With increasing strain, the bandgap of the perovskite decreased, which they suggest is caused by the distortion of PbI_6 octahedra. In addition to the changes in band gap, the strain makes it easier for moisture and oxygen to react with perovskite, increasing the degradation rate.[65]

Studies show that mechanical stress can accelerate moisture, temperature and illumination induced degradation, but the exact mechanisms have not been studied in detail. To increase device stability, strain should be avoided. Strain could be prevented by e.g. lowering perovskite processing temperature and the usage of materials with similar expansion coefficient.[145]

5.1.1.7 Perovskite degradation under electric bias

Light-emitting diodes need to be stable under electric bias. Some PeLEDs have a long shelf life but they degrade under operation. Clearly the operation under electric bias has some effect on PeLEDs, but degradation methods are not well known. For example, Warby et al. studied $CsPbBr_3$ based devices with PEA additives and delaminated the devices after degradation. They studied the perovskite layer with XRD, UV-vis absorbance and SEM, but observed no changes, even though EQE had almost completely degraded.[52]

Xu et al. studied PeLEDs with $MAPbBr_3$ perovskite and architecture of ITO/PEDOT:PSS/TFB/perovskite/TPBi/LiF/Al. They applied a bias of different voltages and found that under 3 V, bias, the EQE slightly improves after 10 seconds, and starts to degrade after that. The EQE improvement is probably caused by migrating ions filling vacancies, leading to a decrease in non-radiative recombination. Under 4 V bias, EQE starts declining immediately, and decline from 3.8% to 0.5% in 50 seconds. Under 5 V or 6 V bias the device fails immediately after 10 seconds. The layer visibly degrades and according to their SEM-EDX studies, there is only Pb and Br left in the degraded spots of the perovskite. They suggest that the degradation undergoes reaction (26).[146]

$$MAPbI_3 \rightarrow MA^+ + PbBr_2 + Br^-$$
$$2Br^- \rightarrow Br_2 + 2e^- \quad (26)$$

It seems that generally a higher voltage and higher current density leads to faster degradation. In principle, IR and red LEDs can operate with lower voltage, since the band gap is smaller. UV and blue LEDs have the largest band gap, and need highest voltage to operate. Additionally, some LEDs do not reach a decent luminance with turn-on voltage, but instead need a higher voltage. If there were methods to decrease the voltage needed to reach satisfactory luminance, those methods would not only increase stability but also luminous power efficiency.

5.1.1.8 Reactions between perovskites and other layers in perovskite light-emitting diodes

Metals from electrodes and inorganic charge transporting layers can react with perovskites. Metals can shift from the electrode to the perovskite layer, and alternatively, some ions can migrate from the perovskite layer to the electrode. Kato et al. found that iodide from the perovskite layer can be detected on top of Ag electrode just one hour after the deposition of silver, even when there is a Spiro-OMeTAD HTL layer between silver electrode and perovskite. Iodide later reacted with silver and formed silver iodide AgI.[147]

Zhao et al. studied PeLEDs with the structure ITO/poly-TPD (HTL)/$MAPbI_3$/TPBi (ETL)/LiF+Al. They found that $MAPbI_3$ degrades with moisture as shown in reaction (21) (in section 5.1.1.3), but when the sample was returned to N_2 atmosphere, only the perovskite that was not covered with Al electrode turned back to $MAPbI_3$. They also studied a PSC device with PCBM/C_{60}/BCP layers between Al electrode and $MAPbI_3$, and observed similar degradation, so they conclude that the interlayers do not participate in the degradation. Based on their studies, aluminum electrode reacts with $MAPbI_3$ in the presence of moisture with reactions (27)–(29).[148]

$$2Al + 4MAPbI_3 + 2H_2O \rightarrow (MA)_4PbI_6 \cdot 2H_2O + 3Pb + 2Al^{3+} + 6I^- \quad (27)$$

$$2Al + 3(MA)_4PbI_6 \cdot 2H_2O \rightarrow 12MAI + 3Pb + 2Al^{3+} + 6I^- \quad (28)$$

$$MAI \rightleftharpoons MA + HI \quad (29)$$

They conclude that in these reactions, water is not the reagent that irreversibly decomposes the perovskite, moisture only enables the diffusion of ions. They expected that $MAPbI_3$ would react with similar redox reactions with other metals, and that similar reactions happen with other perovskites. They deposited layers of aluminum, ytterbium (Yb), chromium (Cr), silver (Ag), and gold (Au) on top of $MAPbI_3$, and layers of Al on top of $CsPbI_3$ and $CsPbBr_3$. Based on XPS studies, every metal except Au reacts with $MAPbI_3$ and Al reacts also with other perovskites to form metallic lead Pb^0.[148]

Yang et al. studied the ZnO:$MAPbI_3$ interface and found that the slightly basic ZnO is capable to deprotonate MA molecules, which leads to formation of methylamine and degradation of the perovskite.[149] Based on this result, it is possible that the contact between a basic layer and perovskite layer can be detrimental for perovskite stability. This could be avoided by substitution of basic layers with non-basic alternatives.

Perovskite materials can react with many metals even through interlayer. It seems possible that non-metal electrodes could enhance stability. One future option could be carbon-based electrodes, such as carbon nanotubes (CNTs) and graphene-based electrodes. Carbon electrodes have advantages such as material availability, price, transparency, and non-toxicity, but common carbon-based electrode materials have higher resistance compared to metal electrodes. Luo et al. fabricated a PSC with PET/graphene/TiO_2/PCBM/$MAPbI_3$/CNTs+Spiro-OMeTAD structure. Compared to their devices with Ag or Au top electrodes, the device with CNT electrode had superior stability in high humidity (70% RH) and elevated temperature (60 °C).[90]

5.1.2 *Other strategies to increase perovskite light-emitting diode stability*

Generally, the morphology of the perovskite film affects its stability and performance. Tiny variations in precursor solution composition can have huge effects in the film. Fassl et al. studied the effect of small deviations in precursor solution on PSC performance. They prepared $MAPbI_3$ perovskite from MAI and lead acetate ($PbAc_2$), where the stoichiometric ratio of MAI to $PbAc_2$ is 3. The highest power conversion efficiency (PCE) was 15.6%, received with the ratio of 3.055, whereas the lowest PCE was under 13.5% with ratio of 2.985. The deviation in MAI:$PbAc_2$ affected grain size, hysteresis and stability.[104] Such small deviations can be unintended especially in laboratory scale, because the solution volumes are small.

Excess Pb can be harmful for perovskite stability. In $MAPbBr_3$, which is made from a solution containing MABr and $PbBr_2$, the film contained a small amount of metallic lead when the stoichiometry of precursors was 1:1, but no metallic lead was detected when the stoichiometry was slightly changed to MABr:$PbBr_2$ 1.05:1.[6] On the other hand, Yuan et al. studied different stoichiometries of $FA_{0.9}Cs_{0.1}PbI_3$, and achieved the highest EQE when the ratio of x:PbI_2 (x= 0.9 FAI+ 0.1 CsI) is 2.5:1. With stoichiometric ratio (1:1), only a non-radiative non-perovskite phase forms.[150] A good optimization of precursor solution is needed to form a pure layer of perovskite with no excess lead and no non-perovskite phases.

Xiao et al. studied perovskite film formation from precursor solution of BAX:MAX:PbX_2, where $X=I^-$ or Br^-. They speculate that the faster reaction rate of reaction (30) compared to reaction (31) (X = I, Br) leads to formation of pure $MAPbX_3$, and BA acts only as a surfactant.

$$MAX + PbX_2 \rightarrow MAPbX_3 \tag{30}$$

$$2BAX + PbX_2 \rightarrow BA_2PbX_4 \tag{31}$$

When BAX:MAX ratio is higher than 6:10, $BA_2MA_{n-1}Pb_nX_{3n+1}$ phases can be detected with XRD, but with ratios up to 4:10 only pure $MAPbX_3$ phase is detected.[62] As an additive, BAX reduces perovskite grain size and surface roughness. With an optimal ratio (4:10), 3D perovskite forms small grains with BA on grain surfaces and boundaries. BA on the grain boundaries and surfaces increases stability. In addition, devices with BA have lower current and luminance hysteresis with I and Br. Ion migration is a known cause of hysteresis, and Xiao et al. suggest that since ion migration mostly happens on grain boundaries, BA on grain boundaries can prevent ion migration.[62]

5.1.3 *Summary of methods to increase perovskite light-emitting diode stability*

Various methods to increase PeLED stability were introduced in previous sections. These methods are shortly summarized in this section. The strategies can be roughly divided to: (1) Substitution of perovskite precursor materials with more stable options. (2) Perovskite layer additives. (3) Altering perovskite layer morphology. (4) Substitution or modification of other layers in PeLED.

Strategy (1) increases the intrinsic stability of the perovskite material. Stability improvement is in most cases done with A-site cation substitution, since lead is the only widely used B-site cation, and X-site substitution has a very large effect on bandgap, leading to a large shift in emission wavelength. A-site cation substitution includes usage of long cations to form 2D/3D perovskite structures. A good choice of A-site cation composition can reduce degradation affected by moisture, oxygen, and illumination, increase thermal and mechanical stability, and reduce ion migration. In addition, perovskites with certain A-site cation compositions do not have non-perovskite phases, and A-site cation engineering can lead to more stable photoactive phases.

Strategy (2) includes the addition of any additional compounds to the precursor solution. Many different additives are used, such as alkali-metal halide salts, polymers, and organic molecules with specific functional groups such as amino group ($–NH_2$) and ether-group (R–O–R'). The function of additives can be e.g., to fill defects in perovskite layer or to passivate perovskite grain boundaries. The ion migration in perovskites correlates with defect density, and filling defect sites can hinder it. Passivation of grain boundaries can increase stability in multiple ways: thermal, moisture, and oxygen induced degradation starts from the grain surfaces, and with successful grain surface passivation, perovskite stability can be increased.

Strategy (3) is more of a fine-tuning after strategies (1) and (2), and it is in some cases achieved with additives, partly overlapping with strategy (2). Morphology can affect stability in multiple ways: small crystal size is beneficial for efficiency, but increases the formation of superoxide, which leads to faster oxygen-induced degradation. A rough film surface can lead to uneven interfaces with adjacent layers, which can lead to reduced stability. The morphology can be modified e.g., with film preparation parameter tuning and additives.

Strategy (4) is not directly related to the perovskite material, but it can affect the stability of perovskite layer. The other layers can contain materials that readily react with perovskites. In addition, the degradation products of perovskites or some other materials can be reactive with other materials, which can speed up the degradation. It is known that some metals can react with perovskites, and that a direct contact with metals and perovskites should be avoided. Basic materials, such as ZnO, can deprotonate organic cations in perovskites. This can be avoided e.g., by substitution of basic materials with non-basic materials. It is

important to make sure that all materials, especially materials used in adjacent layers, are functional together.

It is important to keep in mind that methods to increase stability are not universal and same methods do not work with every perovskite. As an example, there are studies where the addition of long cations to form a 2D/3D perovskite structures increases the stability, but for Warby et al. it did the opposite. They studied a system of $CsPbBr_3$ with PEA ($PEA_2Cs_{n+1}Pb_nBr_{3n+1}$), with varying ratio of PEABr and $CsPbBr_3$ in the precursor solution. They reached the highest EQE (12.1%) with a PEA:Cs ratio 0.4:1, which was superior compared to EQE with $CsPbBr_3$ (0.24%). However, the device lifetime T_{50} of the champion $PEABr_{0.4}CsPbBr_3$ device was only 203 s, which is poor compared to the lifetime of $CsPbBr_3$ device (9.3 h). The 3D perovskite had the highest T_{50}, and device lifetime decreased when the amount of PEA was increased. In this study, T_{50} was measured as a drop in EQE under constant current density of 10 mA cm^{-2}.[52] This is also a good example of the conflict between stability and efficiency: in some cases, the improvement of stability decreases efficiency, and vice versa. Researchers need to continuously evaluate many different aspects of their studies.

The stability of the PeLEDs is not that great yet, but the technology is relatively new, and not that much research has been focusing on the stability. It is relevant to compare PeLED stability to PSC and OLED stability: In 2017, 8 years after the first paper on perovskite solar cells, Grancini et al. released a paper on a 10x10 cm^2 PSC module that maintained its PCE for over 10 000 hours in 55 °C and 1 sun illumination.[151] In 2010, Panasonic reported a white OLED with T_{50} of over 40 000 hours, measured at 1000 cd m^{-2}.[152] Based on the development of PSC and OLED technologies, it is likely that the stability of PeLEDs can be increased significantly, but whether it is enough for large-scale commercialization, and when, remains to be seen.

5.2 Environmental and health issues

When discussing environmental and health issues, it is important to take into account the entire life cycle of the product. First, the manufacturing of the product needs to be safe for workers and the environmental contamination needs to be minimized. The product needs to be safe to use as long as it is functional, and even when it breaks. After it is no longer used,

it needs to be safe to recycle without environmental contamination or health risks. In this section, lead and solvents are discussed. These are major, but not the only issues concerning the manufacturing of perovskites.

5.2.1 *Lead*

5.2.1.1 Issues with lead-containing perovskites

Lead is on the list of ten chemicals of major public health concern by World Health Organization (WHO). WHO instructs that non-essential uses of lead such as leaded paints, leaded petrol and leaded glass should be eliminated.[153] WHO also recommends to eliminate the usage of lead in homes, schools, school materials and children's toys.[154] If these recommendations are looked in the perspective of PeLEDs, it is necessary to define if PeLEDs are essential, since there are other non-lead-containing LED technologies. If lead-containing PeLEDs can significantly outperform non-lead-containing alternatives, or they can enable unique applications, they can be defined to be essential. Yet even in that case, the safety is extremely important, and it is a valid question whether the usage of lead containing PeLEDs in applications such as children's toys should be restricted.

In addition to recommendations by WHO, there is legislation that restricts the usage of lead. European Union (EU) has a directive (2011/65/EU) that restricts the lead content of any homogenous material used in electrical and electronic equipment to the maximum of 0.1 wt%.[155] There are multiple reasons why a product can be exempted from the directive, such as greater positive benefits (environmental, health or safety) compared to negative impacts, and the directive does not apply to e.g. military and space equipment. If the PeLEDs can enable unique applications or greatly outperform other LEDs, it is possible that PeLEDs could be excluded. It is also possible that the usage of PeLEDs in some specific applications where the safety can be easily controlled could be allowed. For example, the directive does not apply to *photovoltaic panels intended to be used in a system that is designed, assembled and installed by professionals for permanent use at a defined location to produce energy from solar light for public, commercial, industrial and residential applications*.[155]

Because of toxicity and strict legislation, lead is already recycled with a high rate. In 2012, global lead production was a bit over 10 million tons, of which secondary lead production was over 60 %.[156] In addition, Binek et al. have studied the recycling of PSCs with similar

structure than PeLEDs. They were able to strip down the PSC layer by layer, and they were able to reuse the PbI_2 from $MAPbI_3$ perovskite in new cells three times without affecting the cell performance.[157] based on these results, PbI_2 is easy to recover from $MAPbI_3$ based devices, and it can be readily reused to build new devices.

Studies show that the in perovskite is more bioavailable for plants than the lead species that are naturally in soil. The bioavailability of lead is important to study for multiple reasons: First of all, it can be hazardous for the plants, and secondly, food is one of the most general ways for lead to enter human body.[158] In addition, the bioavailability at the production is also a risk, since the perovskites are often solution processed from water-miscible solvents.

The amount of lead in PeLEDs is really small, and it would be only a tiny part of the total amount of lead used. An evaluation of lead emissions and toxicity potential for PSCs was released in 2019. In the evaluation they estimate that the amount of lead in a one micrometer layer of perovskite is around 1.4 g m^{-2}. They estimate that if all energy generation in the USA would be replaced by PSCs, the amount of lead used in the PSCs would be around 17000 tons, which is around 0.17% of world lead production.[159] The perovskite layer in PeLEDs is much thinner than in PSCs, so the amount of lead in PeLEDs is even smaller. If the same density is used, a 300 nm layer would contain 0.42 g m^{-2} lead, and a 30 nm layer would contain 0.042 g m^{-2} lead. Perovskite layer density depends on perovskite composition and morphology.

5.2.1.2 Lead free perovskites

Lead-free PeLEDs have been studied. As illustrated in chapter 3, there is a huge amount of possible perovskite and perovskite-like structures, and there are many lead-free possibilities. Ning et al. propose design rules for lead-free perovskite materials (Figure 45).

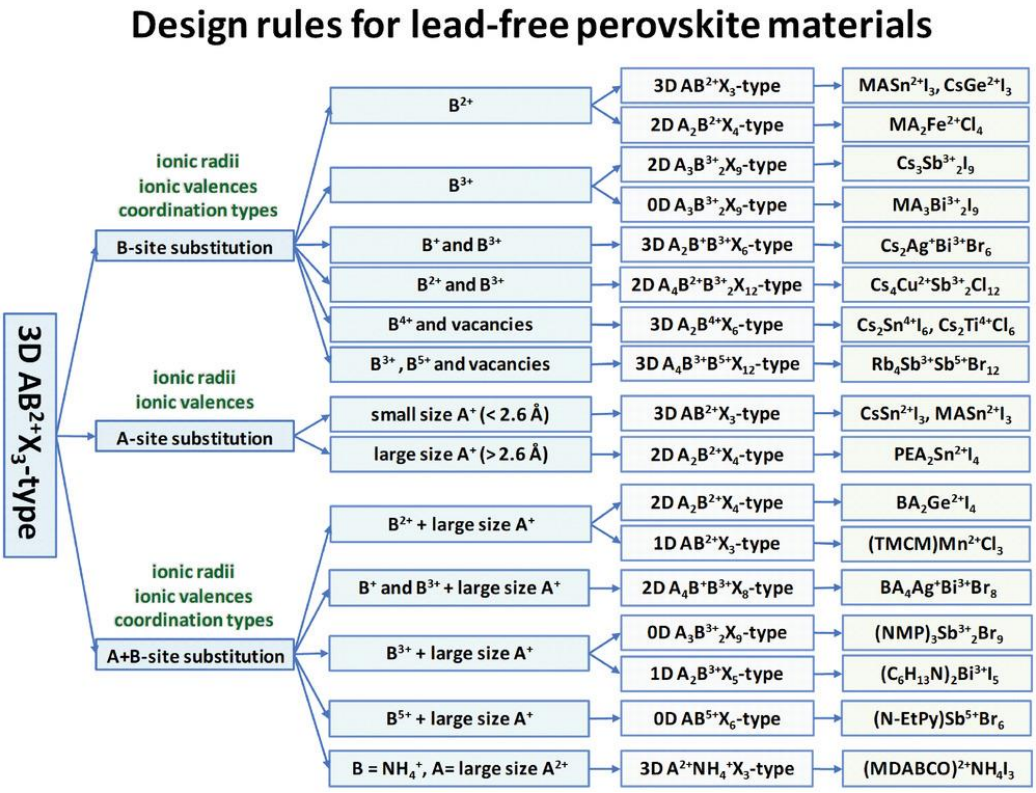

Figure 45. Design rules for lead-free perovskite materials. Reprinted with permission.[160] © 2019 WILEY-VCH Verlag GmbH & Co. KGaA, Weinheim

One common and obvious option is to substitute lead with some other metal with +2 charge, like tin (Sn^{2+}), which is in the same group in previous period and has a similar electron structure with lead. This has proven difficult, since Sn^{2+} easily oxidizes to Sn^{4+}, resulting in the degradation of the perovskite. Gao et al. accomplished a PSC with Cs-doped $FASnI_3$ that maintained 90 % of power-conversion efficiency after 2000 hours in N_2 atmosphere. This demonstrates that the stability of Sn based devices can be increased. The best perovskite composition was $FA_{0.92}Cs_{0.08}SnI_3$ and it had power conversion efficiency of 6.08%. The efficiency is still far from the efficiency of best lead-based PSCs, but at least this proves that the stability is not a critical issue in the development of tin-based perovskite devices. According to XPS measurements, the addition of Cs decreases the amount of Sn^{4+} in the perovskite layer.[161]

Other option to replace lead is double perovskites with A_2BCX_6 structure. Volonakis et al. reported that double perovskites exhibit promising optoelectronic properties. The properties were studied computationally, and a promising material, $Cs_2BiAgCl_6$ was synthetized and characterized.[34]

Lead can be only partly substituted: Zhang et al. used a mixed metal-cation in $CsPb_{1-x}Sn_xBr_3$ with varying x and used it in efficient PeLEDs. Increasing lead content resulted in a blue shift of emission. The bandgap shifts from 2.38 eV, 520 nm (x=0) to 2.50 eV, 496 nm (x=0.7). The best performance was achieved with x=0.3, which was even better than the performance of the PeLED without tin.[41]

5.2.2 *Harmful solvents*

Perovskite films are often fabricated by spin coating or printing methods from a precursor solution. Most commonly, the precursor materials are dissolved in an organic solvent. For example in the case of $FAPbBr_3$ perovskite, formamidinium bromide (FABr) and lead (II) bromide ($PbBr_2$) would be used in 1:1 ratio to receive a 1:1:3 ratio of FA:Pb:Br.

The number of solvents is limited because lead halides are insoluble in many organic solvents. Polar aprotic organic solvents, such as *N,N*-dimethylformamide (DMF) (**38**), dimethyl sulfoxide (DMSO) (**39**), acetonitrile (AcN) (**40**) and γ-butyrolactone (GBL) (**41**) are commonly used in perovskite solutions. These solvents contain a C=O, C≡N or S=O bond that can interact with lead atoms. The chemical structure of these solvents is presented in Figure 46.

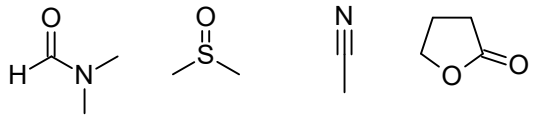

Figure 46. Organic solvents used in the perovskite film fabrication.

DMF is the most common solvent in the perovskite precursor solutions. In laboratory scale it can be used rather safely, but in larger scale it is harder to keep the process safe and risks are much higher. It has caused severe liver toxicity, and its use should be restricted.[162] DMSO can easily penetrate skin, and the dissolved compounds can get absorbed in the body. All solvents listed in Figure 46 are water miscible, which increases the bioavailability and risk of pollution.[163]

In many cases, an anti-solvent is used to enhance perovskite film quality. Anti-solvent is a solvent in which perovskite precursor is insoluble, and it is used to control morphology,

grain size and layer thickness in perovskite layer formation. For example, in spin coating, anti-solvent is dropped on the spinning sample after the perovskite solution. The anti-solvent mixes with the precursor solution, which leads to a fast crystallization of perovskite. The morphology of perovskite layer can be modified by changing the anti-solvent dropping time. A common anti-solvent in PeLED fabrication is toluene, which is toxic. Chlorobenzene, which is also toxic, is a common anti-solvent used in PSC fabrication. Recently, there have been research about green and non-toxic alternatives for chlorobenzene, such as tetraethyl orthocarbonate.[164] One way to get rid of toxic anti-solvents is to use gas-quenching, where an inert gas, in these cases nitrogen (N_2) or argon (Ar), is blown on the sample after precursor solution deposition.[165–167] Gas-quenching is more environmentally friendly than anti-solvent quenching, and it is easier to upscale to large scale production.

5.3 Challenges in perovskite light-emitting diode efficiency

The efficiency of green and red PeLEDs has improved fast, but the efficiency of blue PeLEDs is lagging behind. Blue PeLEDs are generally made with a mixed bromide and chloride perovskite, which leads to phase segregation and formation of chloride and bromide rich phases. Pure 2D perovskites have a blue-shifted emission compared to their 3D equivalents, and some 2D perovskites have a suitable blue emission with only bromide as the X-site anion. To the best of my knowledge, the highest EQE for a blue LED is 9.5% by Liu et al. (2019).[57] The details of blue, green, red and IR PeLEDs with highest EQE-values are presented in Appendix 1.

A lot of PeLED research is based on successful development of PSCs. The optimal band gap for an absorbing material in a solar cell is around 1.35 eV (918 nm), which is in the IR-area. Thus, the ETL and HTL materials that are developed for PSCs work with red and IR PeLEDs, and the higher the perovskite band gap, the worse the energy level alignment is. It is challenging to find the optimal charge transporting materials for blue LEDs. The deep valence band of blue-emitting materials makes hole injection especially hard.

Even though the efficiency of green and red PeLEDs is much higher than blue PeLEDs, it is still behind OLEDs and inorganic LEDs. The efficiency can be further improved e.g., by optimizing the structures and interfaces, and ensuring effective and even charge injection.

6 SUMMARY AND CONCLUSIONS

PeLEDs have the potential to revolutionize the display and lighting market, since solution processing and abundancy of elements used in perovskites enables easy and inexpensive manufacturing. Perovskite light-emitting diodes are a rapidly developing technology that can not only replace the existing LED technologies in some applications, but also introduce new applications for LEDs due to the possibility of making transparent and flexible LEDs with high color purity.

There is a huge number of perovskites, and many remain undiscovered. The most common 3D perovskites in PeLEDs are methylammonium, formamidinium and cesium lead halides In addition, perovskite-like 2D structures and 2D/3D perovskite structures are being studied.

There are multiple challenges in PeLED development, such as performance, stability, and environmental issues. The development of PeLEDs has been fast compared to other LED technologies, and the development has not shown signs of slowing down. The efficiencies of green and red PeLEDs are already reasonably high, and now that the research community has proven that the luminance of PeLEDs is good, the focus of the research should shift more to other topics such as development of blue PeLEDs, increasing stability, production upscaling, and environmental issues. The blue emission has been hardest also for inorganic LEDs and OLEDs, but the development has been successful. In 2014, the Nobel Prize in Physics was awarded to Isamu Akasaki, Hiroshi Amano, and Shuji Nakamura for the invention of blue LED. They made the breakthrough in bright blue LEDs in 1993, over three decades after the first visible emission LEDs were demonstrated.

At present, the stability of PeLEDs is nowhere near sufficient for any real applications, but if the development is compared to relevant technologies such as PSC and OLED, it is likely that the stability can be increased significantly. There are many ways to improve device stability, such as substitution of perovskite components, changing perovskite morphology, additives, and optimization of device architecture.

Another issue is the environmental effects of PeLEDs. Lead is toxic and its usage in consumer goods is rightly strictly restricted. The development of lead-free perovskites is a challenge not only for PeLEDs but also for perovskite solar cells and all other technologies

that use lead halide perovskites. The strict legislation forces the researchers to take the toxicity of lead seriously, and it will likely direct the development of PeLEDs to the direction where the amount of lead is minimized, and possibly avoided.

It is very likely that the most stable PeLED is not the most efficient, and the most efficient PeLED is probably more expensive to manufacture than slightly less efficient PeLED. There will be compromises, and since there are multiple very distinct applications for PeLEDs, there is a call for multiple distinct types of PeLEDs. Some applications require very high color purity and illuminance, whereas some applications can settle for a modest performance but require cheap price.

REFERENCES

1. Era, M.; Morimoto, S.; et al. Organic-Inorganic Heterostructure Electroluminescent Device Using a Layered Perovskite Semiconductor $(C_6H_5C_2H_4NH_3)_2PbI_4$. *Appl. Phys. Lett.* **1994**, *65* (6), 676–678. https://doi.org/10.1063/1.112265.
2. Tan, Z.-K.; Moghaddam, R. S.; et al. Bright Light-Emitting Diodes Based on Organometal Halide Perovskite. *Nat. Nanotechnol.* **2014**, *9* (9), 687–692. https://doi.org/10.1038/nnano.2014.149.
3. Lu, M.; Zhang, Y.; et al. Metal Halide Perovskite Light-Emitting Devices: Promising Technology for Next-Generation Displays. *Adv. Funct. Mater.* **2019**, *29* (30), 1–35. https://doi.org/10.1002/adfm.201902008.
4. Nicole Buccitelli; Elliott, C.; et al. 2015 U .S. Lighting Market Characterization. United Stated Department of Energy 2017.
5. Guidehouse, I.; Elliott, C.; et al. Adoption of Light-Emitting Diodes in Common Lighting Applications. *U.S. Dep. Energy Rep.* **2020**.
6. Cho, H.; Jeong, S. H.; et al. Overcoming the Electroluminescence Efficiency Limitations of Perovskite Light-Emitting Diodes. *Science* **2015**, *350* (6265), 1222–1225. https://doi.org/10.1126/science.aad1818.
7. Bhatnagar, P. K. Organic Light-Emitting Diodes—A Review. In *Nanomaterials and Their Applications*; Springer, Singapore, **2018**; pp 261–287. https://doi.org/10.1007/978-981-10-6214-8_10.
8. Stranks, S. D.; Hoye, R. L. Z.; et al. The Physics of Light Emission in Halide Perovskite Devices. *Adv. Mater.* **2019**, *31* (47). https://doi.org/10.1002/adma.201803336.
9. Schubert, E. F. *Light-Emitting Diodes*; Cambridge University Press: Cambridge, **2006**. https://doi.org/10.1017/CBO9780511790546.
10. CIE chromaticity diagram https://upload.wikimedia.org/wikipedia/commons/b/b0/CIExy1931.png (accessed Nov 6, 2020).
11. Dai, S. W.; Hsu, B. W.; et al. Perovskite Quantum Dots with Near Unity Solution and Neat-Film Photoluminescent Quantum Yield by Novel Spray Synthesis. *Adv. Mater.* **2018**, *30* (7), 1–8. https://doi.org/10.1002/adma.201705532.
12. Gartner Says Global Smartphone Sales Fell Slightly in the Fourth Quarter of 2019

https://www.gartner.com/en/newsroom/press-releases/2020-03-03-gartner-says-global-smartphone-sales-fell-slightly-in (accessed Nov 6, 2020).

13. Dursun, I.; Shen, C.; et al. Perovskite Nanocrystals as a Color Converter for Visible Light Communication. *ACS Photonics* **2016**, *3* (7), 1150–1156. https://doi.org/10.1021/acsphotonics.6b00187.
14. Bao, C.; Xu, W.; et al. Bidirectional Optical Signal Transmission between Two Identical Devices Using Perovskite Diodes. *Nat. Electron.* **2020**, *3* (3), 156–164. https://doi.org/10.1038/s41928-020-0382-3.
15. Yin, Y.; Hu, Z.; et al. Full-Color Micro-LED Display with $CsPbBr_3$ Perovskite and CdSe Quantum Dots as Color Conversion Layers. *Adv. Mater. Technol.* **2020**, *2000251*, 1–6. https://doi.org/10.1002/admt.202000251.
16. International Telecommunication Union - ITU-R. *Parameter Values for Ultra-High Definition Television Systems for Production and International Programme Exchange*; **2015**.
17. CIE 1931 chromaticity diagram with Rec. 2020 color space coordinates https://upload.wikimedia.org/wikipedia/commons/b/b6/CIExy1931_Rec_2020.svg (accessed Nov 6, 2020).
18. He, Z.; Zhang, C.; et al. Tailoring the Spectrum: Low-Cost Perovskite-Polymer Composites. *Inf. Disp. (1975).* **2020**, *36* (1), 10–15. https://doi.org/10.1002/msid.1084.
19. Geske, T.; Bade, S. G. R.; et al. Organometal Halide Perovskites for Next Generation Fully Printed and Flexible LEDs and Displays. In *Flexible and Stretchable Medical Devices*; Takei, K., Ed.; Wiley-VCH Verlag GmbH & Co. KGaA, **2018**; pp 199–214. https://doi.org/10.1002/9783527804856.ch8.
20. Korshunova, K.; Winterfeld, L.; et al. Thermodynamic Stability of Mixed Pb:Sn Methyl-Ammonium Halide Perovskites. *Phys. Status Solidi Basic Res.* **2016**, *253* (10), 1907–1915. https://doi.org/10.1002/pssb.201600136.
21. Yang, Y.; Song, J.; et al. Ammonium-Iodide-Salt Additives Induced Photovoltaic Performance Enhancement in One-Step Solution Process for Perovskite Solar Cells. *J. Alloys Compd.* **2016**, *684*, 84–90. https://doi.org/10.1016/j.jallcom.2016.05.154.
22. Akbulatov, A. F.; Frolova, L. A.; et al. Hydrazinium-Loaded Perovskite Solar Cells with Enhanced Performance and Stability. *J. Mater. Chem. A* **2016**, *4* (47), 18378–18382. https://doi.org/10.1039/c6ta08215g.
23. Pering, S. R.; Deng, W.; et al. Azetidinium Lead Iodide for Perovskite Solar Cells. *J.*

Mater. Chem. A **2017**, *5* (39), 20658–20665. https://doi.org/10.1039/c7ta07545f.

24. Hsu, H. L.; Chang, C. C.; et al. High-Performance and High-Durability Perovskite Photovoltaic Devices Prepared Using Ethylammonium Iodide as an Additive. *J. Mater. Chem. A* **2015**, *3* (17), 9271–9277. https://doi.org/10.1039/c5ta01563d.
25. Singh, P.; Mukherjee, R.; et al. Acetamidinium-Substituted Methylammonium Lead Iodide Perovskite Solar Cells with Higher Open-Circuit Voltage and Improved Intrinsic Stability. *ACS Appl. Mater. Interfaces* **2020**, *12* (12), 13982–13987. https://doi.org/10.1021/acsami.0c00663.
26. Marco, N. De; Zhou, H.; et al. Guanidinium: A Route to Enhanced Carrier Lifetime and Open-Circuit Voltage in Hybrid Perovskite Solar Cells. *Nano Lett.* **2016**, *16* (2), 1009–1016. https://doi.org/10.1021/acs.nanolett.5b04060.
27. Shi, Y.; Xi, J.; et al. Rubidium Doping for Enhanced Performance of Highly Efficient Formamidinium-Based Perovskite Light-Emitting Diodes. *ACS Appl. Mater. Interfaces* **2018**, *10* (11), 9849–9857. https://doi.org/10.1021/acsami.8b00079.
28. Nam, J. K.; Chai, S. U.; et al. Potassium Incorporation for Enhanced Performance and Stability of Fully Inorganic Cesium Lead Halide Perovskite Solar Cells. *Nano Lett.* **2017**, *17* (3), 2028–2033. https://doi.org/10.1021/acs.nanolett.7b00050.
29. Bu, T.; Liu, X.; et al. A Novel Quadruple-Cation Absorber for Universal Hysteresis Elimination for High Efficiency and Stable Perovskite Solar Cells. *Energy Environ. Sci.* **2017**, *10* (12), 2509–2515. https://doi.org/10.1039/C7EE02634J.
30. Bag, S.; Durstock, M. F. Large Perovskite Grain Growth in Low-Temperature Solution-Processed Planar p-i-n Solar Cells by Sodium Addition. *ACS Appl. Mater. Interfaces* **2016**, *8* (8), 5053–5057. https://doi.org/10.1021/acsami.5b11494.
31. Li, N.; Song, L.; et al. Stabilizing Perovskite Light-Emitting Diodes by Incorporation of Binary Alkali Cations. *Adv. Mater.* **2020**, *32* (17), 1907786. https://doi.org/10.1002/adma.201907786.
32. Kieslich, G.; Sun, S.; et al. Solid-State Principles Applied to Organic–Inorganic Perovskites: New Tricks for an Old Dog. *Chem. Sci.* **2014**, *5* (12), 4712–4715. https://doi.org/10.1039/c4sc02211d.
33. Bartel, C. J.; Sutton, C.; et al. New Tolerance Factor to Predict the Stability of Perovskite Oxides and Halides. *Sci. Adv.* **2019**, *5* (2), eaav0693. https://doi.org/10.1126/sciadv.aav0693.
34. Volonakis, G.; Filip, M. R.; et al. Lead-Free Halide Double Perovskites via Heterovalent Substitution of Noble Metals. *J. Phys. Chem. Lett.* **2016**, *7* (7), 1254–

1259. https://doi.org/10.1021/acs.jpclett.6b00376.

35. Luo, J.; Wang, X.; et al. Efficient and Stable Emission of Warm-White Light from Lead-Free Halide Double Perovskites. *Nature* **2018**, *563* (7732), 541–545. https://doi.org/10.1038/s41586-018-0691-0.

36. Colella, S.; Mosconi, E.; et al. $MAPbI_{3-x}Cl_x$ Mixed Halide Perovskite for Hybrid Solar Cells: The Role of Chloride as Dopant on the Transport and Structural Properties. *Chem. Mater.* **2013**, *25* (22), 4613–4618. https://doi.org/10.1021/cm402919x.

37. Jiang, Q.; Rebollar, D.; et al. Pseudohalide-Induced Moisture Tolerance in Perovskite $CH_3NH_3Pb(SCN)_2I$ Thin Films. *Angew. Chemie - Int. Ed.* **2015**, *54* (26), 7617–7620. https://doi.org/10.1002/anie.201503038.

38. Kieslich, G.; Sun, S.; et al. An Extended Tolerance Factor Approach for Organic-Inorganic Perovskites. *Chem. Sci.* **2015**, *6* (6), 3430–3433. https://doi.org/10.1039/c5sc00961h.

39. Travis, W.; Glover, E. N. K.; et al. On the Application of the Tolerance Factor to Inorganic and Hybrid Halide Perovskites: A Revised System. *Chem. Sci.* **2016**, *7* (7), 4548–4556. https://doi.org/10.1039/c5sc04845a.

40. Li, Y.; Liu, F. Z.; et al. Formamidinium-Based Lead Halide Perovskites: Structure, Properties, and Fabrication Methodologies. *Small Methods* **2018**, *2* (7), 1700387. https://doi.org/10.1002/smtd.201700387.

41. Zhang, X.; Cao, W.; et al. Efficient Light-Emitting Diodes Based on Green Perovskite Nanocrystals with Mixed-Metal Cations. *Nano Energy* **2016**, *30* (August), 511–516. https://doi.org/10.1016/j.nanoen.2016.10.039.

42. Noh, J. H.; Im, S. H.; et al. Chemical Management for Colorful, Efficient, and Stable Inorganic–Organic Hybrid Nanostructured Solar Cells. *Nano Lett.* **2013**, *13* (4), 1764–1769. https://doi.org/10.1021/nl400349b.

43. Zhang, X.; Liu, H.; et al. Hybrid Perovskite Light-Emitting Diodes Based on Perovskite Nanocrystals with Organic–Inorganic Mixed Cations. *Adv. Mater.* **2017**, *29* (18), 1606405. https://doi.org/10.1002/adma.201606405.

44. Vegard, L. Die Konstitution Der Mischkristalle Und Die Raumfüllung Der Atome. *Zeitschrift für Phys.* **1921**, *5* (1), 17–26. https://doi.org/10.1007/BF01349680.

45. Sutanto, A. A.; Queloz, V. I. E.; et al. Pushing the Limit of Cs Incorporation into $FAPbBr_3$ Perovskite to Enhance Solar Cells Performances. *APL Mater.* **2019**, *7* (4). https://doi.org/10.1063/1.5087246.

46. Vassilakopoulou, A.; Papadatos, D.; et al. Light Emitting Diodes Based on Blends of Quasi-2D Lead Halide Perovskites Stabilized within Mesoporous Silica Matrix. *Microporous Mesoporous Mater.* **2017**, *249*, 165–175. https://doi.org/10.1016/j.micromeso.2017.05.001.

47. Lee, H.; Kim, H.; et al. Efficient Ruddlesden–Popper Perovskite Light-Emitting Diodes with Randomly Oriented Nanocrystals. *Adv. Funct. Mater.* **2019**, *29* (27), 1901225. https://doi.org/10.1002/adfm.201901225.

48. Na Quan, L.; Ma, D.; et al. Edge Stabilization in Reduced-Dimensional Perovskites. *Nat. Commun.* **2020**, *11*. https://doi.org/10.1038/s41467-019-13944-2.

49. Quan, L. N.; Yuan, M.; et al. Ligand-Stabilized Reduced-Dimensionality Perovskites. *J. Am. Chem. Soc.* **2016**, *138* (8), 2649–2655. https://doi.org/10.1021/jacs.5b11740.

50. Smith, I. C.; Hoke, E. T.; et al. A Layered Hybrid Perovskite Solar-Cell Absorber with Enhanced Moisture Stability. *Angew. Chemie - Int. Ed.* **2014**, *53* (42), 11232–11235. https://doi.org/10.1002/anie.201406466.

51. Sutanto, A. A.; Szostak, R.; et al. In Situ Analysis Reveals the Role of 2D Perovskite in Preventing Thermal-Induced Degradation in 2D/3D Perovskite Interfaces. *Nano Lett.* **2020**, *20* (5), 3992–3998. https://doi.org/10.1021/acs.nanolett.0c01271.

52. Warby, J. H.; Wenger, B.; et al. Revealing Factors Influencing the Operational Stability of Perovskite Light-Emitting Diodes. *ACS Nano* **2020**, *14* (7), 8855–8865. https://doi.org/10.1021/acsnano.0c03516.

53. Shen, Y.; Li, M. N.; et al. Rational Interface Engineering for Efficient Flexible Perovskite Light-Emitting Diodes. *ACS Nano* **2020**, *14* (5), 6107–6116. https://doi.org/10.1021/acsnano.0c01908.

54. Vassilakopoulou, A.; Papadatos, D.; et al. Room Temperature Light Emitting Diode Based on 2D Hybrid Organic-Inorganic Low Dimensional Perovskite Semiconductor. *Appl. Mater. Today* **2016**, *5*, 128–133. https://doi.org/10.1016/j.apmt.2016.09.004.

55. Vareli, I.; Vassilakopoulou, A.; et al. Defect Variants Based on the 2D Hybrid Organic-Inorganic Low-Dimensional Semiconductor (4-Fluoro-Phenethylamine-H)$_2$PbBr$_4$ for Fabrication of Single-Layer Deep Blue LEDs. *ACS Appl. Nano Mater.* **2018**, *1* (5), 2129–2142. https://doi.org/10.1021/acsanm.8b00207.

56. He, Z.; Liu, Y.; et al. High-Efficiency Red Light-Emitting Diodes Based on Multiple Quantum Wells of Phenylbutylammonium-Cesium Lead Iodide Perovskites. *ACS Photonics* **2019**, *6* (3), 587–594. https://doi.org/10.1021/acsphotonics.8b01435.

57. Liu, Y.; Cui, J.; et al. Efficient Blue Light-Emitting Diodes Based on Quantum-

Confined Bromide Perovskite Nanostructures. *Nat. Photonics* **2019**, *13* (11), 760–764. https://doi.org/10.1038/s41566-019-0505-4.

58. Wang, N.; Cheng, L.; et al. Perovskite Light-Emitting Diodes Based on Solution-Processed Self-Organized Multiple Quantum Wells. *Nat. Photonics* **2016**, *10* (11), 699–704. https://doi.org/10.1038/nphoton.2016.185.
59. Chaudhary, B.; Koh, T. M.; et al. Mixed-Dimensional Naphthylmethylammonium-Methylammonium Lead Iodide Perovskites with Improved Thermal Stability. *Sci. Rep.* **2020**, *10* (1), 429. https://doi.org/10.1038/s41598-019-57015-4.
60. Chen, H.; Lin, J.; et al. Structural and Spectral Dynamics of Single-Crystalline Ruddlesden-Popper Phase Halide Perovskite Blue Light-Emitting Diodes. *Sci. Adv.* **2020**, *6* (4), eaay4045. https://doi.org/10.1126/sciadv.aay4045.
61. Alehdaghi, H.; Kanwat, A.; et al. Quasi-2D Organic Cation-Doped Formamidinium Lead Bromide ($FAPbBr_3$) Perovskite Light-Emitting Diodes by Long Alkyl Chain. *Org. Electron.* **2020**, *79*, 105626. https://doi.org/10.1016/j.orgel.2020.105626.
62. Xiao, Z.; Kerner, R. A.; et al. Efficient Perovskite Light-Emitting Diodes Featuring Nanometre-Sized Crystallites. *Nat. Photonics* **2017**, *11* (2), 108–115. https://doi.org/10.1038/nphoton.2016.269.
63. Wygant, B. R.; Ye, A. Z.; et al. Probing the Degradation Chemistry and Enhanced Stability of 2D Organolead Halide Perovskites. *J. Am. Chem. Soc.* **2019**, *141* (45), 18170–18181. https://doi.org/10.1021/jacs.9b08895.
64. Xiao, X.; Dai, J.; et al. Suppressed Ion Migration along the In-Plane Direction in Layered Perovskites. *ACS Energy Lett.* **2018**, *3* (3), 684–688. https://doi.org/10.1021/acsenergylett.8b00047.
65. Wang, S.; Gong, Z.; et al. The Strain Effects in 2D Hybrid Organic-Inorganic Perovskite Microplates: Bandgap, Anisotropy and Stability. *Nanoscale* **2020**, *12* (12), 6644–6650. https://doi.org/10.1039/d0nr00657b.
66. Vassilakopoulou, A.; Papadatos, D.; et al. Mixtures of Quasi-Two and Three Dimensional Hybrid Organic-Inorganic Semiconducting Perovskites for Single Layer LED. *J. Alloys Compd.* **2017**, *692*, 589–598. https://doi.org/10.1016/j.jallcom.2016.09.076.
67. Chiba, T.; Hayashi, Y.; et al. Anion-Exchange Red Perovskite Quantum Dots with Ammonium Iodine Salts for Highly Efficient Light-Emitting Devices. *Nat. Photonics* **2018**, *12* (11), 681–687. https://doi.org/10.1038/s41566-018-0260-y.
68. Lin, Y.; Bai, Y.; et al. Enhanced Thermal Stability in Perovskite Solar Cells by

Assembling 2D/3D Stacking Structures. *J. Phys. Chem. Lett.* **2018**, *9* (3), 654–658. https://doi.org/10.1021/acs.jpclett.7b02679.

69. Akkerman, Q. A.; Manna, L. What Defines a Halide Perovskite? *ACS Energy Lett.* **2020**, *5* (2), 604–610. https://doi.org/10.1021/acsenergylett.0c00039.
70. Breternitz, J.; Schorr, S. What Defines a Perovskite? *Adv. Energy Mater.* **2018**, *8* (34), 1–2. https://doi.org/10.1002/aenm.201802366.
71. Protesescu, L.; Yakunin, S.; et al. Nanocrystals of Cesium Lead Halide Perovskites ($CsPbX_3$, X=Cl, Br, and I): Novel Optoelectronic Materials Showing Bright Emission with Wide Color Gamut. *Nano Lett.* **2015**, *15* (6), 3692–3696. https://doi.org/10.1021/nl5048779.
72. Xing, G.; Mathews, N.; et al. Low-Temperature Solution-Processed Wavelength-Tunable Perovskites for Lasing. *Nat. Mater.* **2014**, *13* (5), 476–480. https://doi.org/10.1038/nmat3911.
73. Song, J.; Li, J.; et al. Quantum Dot Light-Emitting Diodes Based on Inorganic Perovskite Cesium Lead Halides ($CsPbX_3$). *Adv. Mater.* **2015**, *27* (44), 7162–7167. https://doi.org/10.1002/adma.201502567.
74. Kumar, S.; Jagielski, J.; et al. Ultrapure Green Light-Emitting Diodes Using Two-Dimensional Formamidinium Perovskites: Achieving Recommendation 2020 Color Coordinates. *Nano Lett.* **2017**, *17* (9), 5277–5284. https://doi.org/10.1021/acs.nanolett.7b01544.
75. Lu, C. H.; Hu, J.; et al. Control of Morphology, Photoluminescence, and Stability of Colloidal Methylammonium Lead Bromide Nanocrystals by Oleylamine Capping Molecules. *J. Colloid Interface Sci.* **2016**, *484*, 17–23. https://doi.org/10.1016/j.jcis.2016.08.047.
76. Huang, J.; Wu, Y. H.; et al. Control of Oleylamine to Perovskite Ratio in Synthesis of $MAPbBr_3$ Nanoparticles. *Chem. Phys. Lett.* **2018**, *702*, 21–25. https://doi.org/10.1016/j.cplett.2018.04.057.
77. Li, J.; Bade, S. G. R.; et al. Single-Layer Light-Emitting Diodes Using Organometal Halide Perovskite/Poly(Ethylene Oxide) Composite Thin Films. *Adv. Mater.* **2015**, *27* (35), 5196–5202. https://doi.org/10.1002/adma.201502490.
78. Li, J.; Shan, X.; et al. Single-Layer Halide Perovskite Light-Emitting Diodes with Sub-Band Gap Turn-On Voltage and High Brightness. *J. Phys. Chem. Lett.* **2016**, *7* (20), 4059–4066. https://doi.org/10.1021/acs.jpclett.6b01942.
79. Zhao, L.; Lee, K. M.; et al. Improved Outcoupling Efficiency and Stability of

Perovskite Light-Emitting Diodes Using Thin Emitting Layers. *Adv. Mater.* **2019**, *31* (2), 1805836. https://doi.org/10.1002/adma.201805836.

80. Jung, Y. J.; Cho, S. Y.; et al. Influence of Indium-Tin-Oxide and Emitting-Layer Thicknesses on Light Outcoupling of Perovskite Light-Emitting Diodes. *Nano Converg.* **2019**, *6* (1). https://doi.org/10.1186/s40580-019-0196-z.
81. Shi, Y.; Wu, W.; et al. A Strategy for Architecture Design of Crystalline Perovskite Light-Emitting Diodes with High Performance. *Adv. Mater.* **2018**, *30* (25), 1–10. https://doi.org/10.1002/adma.201800251.
82. Kim, Y. H.; Cho, H.; et al. Multicolored Organic/Inorganic Hybrid Perovskite Light-Emitting Diodes. *Adv. Mater.* **2015**, *27* (7), 1248–1254. https://doi.org/10.1002/adma.201403751.
83. Seo, H.-K.; Kim, H.; et al. Efficient Flexible Organic/Inorganic Hybrid Perovskite Light-Emitting Diodes Based on Graphene Anode. *Adv. Mater.* **2017**, *29* (12), 1605587. https://doi.org/10.1002/adma.201605587.
84. Kumar, A.; Zhou, C. The Race to Replace Tin-Doped Indium Oxide: Which Material Will Win? *ACS Nano* **2010**, *4* (1), 11–14. https://doi.org/10.1021/nn901903b.
85. Xie, C.; Zhao, X.; et al. Transparent Near-Infrared Perovskite Light-Emitting Diodes. *Nat. Commun.* **2020**, *11* (1), 1–5. https://doi.org/10.1038/s41467-020-18110-7.
86. Tao, S.; Schmidt, I.; et al. Absolute Energy Level Positions in Tin- and Lead-Based Halide Perovskites. *Nat. Commun.* **2019**, *10* (1), 1–10. https://doi.org/10.1038/s41467-019-10468-7.
87. Subbiah, A. S.; Agarwal, S.; et al. Stable p–i–n $FAPbBr_3$ Devices with Improved Efficiency Using Sputtered ZnO as Electron Transport Layer. *Adv. Mater. Interfaces* **2017**, *4* (8). https://doi.org/10.1002/admi.201601143.
88. Wang, H.; Yu, H.; et al. Efficient Perovskite Light-Emitting Diodes Based on a Solution-Processed Tin Dioxide Electron Transport Layer. *J. Mater. Chem. C* **2018**, *6* (26), 6996–7002. https://doi.org/10.1039/C8TC01871E.
89. Ling, Y.; Tian, Y.; et al. Enhanced Optical and Electrical Properties of Polymer-Assisted All-Inorganic Perovskites for Light-Emitting Diodes. *Adv. Mater.* **2016**, *28* (40), 8983–8989. https://doi.org/10.1002/adma.201602513.
90. Luo, Q.; Ma, H.; et al. All-Carbon-Electrode-Based Endurable Flexible Perovskite Solar Cells. *Adv. Funct. Mater.* **2018**, *28* (11), 1–8. https://doi.org/10.1002/adfm.201706777.
91. Li, G.; Tan, Z.-K.; et al. Efficient Light-Emitting Diodes Based on Nanocrystalline

Perovskite in a Dielectric Polymer Matrix. *Nano Lett.* **2015**, *15* (4), 2640–2644. https://doi.org/10.1021/acs.nanolett.5b00235.

92. Zhao, B.; Bai, S.; et al. High-Efficiency Perovskite–Polymer Bulk Heterostructure Light-Emitting Diodes. *Nat. Photonics* **2018**, *12* (12), 783–789. https://doi.org/10.1038/s41566-018-0283-4.
93. Kim, D. H.; Kim, Y. C.; et al. Enhanced Brightness of Red Light-Emitting Diodes Based on $CsPbBr_xI_{3-x}$–PEOXA Composite Films. *J. Alloys Compd.* **2020**, *845*. https://doi.org/10.1016/j.jallcom.2020.156272.
94. Cho, H.; Kim, J. S.; et al. High-Efficiency Polycrystalline Perovskite Light-Emitting Diodes Based on Mixed Cations. *ACS Nano* **2018**, *12* (3), 2883–2892. https://doi.org/10.1021/acsnano.8b00409.
95. Goetz, K. P.; Taylor, A. D.; et al. Shining Light on the Photoluminescence Properties of Metal Halide Perovskites. *Adv. Funct. Mater.* **2020**. https://doi.org/10.1002/adfm.201910004.
96. Zhao, X.; Tan, Z. K. Large-Area near-Infrared Perovskite Light-Emitting Diodes. *Nat. Photonics* **2019**, *14* (April). https://doi.org/10.1038/s41566-019-0559-3.
97. Anaya, M.; Rand, B. P.; et al. Best Practices for Measuring Emerging Light-Emitting Diode Technologies. *Nat. Photonics* **2019**, *13* (12), 818–821. https://doi.org/10.1038/s41566-019-0543-y.
98. Wang, F.; Liu, X.-K.; et al. Chapter 1 - Fundamentals of Solar Cells and Light-Emitting Diodes. In *Micro and Nano Technologies*; Gao, F. B. T.-A. N. for S. C. and L. E. D., Ed.; Elsevier, **2019**; pp 1–35. https://doi.org/https://doi.org/10.1016/B978-0-12-813647-8.00001-1.
99. Airam LED 2700K https://www.airam.fi/en/product/v11382/4713775/ledop-p45-8w-827-e27-bx/182 (accessed Nov 5, 2020).
100. Li, G.; Rivarola, F. W. R.; et al. Highly Efficient Perovskite Nanocrystal Light-Emitting Diodes Enabled by a Universal Crosslinking Method. *Adv. Mater.* **2016**, *28* (18), 3528–3534. https://doi.org/10.1002/adma.201600064.
101. Khenkin, M. V.; Katz, E. A.; et al. Consensus Statement for Stability Assessment and Reporting for Perovskite Photovoltaics Based on ISOS Procedures. *Nat. Energy* **2020**, *5* (1), 35–49. https://doi.org/10.1038/s41560-019-0529-5.
102. Wang, H.; Kosasih, F. U.; et al. Perovskite-Molecule Composite Thin Films for Efficient and Stable Light-Emitting Diodes. *Nat. Commun.* **2020**, *11* (1), 1–9. https://doi.org/10.1038/s41467-020-14747-6.

103. Cho, H.; Wolf, C.; et al. High-Efficiency Solution-Processed Inorganic Metal Halide Perovskite Light-Emitting Diodes. *Adv. Mater.* **2017**, *29* (31), 1700579. https://doi.org/10.1002/adma.201700579.

104. Fassl, P.; Lami, V.; et al. Fractional Deviations in Precursor Stoichiometry Dictate the Properties, Performance and Stability of Perovskite Photovoltaic Devices. *Energy Environ. Sci.* **2018**, *11* (12), 3380–3391. https://doi.org/10.1039/C8EE01136B.

105. Yang, J. N.; Song, Y.; et al. Potassium Bromide Surface Passivation on $CsPbI_{3-X}Br_x$ Nanocrystals for Efficient and Stable Pure Red Perovskite Light-Emitting Diodes. *J. Am. Chem. Soc.* **2020**, *142* (6), 2956–2967. https://doi.org/10.1021/jacs.9b11719.

106. Liu, G.; Zheng, H.; et al. Interface Passivation Treatment by Halogenated Low-Dimensional Perovskites for High-Performance and Stable Perovskite Photovoltaics. *Nano Energy* **2020**, 104753. https://doi.org/10.1016/j.nanoen.2020.104753.

107. Lin, K.; Xing, J.; et al. Perovskite Light-Emitting Diodes with External Quantum Efficiency Exceeding 20 per Cent. *Nature* **2018**, *562* (7726), 245–248. https://doi.org/10.1038/s41586-018-0575-3.

108. Bing, J.; Kim, J.; et al. The Impact of a Dynamic Two-Step Solution Process on Film Formation of $Cs_{0.15}(MA_{0.7}FA_{0.3})_{0.85}PbI_3$ Perovskite and Solar Cell Performance. *Small* **2019**, *15* (9), 1–15. https://doi.org/10.1002/smll.201804858.

109. Zhao, Y.; Yang, R.; et al. Stabilizing $CsPbBr_3$ Quantum Dots with Conjugated Aromatic Ligands and Their Regulated Optical Behaviors. *Chem. Eng. J.* **2020**. https://doi.org/10.1016/j.cej.2020.124453.

110. Brandon, D.; Kaplan, W. D. *Wiley: Microstructural Characterization of Materials, 2nd Edition - David Brandon, Wayne D. Kaplan*, Second.; John Wiley & Sons, Ed.; **2008**.

111. Wang, J.; Song, C.; et al. All-Solution-Processed Pure Formamidinium-Based Perovskite Light-Emitting Diodes. *Adv. Mater.* **2018**, *30* (39), 1804137. https://doi.org/10.1002/adma.201804137.

112. Stoumpos, C. C.; Malliakas, C. D.; et al. Semiconducting Tin and Lead Iodide Perovskites with Organic Cations: Phase Transitions, High Mobilities, and near-Infrared Photoluminescent Properties. *Inorg. Chem.* **2013**, *52* (15), 9019–9038. https://doi.org/10.1021/ic401215x.

113. McGettrick, J. D.; Hooper, K.; et al. Sources of Pb(0) Artefacts during XPS Analysis of Lead Halide Perovskites. *Mater. Lett.* **2019**, *251*, 98–101. https://doi.org/10.1016/j.matlet.2019.04.081.

114. Akbulatov, A. F.; Martynenko, V. M.; et al. Intrinsic Thermal Decomposition Pathways of Lead Halide Perovskites $APbX_3$. *Sol. Energy Mater. Sol. Cells* **2020**, *213*, 110559. https://doi.org/10.1016/j.solmat.2020.110559.
115. European Union. Technology readiness levels (TRL); Extract from Part 19 - Commission Decision C(2014)4995 https://ec.europa.eu/research/participants/data/ref/h2020/wp/2014_2015/annexes/h2020-wp1415-annex-g-trl_en.pdf (accessed Nov 9, 2020).
116. Senocrate, A.; Kim, G. Y.; et al. Thermochemical Stability of Hybrid Halide Perovskites. *ACS Energy Lett.* **2019**, *4* (12), 2859–2870. https://doi.org/10.1021/acsenergylett.9b01605.
117. Fu, F.; Pisoni, S.; et al. I_2 Vapor-Induced Degradation of Formamidinium Lead Iodide Based Perovskite Solar Cells under Heat-Light Soaking Conditions. *Energy Environ. Sci.* **2019**, *12* (10), 3074–3088. https://doi.org/10.1039/c9ee02043h.
118. Nagabhushana, G. P.; Shivaramaiah, R.; et al. Direct Calorimetric Verification of Thermodynamic Instability of Lead Halide Hybrid Perovskites. *Proc. Natl. Acad. Sci. U. S. A.* **2016**, *113* (28), 7717–7721. https://doi.org/10.1073/pnas.1607850113.
119. Juarez-Perez, E. J.; Ono, L. K.; et al. Photodecomposition and Thermal Decomposition in Methylammonium Halide Lead Perovskites and Inferred Design Principles to Increase Photovoltaic Device Stability. *J. Mater. Chem. A* **2018**, *6* (20), 9604–9612. https://doi.org/10.1039/c8ta03501f.
120. Fan, Z.; Xiao, H.; et al. Layer-by-Layer Degradation of Methylammonium Lead Tri-Iodide Perovskite Microplates. *Joule* **2017**, *1* (3), 548–562. https://doi.org/10.1016/j.joule.2017.08.005.
121. Poglitsch, A.; Weber, D. Dynamic Disorder in Methylammoniumtrihalogenoplumbates (II) Observed by Millimeter-Wave Spectroscopy. *J. Chem. Phys.* **1987**, *87* (11), 6373–6378. https://doi.org/10.1063/1.453467.
122. Li, Z.; Yang, M.; et al. Stabilizing Perovskite Structures by Tuning Tolerance Factor: Formation of Formamidinium and Cesium Lead Iodide Solid-State Alloys. *Chem. Mater.* **2016**, *28* (1), 284–292. https://doi.org/10.1021/acs.chemmater.5b04107.
123. Fabini, D. H.; Stoumpos, C. C.; et al. Reentrant Structural and Optical Properties and Large Positive Thermal Expansion in Perovskite Formamidinium Lead Iodide. *Angew. Chemie* **2016**, *128* (49), 15618–15622. https://doi.org/10.1002/ange.201609538.

124. Schueller, E. C.; Laurita, G.; et al. Crystal Structure Evolution and Notable Thermal Expansion in Hybrid Perovskites Formamidinium Tin Iodide and Formamidinium Lead Bromide. *Inorg. Chem.* **2018**, *57* (2), 695–701. https://doi.org/10.1021/acs.inorgchem.7b02576.

125. Stoumpos, C. C.; Malliakas, C. D.; et al. Crystal Growth of the Perovskite Semiconductor $CsPbBr_3$: A New Material for High-Energy Radiation Detection. *Cryst. Growth Des.* **2013**, *13* (7), 2722–2727. https://doi.org/10.1021/cg400645t.

126. Yun, J. S.; Kim, J.; et al. Humidity-Induced Degradation via Grain Boundaries of $HC(NH_2)_2PbI_3$ Planar Perovskite Solar Cells. *Adv. Funct. Mater.* **2018**, *28* (11), 1705363. https://doi.org/10.1002/adfm.201705363.

127. Yi, C.; Luo, J.; et al. Entropic Stabilization of Mixed A-Cation ABX_3 Metal Halide Perovskites for High Performance Perovskite Solar Cells. *Energy Environ. Sci.* **2016**, *9* (2), 656–662. https://doi.org/10.1039/C5EE03255E.

128. Saliba, M.; Matsui, T.; et al. Cesium-Containing Triple Cation Perovskite Solar Cells: Improved Stability, Reproducibility and High Efficiency. *Energy Environ. Sci.* **2016**, *9* (6), 1989–1997. https://doi.org/10.1039/c5ee03874j.

129. Leguy, A. M. A.; Hu, Y.; et al. Reversible Hydration of $CH_3NH_3PbI_3$ in Films, Single Crystals, and Solar Cells. *Chem. Mater.* **2015**, *27* (9), 3397–3407. https://doi.org/10.1021/acs.chemmater.5b00660.

130. Christians, J. A.; Miranda Herrera, P. A.; et al. Transformation of the Excited State and Photovoltaic Efficiency of $CH_3NH_3PbI_3$ Perovskite upon Controlled Exposure to Humidified Air. *J. Am. Chem. Soc.* **2015**, *137* (4), 1530–1538. https://doi.org/10.1021/ja511132a.

131. Lee, J. W.; Kim, D. H.; et al. Formamidinium and Cesium Hybridization for Photo- and Moisture-Stable Perovskite Solar Cell. *Adv. Energy Mater.* **2015**, *5* (20). https://doi.org/10.1002/aenm.201501310.

132. Marchezi, P. E.; Therézio, E. M.; et al. Degradation Mechanisms in Mixed-Cation and Mixed-Halide $Cs_xFA_{1-x}Pb(Br_yI_{1-y})_3$ Perovskite Films under Ambient Conditions. *J. Mater. Chem. A* **2020**, *8* (18), 9302–9312. https://doi.org/10.1039/D0TA01201G.

133. Fairfield, D. J.; Sai, H.; et al. Structure and Chemical Stability in Perovskite-Polymer Hybrid Photovoltaic Materials. *J. Mater. Chem. A* **2019**, *7* (4), 1687–1699. https://doi.org/10.1039/c8ta07545j.

134. Eperon, G. E.; Habisreutinger, S. N.; et al. The Importance of Moisture in Hybrid Lead Halide Perovskite Thin Film Fabrication. *ACS Nano* **2015**, *9* (9), 9380–9393.

https://doi.org/10.1021/acsnano.5b03626.

135. Aristidou, N.; Eames, C.; et al. Fast Oxygen Diffusion and Iodide Defects Mediate Oxygen-Induced Degradation of Perovskite Solar Cells. *Nat. Commun.* **2017**, *8*, 15218. https://doi.org/10.1038/ncomms15218.
136. Eames, C.; Frost, J. M.; et al. Ionic Transport in Hybrid Lead Iodide Perovskite Solar Cells. *Nat. Commun.* **2015**, *6* (1), 7497. https://doi.org/10.1038/ncomms8497.
137. Wei, Z.; Xing, J. The Rise of Perovskite Light-Emitting Diodes. *J. Phys. Chem. Lett.* **2019**, *10* (11), 3035–3042. https://doi.org/10.1021/acs.jpclett.9b00277.
138. DeQuilettes, D. W.; Zhang, W.; et al. Photo-Induced Halide Redistribution in Organic-Inorganic Perovskite Films. *Nat. Commun.* **2016**, *7* (May). https://doi.org/10.1038/ncomms11683.
139. Hoke, E. T.; Slotcavage, D. J.; et al. Reversible Photo-Induced Trap Formation in Mixed-Halide Hybrid Perovskites for Photovoltaics. *Chem. Sci.* **2015**, *6* (1), 613–617. https://doi.org/10.1039/C4SC03141E.
140. Wu, T.; Li, J.; et al. High-Performance Perovskite Light-Emitting Diode with Enhanced Operational Stability Using Lithium Halide Passivation. *Angew. Chemie Int. Ed.* **2020**, *59* (10), 4099–4105. https://doi.org/10.1002/anie.201914000.
141. Xu, W.; Hu, Q.; et al. Rational Molecular Passivation for High-Performance Perovskite Light-Emitting Diodes. *Nat. Photonics* **2019**, *13* (6), 418–424. https://doi.org/10.1038/s41566-019-0390-x.
142. Rolston, N.; Watson, B. L.; et al. Mechanical Integrity of Solution-Processed Perovskite Solar Cells. *Extrem. Mech. Lett.* **2016**, *9*, 353–358. https://doi.org/10.1016/j.eml.2016.06.006.
143. Zhao, L.; Rolston, N.; et al. Influence of Bulky Organo-Ammonium Halide Additive Choice on the Flexibility and Efficiency of Perovskite Light-Emitting Devices. *Adv. Funct. Mater.* **2018**, *28* (31), 1–9. https://doi.org/10.1002/adfm.201802060.
144. Zhao, J.; Deng, Y.; et al. Strained Hybrid Perovskite Thin Films and Their Impact on the Intrinsic Stability of Perovskite Solar Cells. *Sci. Adv.* **2017**, *3* (11), eaao5616. https://doi.org/10.1126/sciadv.aao5616.
145. Boyd, C. C.; Cheacharoen, R.; et al. Understanding Degradation Mechanisms and Improving Stability of Perovskite Photovoltaics. *Chem. Rev.* **2019**, *119* (5), 3418–3451. https://doi.org/10.1021/acs.chemrev.8b00336.
146. Xu, B.; Wang, W.; et al. Electric Bias Induced Degradation in Organic-Inorganic Hybrid Perovskite Light-Emitting Diodes. *Sci. Rep.* **2018**, *8* (1), 15799.

https://doi.org/10.1038/s41598-018-34034-1.

147. Kato, Y.; Ono, L. K.; et al. Silver Iodide Formation in Methyl Ammonium Lead Iodide Perovskite Solar Cells with Silver Top Electrodes. *Adv. Mater. Interfaces* **2015**, *2* (13), 2–7. https://doi.org/10.1002/admi.201500195.

148. Zhao, L.; Kerner, R. A.; et al. Redox Chemistry Dominates the Degradation and Decomposition of Metal Halide Perovskite Optoelectronic Devices. *ACS Energy Lett.* **2016**, *1* (3), 595–602. https://doi.org/10.1021/acsenergylett.6b00320.

149. Yang, J.; Siempelkamp, B. D.; et al. Origin of the Thermal Instability in $CH_3NH_3PbI_3$ Thin Films Deposited on ZnO. *Chem. Mater.* **2015**, *27* (12), 4229–4236. https://doi.org/10.1021/acs.chemmater.5b01598.

150. Yuan, Z.; Miao, Y.; et al. Unveiling the Synergistic Effect of Precursor Stoichiometry and Interfacial Reactions for Perovskite Light-Emitting Diodes. *Nat. Commun.* **2019**, *10* (1), 1–9. https://doi.org/10.1038/s41467-019-10612-3.

151. Grancini, G.; Roldán-Carmona, C.; et al. One-Year Stable Perovskite Solar Cells by 2D/3D Interface Engineering. *Nat. Commun.* **2017**, *8*, 1–8. https://doi.org/10.1038/ncomms15684.

152. Komoda, T.; Tsuji, H.; et al. 66.4: Invited Paper: High-Quality White OLEDs and Resource Saving Fabrication Processes for Lighting Application. *48th Annu. SID Symp. Semin. Exhib. 2010, Disp. Week 2010* **2010**, *2*, 993–996. https://doi.org/10.1889/1.3500653.

153. World Health Organization. International Programme on Chemical Safety: Ten chemicals of major public health concern https://www.who.int/ipcs/assessment/public_health/chemicals_phc/en/ (accessed Nov 6, 2020).

154. World Health Organization. Exposure to lead: A major public health concern https://apps.who.int/iris/bitstream/handle/10665/329953/WHO-CED-PHE-EPE-19.4.7-eng.pdf?ua=1 (accessed Nov 6, 2020).

155. European Union. Directive 2011/65/EU of the European Parliament and of the Council of 8 June 2011 on the Restriction of the Use of Certain Hazardous Substances in Electrical and Electronic Equipment. *Official Journal* **2011**, *L* (174), 88–110.

156. Zhang, W.; Yang, J.; et al. A Critical Review on Secondary Lead Recycling Technology and Its Prospect. *Renew. Sustain. Energy Rev.* **2016**, *61*, 108–122. https://doi.org/10.1016/j.rser.2016.03.046.

157. Binek, A.; Petrus, M. L.; et al. Recycling Perovskite Solar Cells to Avoid Lead Waste.

ACS Appl. Mater. Interfaces **2016**, *8* (20), 12881–12886. https://doi.org/10.1021/acsami.6b03767.

158. Li, J.; Cao, H. L.; et al. Biological Impact of Lead from Halide Perovskites Reveals the Risk of Introducing a Safe Threshold. *Nat. Commun.* **2020**, *11* (1), 1–5. https://doi.org/10.1038/s41467-019-13910-y.
159. Billen, P.; Leccisi, E.; et al. Comparative Evaluation of Lead Emissions and Toxicity Potential in the Life Cycle of Lead Halide Perovskite Photovoltaics. *Energy* **2019**, *166*, 1089–1096. https://doi.org/10.1016/j.energy.2018.10.141.
160. Ning, W.; Gao, F. Structural and Functional Diversity in Lead-Free Halide Perovskite Materials. *Adv. Mater.* **2019**, *31* (22), 1900326. https://doi.org/10.1002/adma.201900326.
161. Gao, W.; Ran, C.; et al. Robust Stability of Efficient Lead-Free Formamidinium Tin Iodide Perovskite Solar Cells Realized by Structural Regulation. *J. Phys. Chem. Lett.* **2018**, *9* (24), 6999–7006. https://doi.org/10.1021/acs.jpclett.8b03194.
162. Kim, T. H.; Kim, S. G. Clinical Outcomes of Occupational Exposure to N,N-Dimethylformamide: Perspectives from Experimental Toxicology. *Saf. Health Work* **2011**, *2* (2), 97–104. https://doi.org/10.5491/SHAW.2011.2.2.97.
163. Babayigit, A.; Ethirajan, A.; et al. Toxicity of Organometal Halide Perovskite Solar Cells. *Nat. Mater.* **2016**, *15* (3), 247–251. https://doi.org/10.1038/nmat4572.
164. Wang, M.; Fu, Q.; et al. Systematic Optimization of Perovskite Solar Cells via Green Solvent Systems. *Chem. Eng. J.* **2020**, *387* (January). https://doi.org/10.1016/j.cej.2019.123966.
165. Kim, T.; Kim, J.-H.; et al. All-Solution-Processed Organic–Inorganic Hybrid Perovskite Light-Emitting Diodes under Ambient Air. *Phys. status solidi* **2019**, *216* (22), 1900642. https://doi.org/10.1002/pssa.201900642.
166. Prakasam, V.; Tordera, D.; et al. Large Area Perovskite Light-Emitting Diodes by Gas-Assisted Crystallization. *J. Mater. Chem. C* **2019**, *7* (13), 3795–3801. https://doi.org/10.1039/c8tc06482b.
167. Huang, F.; Dkhissi, Y.; et al. Gas-Assisted Preparation of Lead Iodide Perovskite Films Consisting of a Monolayer of Single Crystalline Grains for High Efficiency Planar Solar Cells. *Nano Energy* **2014**, *10*, 10–18. https://doi.org/10.1016/j.nanoen.2014.08.015.

Appendix 1 Perovskite light-emitting diodes with highest EQE-values

Table A1. Details of blue, green, red and IR PeLEDs with highest EQE values.

Color	EL (nm)	Perovskite and additives	Device architecture	EQE (%)	Stability	Reference
Blue	483	$FA_{0.3}Cs_{0.7}PbBr_3$ and PBABr 2D/3D perovskite	Glass/ITO/NiOx/TFB/PVK/ perovskite/TPBi/LiF/Al p-i-n	9.5	T_{50}=250 s Constant current density 1 mA cm^{-2}	[57]
Green	512	$CsPbBr_3$ and PEABr 2D/3D perovskite PEO additive	PET/AgNW/ZnO/PEDOT:PSS/ perovskite/TPBi/LiF/Al p-i-n	24.5	T_{50}=453.4 min Constant luminance 100 cd m^{-2}	[53]
Red	653	$CsPb(Br/I)_3$ Quantum dots with OA	Glass/ITO/PEDOT:PSS/poly-TPD/perovskite/TPBi/lithium 8-quinolate (Liq)/Al p-i-n	21.3	T_{50}=5 min Constant current density 1.25 mA cm^{-2}	[67]
IR	800	$FAPbI_3$ ODEA passivation	Glass/ITO/ZnO:PEIE/ perovskite/MoO_x/Au n-i-p	21.6	T_{50}=1200 min Constant current density 25 mA cm^{-2}	[141]